

8-2018

14-3-3 Protein Rad24 and its Effect on Mid1 Localization and Contractile Acto- Myosin Ring Assembly During Cytokinesis in *S. pombe*

Anissa P. Grawe
Grand Valley State University

Follow this and additional works at: <https://scholarworks.gvsu.edu/theses>

 Part of the [Cell and Developmental Biology Commons](#)

Recommended Citation

Grawe, Anissa P., "14-3-3 Protein Rad24 and its Effect on Mid1 Localization and Contractile Acto- Myosin Ring Assembly During Cytokinesis in *S. pombe*" (2018). *Masters Theses*. 891.
<https://scholarworks.gvsu.edu/theses/891>

This Thesis is brought to you for free and open access by the Graduate Research and Creative Practice at ScholarWorks@GVSU. It has been accepted for inclusion in Masters Theses by an authorized administrator of ScholarWorks@GVSU. For more information, please contact scholarworks@gvsu.edu.

14-3-3 Protein Rad24 and its Effect on Mid1 Localization and Contractile Acto-Myosin Ring Assembly During Cytokinesis in *S. pombe*

Anissa Pedersen Grawe

A thesis submitted to the Graduate Faculty of

GRAND VALLEY STATE UNIVERSITY

In

Partial Fulfillment of the Requirements

For the Degree of

Master of Science

Department of Cell and Molecular Biology

August 2018

Dedication

I dedicate this work to my two sons, Gunnar Gordon Grawe and Tobin Axel Roger Grawe, and to my brother Chris Lee Pedersen, whom I never met. He died from rhabdomyosarcoma in 1968, at age 9. I know that my interest in science and research has undoubtedly come from his death at such a young age. My hope is that were he diagnosed today, scientific advancements made possible by basic science research since then could have saved him, and that hope makes me optimistic and inspired by the power of what research can do.

Acknowledgements

I would like to thank my committee members, Matthew Christians, Agnieszka Szarecka, and especially Dawn Hart for teaching me so much about the wonderful model organism fission yeast, scientific writing, and cell division. A special thanks goes to Dr. Szarecka for her help with modeling Mid1, and a very special thanks goes to Sango Otieno in the Statistical Counseling Center for helping with the analysis of all the confocal data. I would like to thank the Cell and Molecular Biology Department, the Graduate Studies Department, and the National Science Foundation for funding my research project. And most of all, I would like to thank my husband Sam for being my partner in life and supporting me through the entire graduate school process.

Abstract

In animal and yeast cells, cell division (cytokinesis) is facilitated by the formation of a contractile acto-myosin ring (CAR). Proper CAR formation and constriction is heavily reliant on the temporal regulation, phosphorylation, and localization of key proteins. In the fission yeast *S. pombe*, Mid1 is an important dimeric CAR scaffolding protein that connects the contractile apparatus to the plasma membrane at the right place and time during cytokinesis. Mid1 is confined to both the nucleus and protein assemblies called nodes during interphase, and transitions to the cell cortex at mitotic entry as nodes mature and coalesce into the CAR. Rad24 is a 14-3-3 protein involved in cell cycle checkpoints known to interact with CAR proteins and some of their regulators. 14-3-3 proteins bind to a conserved consensus phosphorylation motif, RXXpS, which is targeted by Sid2 and other NDR-kinases. The Septation Initiation Network (SIN) is a conserved signaling pathway to facilitate separation of two new daughter cells. Sid2, the terminal kinase of the SIN, has numerous targets in the CAR, including Mid1. Removal of Rad24 has distinct consequences on the timing of major cytokinetic events.

The goal of this thesis is to use fission yeast to characterize the interaction between Rad24 and Mid1, which in turn organizes important CAR components F-actin and Myosin II. Live cell videomicroscopy in *rad24* Δ cells shows that fluorescently tagged Mid1-NeoGreen remains nodal during interphase and returns to the nucleus early after CAR constriction. *rad24* Δ cells also show a delay of F-actin (LifeAct-GFP) and myosin-II (Rlc1-tomato) recruitment to the CAR and deferred CAR constriction. *In vitro* binding assays show that Mid1 and Rad24 interact directly and computational

structural speculation concludes that this interaction occurs most likely while Mid1 is in a monomeric form, after or before nuclear export or import. SIN-dependent phosphorylation of Mid1 has definitive consequences on cell division in fission yeast, and the conserved nature of protein interactions during cytokinesis in *S. pombe* suggests broader implications for the study of cell division and cancer in higher animals.

Table of Contents

Dedication	3
Acknowledgement	4
Abstract	5
Listing of Figures and Tables	8
Abbreviations	10
1 Introduction	11
1.1 Overview	11
1.2 Cytokinesis in Yeast, the Cell Geometry Network, and Mid1 positioning	12
1.3 Nodes and CAR recruitment during the Cell Cycle	14
1.4 Sid2 and the Septation Initiation Network	18
1.5 14-3-3 Proteins and Cell Cycle Checkpoints	23
1.6 Previous work with Sid2 Phosphomutants	25
1.7 Role of Rad24 binding in Mid1 localization	27
1.8 Mid1 Structure and Oligomerization	29
1.9 Hypothesis	35
2 Methods	37
2.1 Strains and Media	37
2.2 Confocal Microscopy	41
2.3 Biochemical Assays	43
2.4 Computational Tools	46
2.5 Statistical Analysis	48
3 Characterization of the Interaction between Mid1 and Rad24	51
3.1 Determination of Phospho-dependence of Mid1 and Mid1 ^{4RXXSA} /Rad24 Interaction	51
3.2 Determination of Phospho-dependence of Rad24/Mid1 Interaction in SIN Mutants	54
3.3 Sequence analysis and structural models of Rad24 and Mid1 N-terminus	58
4 Consequences of Rad24 deletion on timing and morphology of CAR formation	66
4.1 Difference in F-actin distribution between wild type and <i>rad24Δ S. pombe</i>	66
4.2 Difference in Myosin-II and Mid1 distributions in WT and <i>rad24Δ S. pombe</i>	70
4.3 Difference in Mid1 distribution between wild type and <i>rad24Δ S. pombe</i>	77
5 Discussion	79
6 Supplemental	86
7 References	89

Listing of Figures

Figure 1	Mid1 is an important scaffolding protein for correct positioning of the division site.	13
Figure 2	The Cell Cycle.	14
Figure 3	Mid1 and nodes.	15
Figure 4	<i>S. pombe</i> cytokinesis, Septation Initiation Network (SIN) phenotypes, and the SIN cascade.	19
Figure 5	Mid1 localization in SIN mutant phenotypes.	23
Figure 6	Mid1 in phosphomutant and <i>rad24Δ</i> cells: Mid1 shows higher localization to the nucleus in cells lacking <i>rad24</i> .	28
Figure 7	Protein structures of Anillin and Mid1.	30
Figure 8	Mid1 Dimerization Interface and Mid1 protein schematic.	32
Figure 9	Dimerization of Mid1 is important for localization.	33
Figure 10	Concepts of confocal microscopy and Z-plane optical sectioning.	41
Figure 11	Schematic of fluorescence intensity distribution profiles and data processing.	49
Figure 12	Mid1-GFP does not bind more efficiently to GST-Rad24 than Mid14 ^{RXXSA} -GFP.	53
Figure 13	Hyperphosphorylation did not result in Rad24 binding to Mid1 more readily.	56
Figure 14	Motif analysis shows consensus between four yeast Mid1 protein sequences.	60
Figure 15	Phyre2 comparative model of <i>S. pombe</i> Rad24.	61
Figure 16	STAMP structural alignment of putative Mid1 N-terminus (aa 1-582) models rendered in VMD shows consensus around Sid2 phosphosites.	65

Figure 17	<i>rad24</i> Δ cells show a delay in F-actin recruitment to the CAR but premature CAR constriction and septation.	69
Figure 18	<i>rad24</i> Δ cells show delayed Myosin recruitment to the CAR and delays in CAR constriction.	73
Figure 19	<i>rad24</i> Δ cells show cortical adherence of Mid1 during G2 and a premature return to the nucleus.	76
Figure 20	<i>rad24</i> Δ cells show cortical adherence of Mid1 during G2 and a premature return to the nucleus.	78
Figure S1	Delay in Mid1-facilitated assembly of the CAR coincides with a delay in Myosin recruitment to the CAR and deferred CAR constriction.	86
Figure S2	Clustal Omega Multiple Sequence Alignment of yeast Mid1 sequences reveals multiple conserved motifs and serines.	87
Figure S3	Additional Logos from MEME Motif Analysis reveals conserved residues among yeasts.	88

Listing of Tables

Table 1	PCR Primers used in this study.	39
Table 2	<i>S. pombe</i> strains used in this study.	40
Table 3	PSI-BLAST result sequences with Mid1 N-terminus (aa 1-582) as query.	58
Table 4	I-TASSER Models of Mid1 N terminus.	63

Abbreviations

CAR	Contractile Acto-Myosin Ring
SIN	Septation Initiation Network
ATP	Adenosine Triphosphate
CGN	Cell Geometry Network
Rho GTPase	hydrolyzes Guanosine Triphosphate into Guanosine Diphosphate
C2 Domain	Ca ²⁺ -dependent membrane targeting Domain
Rho GEF	Rho Guanine nucleotide Exchange Factor
SAD kinase	Synapses of Amphids Defective kinase
PH	Pleckstrin Homology Domain
DYRK kinase	Dual-specificity Tyrosine-phosphorylation Regulated Kinase
NDR kinase	Nuclear dbf2-related kinase
IQGAP	IQ motif-containing GTPase activating protein
F-actin	Filamentous Actin
PAK	p21-activated Kinase
Ras	Retrovirus-associated DNA sequences GTPase
I-TASSER	Iterative Threading ASSEmbly Refinement

1 Introduction

1.1 Overview

Cell division is evolutionarily conserved from yeast to humans. The important processes that facilitate cell division are shared across highly divergent biological kingdoms, such as fungi and animalia. The fission yeast *Schizosaccharomyces pombe* is a rod shaped unicellular eukaryote that grows by elongation at the tips and divides medially via a contractile acto-myosin ring (CAR) (Hayles and Nurse, 1989; Chang, et al., 1996). The cytokinetic ring, or CAR, is a feature present in both animal and yeast cells and is composed of filamentous actin, which also comprises the microfilaments of the cytoskeleton, and the motor protein myosin-II (Pollard and Wu, 2010). After microtubules, comprised of α and β -tubulin, segregate chromosomes, a pulley system between F-actin and myosin-II in the CAR creates the force necessary for cell cleavage (Pollard and Wu, 2010) in a process similar to a muscle contraction (Vavylonis, et al., 2008).

Diseases such as cancer involve disruptions to the normal cell cycle. Cell division in *S. pombe* is analogous to the cell division process in human cells, which makes yeast a powerful model for the study of cytokinesis and mitosis (Hayles and Nurse, 1989) and their possible roles in disease progression. One of the most important cell division proteins in *S. pombe*, Mid1, shows functional as well as structural similarity with its human homolog, Anillin (Paoletti and Chang, 2000; Sun, et al., 2015). Interestingly, Anillin has been shown to be overexpressed in various human tumors (Hall, et al., 2005). Therefore, a clear understanding of Mid1's localization and its role in cell division

is important, not only for the general knowledge of how cytokinesis proceeds, but for advancing this knowledge to the point that we could find new potential therapies.

1.2 Cytokinesis in Yeast, the Cell Geometry Network, and Mid1 positioning

Spatial indicators of cell geometry, mitotic apparatus, and genetic material that constitute the Cell Geometry Network (CGN) determine the division plane and CAR orientation (Rincon and Paoletti, 2012) in fission yeast cells. Interphase microtubules position the nucleus directly in the cell geometrical center (Tran, et al., 2001), and DYRK kinase Pom1 organizes SAD serine/threonine protein kinase Cdr2 to define the division plane (Martin and Berthelot-Grosjean, 2009). Since *S. pombe* grows only at the cell ends and maintains a constant width throughout cell division, the spatial Pom1 gradient constitutes an internal sensing mechanism for the yeast cell to monitor its own length and volume (Turner, et al., 2012). Entry into mitosis is dependent on Cyclin-dependent kinase (Cdk1) activity (Russell and Nurse, 1986), which is inhibited by Wee1 kinase (Russell and Nurse, 1987), and activated by Cdc25 phosphatase (Gould, et al., 1990). Cdr2 and Cdr1 are Wee1- inhibitory kinases that are themselves inhibited by Pom1 (Bähler and Pringle, 1998).

Negative signaling from Pom1 controlling Cdr2 from the cell tips during interphase, along with positive signaling from nuclear export of Mid1 at mitotic entry, together insure proper division plane placement (Almonacid, et al., 2009). In this sense, Cdr2 serves as a mitotic activator that is localized to the middle of the cell, and Pom1, serving as an inhibitor of Cdr2, is arranged in a gradient originating from the cell ends (Martin and Berthelot-Grosjean, 2009; Almonacid, et al., 2009; Moseley, et al., 2009).

As the cell grows, the amount of inhibitor interacting with the activator decreases, leading to an increase in Cdk1 activity, which drives mitosis (Deng, et al., 2014). Mid1 is an important scaffolding protein that recruits CAR precursors, regulatory elements, and subsequently F-actin and myosin-II, to the division site in fission yeast cells (Wu, et al., 2003).

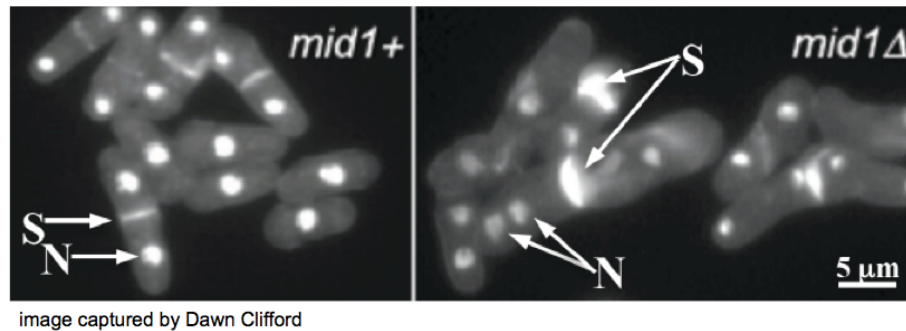


Figure 1. Mid1 is an important scaffolding protein for correct positioning of the division site. Fission yeast cells stained with methyl blue to show cell walls and DAPI to show nuclei. Cells lacking Mid1 have misshapen or tilted septa (S) that do not form in the center of the cell; they also contain multiple septa and nuclei (N).

Mid1 is essential in anchoring the CAR to the cell membrane in the correct place and time during the cell cycle (Sohrmann, et al., 1996). In the absence of Mid1, the septum becomes positioned randomly and at tilted angles (Figure 1), even though the nucleus is positioned normally, indicating that Mid1 is required to unite the location of the nucleus with the division site (Chang, et al., 1996). However, CAR assembly in these *mid1Δ* mutant cells can still proceed via actomyosin filaments through a signaling cascade called the Septation Initiation Network (SIN) rather than by the formation of a cortical network of CAR proteins (Hachet and Simanis, 2008). Even though *mid1Δ* cells are able to eventually divide via these overlapping cytokinetic mechanisms, there are distinct consequences in the morphology of the CAR and timing of CAR assembly due to the lack of *mid1* (Saha and Pollard, 2012a). SIN signaling is important in initiating

separation, the last stage of cytokinesis, and recent connections have developed between the CGN and the SIN (Rincon, et al., 2017). In this respect, both of the major pathways that regulate division plane positioning, the CGN and the SIN, intersect through interactions with Mid1 (Rincon and Paoletti, 2012).

1.3 Nodes and CAR Recruitment during the Cell Cycle

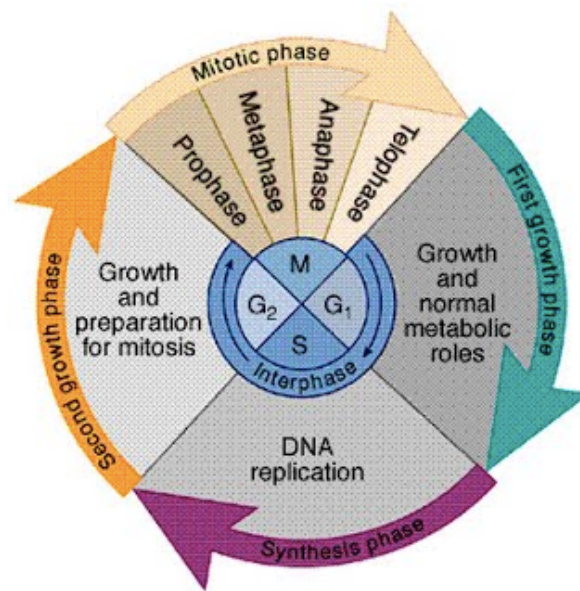


Figure 2. The Cell Cycle. The series of events that occur during cell division to duplicate DNA and produce two daughter cells. G₁, S, and G₂ are growth and DNA synthesis phases collectively termed interphase. Mitosis, when chromosomes condense and are separated, occurs during M phase, and cytokinesis occurs during the late stages of mitosis.

<https://sites.google.com/site/celldivisionhotran/regulation-of-cell-cycle>

The cell cycle contains four stages (Figure 2). G₁, S and G₂, collectively termed interphase, are when the majority of cell growth occurs and DNA in chromosomes is duplicated. The fourth stage, mitosis, is separated into prophase, anaphase,

metaphase, and telophase. Cytokinesis is the process after mitosis by which a cell and its cytoplasmic contents divide to become two daughter cells. During interphase the actin cytoskeleton accumulates as patches and cables in the growing cell tips, and is reorganized during CAR assembly to concentrate at the cell cortex during metaphase (Marks, et al., 1986). When cells enter mitosis, elongation stops and the actin and tubulin cytoskeletons are reorganized in preparation for cytokinesis (Marks, et al., 1986). Chromatin condensation and chromosome separation take place during mitosis and directly precede cytokinesis, when CAR constriction and cell septation occur.

There are two types of heterogeneous protein assemblies called nodes in *S. pombe*, which contain precursors for formation of the CAR (Wu, et al., 2006). During the cell cycle, these two distinct node types eventually fuse to be called cytokinetic nodes

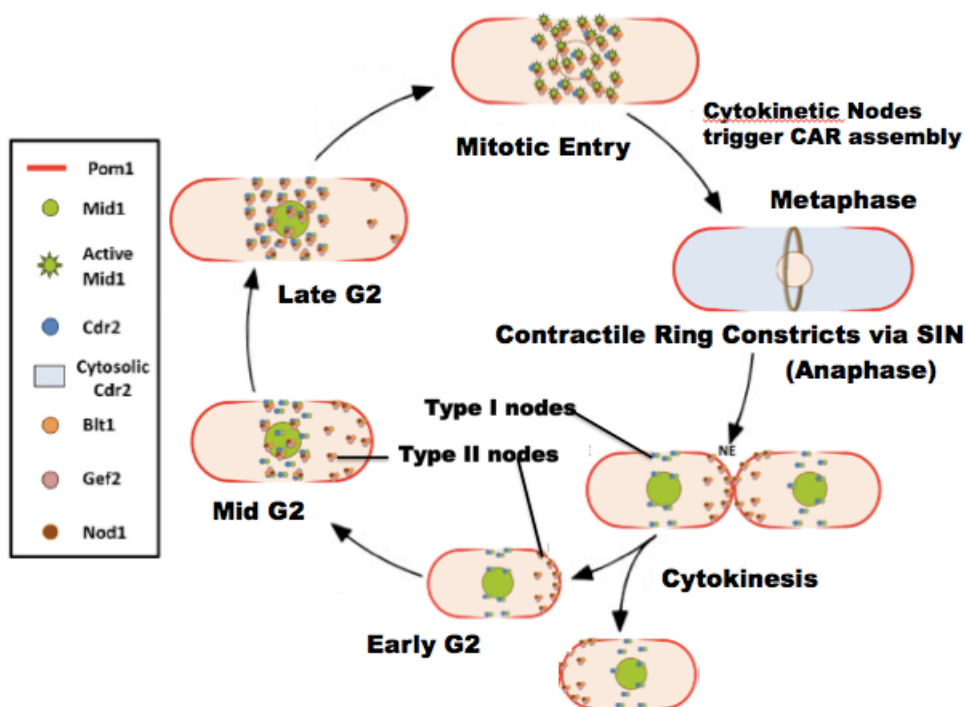


Figure 3. Mid1 and Nodes

Mid1 Localization during the cell cycle. Type I node placement and Type II node migration are also shown. Adapted from Rincon and Paoletti, 2016.

and are organized by Cdr2 in cooperation with Mid1 as it recruits all the necessary proteins to form the functioning machinery of the CAR (Figure 3).

Type I nodes contain Cdr2 as well as Mid1, and are confined to the cell cortex (Akamatsu, et al., 2014). During interphase, a small amount of Mid1 is shuttled between the nucleus and the Type I nodes during early G2, with the majority of Mid1 harbored in the nucleus (Paoletti and Chang, 2000). Pom1, as mentioned previously, exerts a spatial gradient effect by diffusing from the cell ends to regulate Cdr2 and insure medial division plane position (Moseley, et al., 2009). In cells lacking Pom1, Cdr2 spreads toward the non-growing tip (Martin and Berthelot-Grosjean, 2011). Mid1 distribution follows that of Cdr2, which results in mispositioned septa (Celton-Morizur, et al., 2006; Moseley, et al., 2009).

Cdr2 deletion partially rescues the division plane position defects seen in *pom1Δ* cells despite the presence of morphological defects seen in double deletion mutants (Lee and Wu, 2012). This may be due to Mid1's nuclear pool being restored, allowing for nuclear position to provide medial division. Cdr2 is a phosphorylation target of Pom1 *in vitro* (Martin and Berthelot-Grosjean, 2011) and Cdr2 is hyperphosphorylated *in vivo* when Pom1 is overexpressed (Moseley, et al., 2009). Therefore, the protein interactions in Type I nodes are tightly regulated through phosphorylation events, which in turn have an effect on Mid1's localization and ability to anchor the CAR correctly.

Type II nodes have a different composition of proteins during interphase, including Blt1 (another scaffolding protein), Gef2 (a putative Rho-GEF guanine exchange factor), and Nod1 (a Gef2-related protein; Zhu, et al., 2013). Type II nodes arise from the previous contractile ring remnants on the new end (NE, Figure 3) of the

cell and diffuse back to the center where the stationary Mid1-containing Type I nodes capture them in mid to late G2 (Akamatsu, et al., 2014).

In late G2, Type II nodes complete their migration to the cortex and Mid1 facilitates recruitment of key CAR components (Wu, et al., 2006; Laporte, et al., 2011). This singles out Mid1 as the only protein that is a component of both types of nodes. The remaining nuclear Mid1 is exported from the nucleus into the cytoplasm in late G2 just prior to mitosis (Bähler, et al., 1998). Mid1 contains one nuclear localization sequence (aa691-695), a second, longer region associated with nuclear localization that does not contain an NLS (aa450-506), and two nuclear export sequences (NES, aa69-81 and aa763-773) to modulate nuclear shuttling (Paoletti and Chang, 2000).

As Mid1 is exported from the nucleus and becomes associated with the nodes, it serves as a spatial cue for CAR recruitment (Almonacid, et al., 2009). Cdr2 binds Mid1 at the cell cortex (Almonacid et al, 2009) and then gradually dissociates from the nodes and becomes cytoplasmic (Akamatsu, et al., 2014). Polo-like kinase Plo1 exhibits phosphorylation-dependent control over Mid1's nuclear export through a possible modulation of Mid1's NES (Almonacid, et al., 2011). The cytokinetic nodes coalesce into the CAR when IQGAP protein (actin-binding) Rng2, Myosin II, Rlc1 (myosin regulatory light chain), Cdc4 (myosin essential light chain), Cdc12 (formin), and Cdc15 (actin regulator) function together to initiate actin filamentation and bundling (Laporte, et al., 2012).

1.4 Sid2 and the Septation Initiation Network

At the onset of ring constriction, Mid1 dissociates from the ring and is shuttled back to the nucleus (Sohrmann, et al., 1996) while the rest of the ring components facilitate separation through the Septation Initiation Network (SIN) (Krapp, et al., 2004). The SIN is a GTPase- mediated signaling cascade (Figure 4) that triggers the onset of cell cleavage and begins after the chromosomes have separated and the nucleus has divided (McCollum and Gould, 2001). Septation in *S. pombe* requires the synthesis of a new cell wall, which is formed by a tri-layer division septum deposited behind the CAR as it is constricting. This septum is composed primarily of α and $\beta(1,3)$ glucans and is formed by at least 3 glucan synthases, whose catalytic subunits are composed of Bgs1, Bgs4, and Ags1 (Humbel, et al., 2001). Outward turgor pressure, in combination with secreted glucanases to degrade the septum, contribute to the rounding and separation of each new daughter cell's new ends (Cortés, et al., 2012).

In *S. pombe*, the SIN is analogous to the MEN (Mitotic Exit Network) in the budding yeast *Saccharomyces cerevisiae* and the Hippo pathway in humans, which functions in cell growth and proliferation (Hergovich and Hemmings, 2012). It has been shown that LATS1, the human Sid2 homolog, functions as a tumor suppressor by inactivating a proto-oncogene (Hao, et al., 2008; Visser and Yang, 2010) and that deletion of LATS1/2 has a role in tumor growth (Moroishi, et al., 2016).

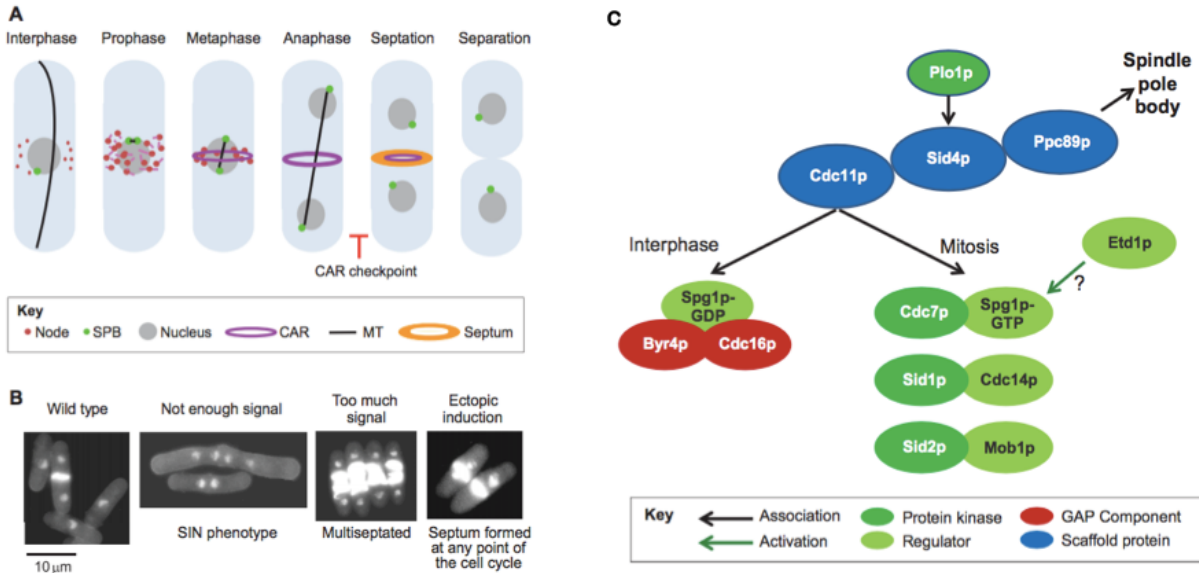


Figure 4. *S. pombe* cytokinesis, Septation Initiation Network (SIN) phenotypes, and the SIN cascade. (A) Schematic representation of cell division in *S. pombe*. In interphase, bundles of microtubules (MT) span the length of the cell to position the nucleus medially; for clarity a single MT bundle is shown. During interphase Mid1 is localized mainly in the nucleus, with a subset found at the cell cortex (nodes). Following entry into mitosis, a spindle is formed and chromosomes are aligned and attached to opposite SPBs. Mid1 is exported from the nucleus, and associates with the nodes, together with other CAR components. These condense together to form the CAR, which contracts at the end of mitosis, guiding septum synthesis. (B) The phenotypic effects of different levels of SIN signaling. Cells were stained with DAPI for DNA and Calcofluor for the septum; original images from Simanis, 2003. Wild-type cells contain a single, medially placed septum. If the SIN does not signal, cells become elongated and multinucleated, whereas the cell becomes multiseptated if SIN signaling is constitutively activated. (C) Protein kinases required for signaling are shown in dark green, with their respective regulatory subunits shown in light green. Scaffolding proteins are shown in blue. Etd1 activates Spg1 through an unknown positive regulatory mechanism. Byr4 and Cdc16 are shown in red to represent their negative regulatory function. Adapted from Simanis, 2015.

As mentioned previously, Mid1's proper placement is required during cytokinesis, and is tied in closely with SIN signaling to initiate correct division plane location and CAR synthesis (Figure 4A; Paoletti and Chang, 2000). *mid1* Δ mutants form ectopic CARs during anaphase when the SIN becomes active (as in Figure 4B), which reinforces Mid1's importance in directing CAR assembly at the right place (Chang, et al., 1996; Sohrmann, et al., 1996). Inactive SIN mutants form a CAR in early mitosis that dissipates in anaphase, which suggests that SIN signaling is required in late mitosis for CAR assembly and maintenance (Balasubramanian, et al., 1998).

SIN signaling originates from the spindle pole bodies (SPBs) to regulate the onset on cytokinesis and septation (Johnson, et al., 2012; Sparks, et al., 1999). The spindle pole bodies are the main microtubule-organizing center (MTOC) in yeast and are analogous to centrosomes in animal cells. SPBs delineate the mitotic spindle and bipolar chromosome segregation to both daughter cells during telophase in cell division.

Scaffolding proteins Sid4 and Cdc11 function together (Figure 4C) to assemble the other SIN components at the SPBs (Chang and Gould, 2000). Byr4 and Cdc16 are partners in a GTPase-activating protein (GAP) complex that negatively regulates GTPase Spg1 at the top of the SIN cascade (Figure 4C; Fankhauser, et al., 1993; Song, et al., 1996; Furge, et al., 1998; Balasubramanian, et al., 1998). Inactivation of Byr4 or Cdc16 results in hyperactive SIN signaling, multiseptated cells, and decoupling of cytokinesis from the rest of the cell cycle (Minet, et al., 1979). In contrast, the cytokinetic failure that results from insufficient SIN signaling causes elongated multinucleate cells, the morphology of which is typically referred to as the SIN phenotype (Figure 4B; Nurse, et al., 1976).

During interphase, kinases Cdk1 and Plo1 (Figure 4C) phosphorylate Byr4 to inhibit GAP activity, which activates the SIN (Rachfall, et al., 2012). Spg1 activation during mitosis by Etd1 (Ethanol-dependent mutant protein 1) sets forth a cascade of three kinases - PAK-related GC kinase Sid1, and serine/threonine NDR (AGC) kinases Sid2 and Cdc7 (Krapp and Simanis, 2008). Etd1 is thought to act as a tie between the CAR and the SIN, and is required for localization of SIN kinases to the SPB and CAR in anaphase (Daga, et al., 2005).

During anaphase when Cdk1 activity is low, Sid1 gathers asymmetrically on the SPBs to activate Sid2 (Guertin, et al., 2000; Sparks, et al., 1999). Sid2 and its activator and binding partner, Mob1, then move to the CAR and initiate constriction (Hou, et al., 2004 and Sparks et al, 1999). Plo1 transiently associates with the CAR early in mitosis (Bähler et al., 1998), while Sid2-Mob1 associate with the CAR in mid-late anaphase (Hou, et al., 2000). It is worth noting that Plo1 regulates both Mid1 and the SIN (Almonacid, et al., 2011; Mulvihill and Hyams, 2002) and that Plo1 is thought to regulate SIN-mediated CAR formation in the absence of Mid1 (Roberts-Galbraith and Gould, 2008). The Sid2-Mob1 kinase complex is thought to transmit the cell division signal from the SPB to the CAR, since it accumulates at the division site immediately prior to cytokinesis (Hou, et al., 2003 and Sparks, et al., 2009). In mutants where both Mid1 and SIN function are compromised, no CAR will form (Hachet and Simanis, 2008).

In fission yeast, Sid2 is the terminal kinase of the SIN (Sparks, et al., 1999) and like other NDR kinase family members, phosphorylates conserved sites containing a consensus RXXpS sequence (Mah, et al., 2005). In SIN-hyperactive mutants, Type I

nodes dispersed from the cell cortex earlier than normal, which is suggestive of SIN-mediated control over the assembly of Type I nodes (Pu, Akamatsu, and Pollard, 2015).

Sid2 plays a role in Cdr2 dissociating from the Type I nodes during interphase before CAR assembly (Rincon, et al., 2017). This precedes Mid1's separation from the fully assembled CAR in late anaphase, at CAR constriction onset. Unpublished data from the Hart lab at GVSU has shown that Sid2 also phosphorylates Mid1 (DeWitt, Gould, and Hart; article in progress), which could play a role in Mid1's dissociation from the CAR after mitosis.

The localization of Mid1 in SIN mutants (Figure 5) shows that when the SIN is hyperactive, as in the *cdc16-116* mutant strain, Mid1-GFP is localized in the nucleus, which suggests that hyperphosphorylation of Mid1-GFP results in a higher fraction of Mid1-GFP shuttling back to the nucleus, or that Sid2 phosphorylation is required for nuclear export. In inactivated SIN mutants such as *sid2-250*, (Figure 5), Mid1-GFP appears to be stuck at nodes and unable to organize the CAR for constriction initiation. Both major pathways that regulate division plane positioning, the CGN - through Cdr2 interacting with Mid1 in Type I nodes - and the SIN - through the SIN's terminal kinase, Sid2, phosphorylating Cdr2 (Rincon, et al., 2017) and Mid1 (DeWitt, Gould, and Hart; article in progress) - converge with Mid1 (Rincon and Paoletti, 2012).

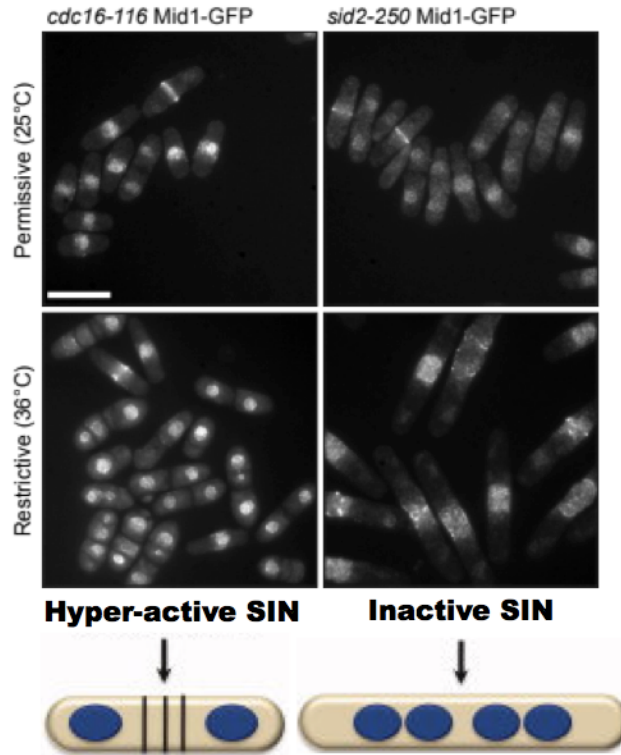


Figure 5. Mid1 localization in SIN mutant phenotypes. In hyperactive SIN strain *cdc16-116*, Mid1-GFP remains nuclear and multiple septa are formed, with an absence of Mid1-GFP at the CAR. In SIN inactive strain *sid2-250*, Mid1-GFP is stuck at nodes and CAR is not able to form. Scale Bar = 10 μ m.

From DeWitt, Gould, and Hart, article in progress; and Johnson, et al., 2012.

1.5 14-3-3 Proteins and Cell Cycle Checkpoints

Cytokinesis proceeds through tightly controlled mechanisms that ensure proper chromosome segregation. The cell cycle is regulated by cyclin-dependent serine/threonine kinases (CDKs) with checkpoints at G1, G2/M (G2 to mitosis transition), and M (metaphase) (Barnum and O'Connell, 2014). CDKs bind to regulatory proteins known as cyclins, and CDK-cyclin complexes regulate downstream targets in cell cycle progression. The M regulatory checkpoint, also known as the spindle or cytokinesis checkpoint, is a mechanism that can halt cell division in metaphase to

prevent cytokinesis until chromosome separation has correctly occurred in anaphase (CAR checkpoint, Figure 5A). The M checkpoint was discovered through a study of $\beta(1,3)$ glucan synthase catalytic subunit mutant *bgs1* (Le Goff, et al., 1999). Some *bgs1* mutants fail to form septa even though they are able to complete mitosis. The *bgs1* cells arrest with an interphase microtubule configuration, with nuclei centered in what would be the two daughter cells (Liu, et al., 2000). Each nuclei in these cells are able to go through S phase, but the nuclei are stalled in G2 and are unable to continue through the M phase, even though the CAR has formed. This is indicative that a failure to complete some aspect of cytokinesis prevents cell cycle progression though mitosis.

In eukaryotic cells, 14-3-3 proteins are highly conserved regulatory molecules that have a variety of ligands including kinases, phosphatases, and transmembrane receptors (Hermeking and Benzinger, 2006; for review). 14-3-3 proteins have also been previously shown to be involved in cell cycle checkpoints (Ford, et al., 1994). In *S. pombe*, Rad24 is a 14-3-3 protein implicated in correct cell cycle checkpoint progression through its binding to a phosphorylated cyclin-dependent phosphatase Cdc25 (Zeng and Piwnica-Worms, 1999). Both replication checkpoint kinases Cds1 and Chk1 kinases regulate the binding of Cdc25 to 14-3-3 proteins as part of the checkpoint response to unreplicated DNA (Zeng, et al., 1998). Chk1 functions redundantly with the kinase Cds1 at the replication checkpoint and both kinases phosphorylate Cdc25 on the same sites, which include serine residues at positions 99, 192 and 359. Mutation of these residues reduces binding of Rad24 to Cdc25 *in vitro* and disrupts the replication checkpoint *in vivo* (Zeng, et al., 1998). Rad24 and other 14-3-3-proteins bind to the phosphorylated Sid2 consensus sequence, RXXpS (Muslin, et al., 1996) in an amphipathic binding cleft.

Potential Sid2 targets were previously identified by comparing proteins that associate with Rad24 when the SIN is turned on or off, revealing coordination between mechanisms of the SIN and the other conserved NDR kinase pathway in *S. pombe*, the MOR pathway (Gupta, et al., 2013). While 14-3-3 proteins were first identified for their role as checkpoint regulators, they interact with binding partners at all stages of cell division, and play diverse regulatory roles.

1.6 Previous work with Sid2 Phosphomutants

In addition to scaffolding the CAR precursors, Mid1 has been shown to interact with Clp1 (Clifford, et al., 2008), a phosphatase and regulator of mitotic exit in *S. pombe* (Chen, et al., 2008). Clp1 dephosphorylates substrates of cyclin-dependent kinase (Wolfe, et al., 2006), and is regulated in part through its localization during the cell cycle (Chen, et al., 2008). Previous research has shown that Sid2 phosphorylation provides a binding site for Rad24, which sequesters Clp1, to the cytoplasm during mitosis (Mishra, et al., 2005). Mutation of six serines in the Sid2 phosphorylation sites to alanine disrupted Rad24 binding, and resulted in Clp1 returning to the nucleus prematurely when compared to wild-type cells (Chen, et al., 2008). This work demonstrated that Sid2 phosphorylation is required for Rad24 to bind to Clp1, and Rad24 is necessary for temporal regulation of CAR assembly and constriction during cytokinesis (Chen, et al., 2008).

Another target of the SIN, the formin Cdc12, is present in the CAR. Sid2 phosphorylation is needed for initiation of actin bundling by Cdc12 during CAR assembly (Bohnert, et al., 2013), and the mutation of phosphorylation sites on Cdc12

results in impaired CAR formation. Actin regulator Cdc15 also requires SIN function to associate with the CAR (Hatchet and Simanis, 2008), although it is unknown whether Sid2 phosphorylates Cdc15 directly. However, there have been 13 RXXS sites identified on Cdc15 that could bind Rad24 even if Sid2 is not the kinase involved (Roberts-Galbraith, et al., 2010). It is highly likely that there may be other targets of SIN function, or Rad24 binding partners, located in the CAR.

A recent study revealed that Rad24 interacts with Cdr2 upon Sid2 phosphorylation and sequesters Cdr2 in the cytoplasm during cell division, and that Cdr2^{RXXS-2A} phosphomutants demonstrated a reduced interaction with Rad24 (Rincon, et al., 2017). This study also showed that in *rad24Δ* cells, Cdr2-mEGFP did not leave the cell cortex during mitosis, was redistributed from the medial cortex toward the cell tips, and that intensity of Cdr2-mEGFP did not increase in the cytoplasm during mitosis. It instead diminished similarly to Cdr2^{RXXS-2A}-mEGFP on the medial cortex due to lateral spreading toward cell tips (Rincon, et al., 2017), confirming that Cdr2 localization is specifically dependent on Sid2 phosphorylation and Rad24 binding.

Previous research has also shown that Cdr2 anchors Mid1 at the cortex through interaction with a sequence in the midpoint of Mid1 (aa400-450) (Almonacid, et al., 2009), a region of the Mid1 protein that is also where the Sid2 phosphorylation sites are located. Sid2 phosphorylates Cdr2 at Rad24 consensus binding sites to release it from the cell cortex in a 14-3-3-dependent manner (Rincon, et al., 2017). Cdr2 association with Rad24 re-localizes it to the cytoplasm and resets the division plane for the next round of cytokinesis (Rincon, et al., 2017).

An unpublished study (DeWitt A, Schneider P, Foxa G, Gould K, and Hart D; article in progress) also determined that Sid2 phosphorylation might modulate binding of Importin1 (Imp1), which facilitates Mid1's re-localization to the nucleus. To test the importance of Sid2 phosphorylation on Mid1, a Mid1^{4RXXSA} phosphomutant cell line was generated with serine mutated to alanine in four Sid2 phosphorylation sites (S329, S432, S464, and S531). When Sid2 phosphorylation is diminished, Mid1^{4RXXSA} concentrates in the nodes during interphase and remains cytoplasmic during CAR constriction instead of migrating back to the nucleus (Figure 6, panel A2). Mid1^{4RXXSA} could potentially be stabilized at the nodes due to the NLS near the amphipathic helix being buried inside the plasma membrane and obscured from Imp1 (DeWitt A, Schneider P, Foxa G, Gould K, and Hart D). Mid1^{4RXXSA} phosphomutants also began cytokinetic events much earlier than WT, and exhibited CAR formation defects (DeWitt A, Schneider P, Foxa G, Gould K, and Hart D; data not shown). Mid1 depends on Sid2 phosphorylation for dispersal from the division site and nodes, but further elucidation is needed to show how Mid1 is retained in the cytoplasm until mitotic exit.

1.7 Role of Rad24 binding in Mid1 localization

Sid2 phosphorylation could also be important in placing Mid1 at key locations during the cell cycle by other means. Rad24 and Mid1 were isolated together in tandem-affinity purification and are known to interact through an unknown mechanism. Sid2 phosphorylation could facilitate direct binding of Rad24 to Mid1, sequestering it in the cytoplasm until the CAR has properly formed, to ensure that cytokinesis is temporally regulated. Rad24 could also stabilize Mid1 oligomers, as there is evidence that only the

monomeric form of Mid1 can be imported to the nucleus (Sun, et al., 2015). Additionally, Rad24 and Imp1 could compete to bind Mid1, creating distinct populations of Mid1 with either Rad24 or Imp1 bound, sending Mid1 to different sites in the cell during division.

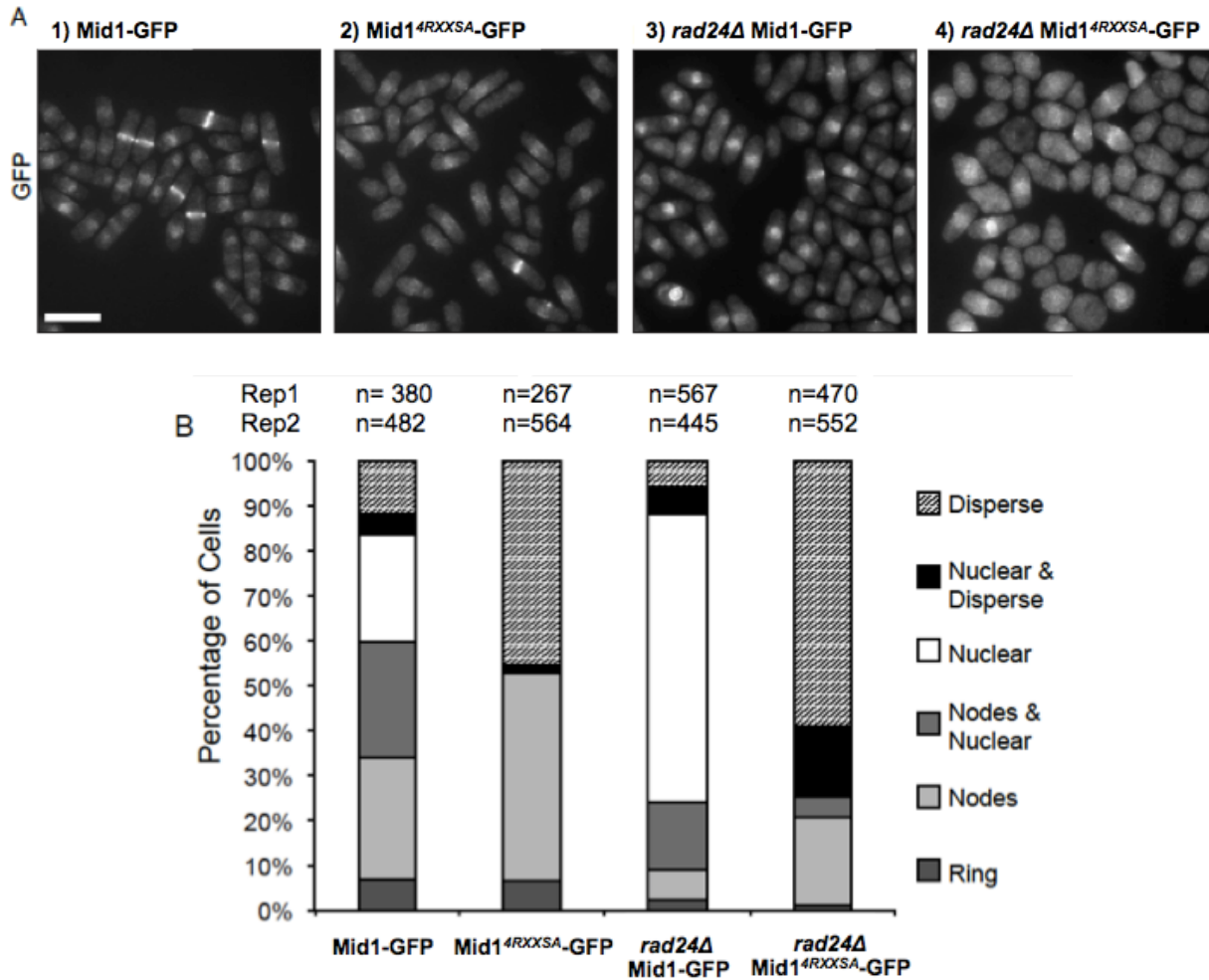


Figure 6. Mid1 in phosphomutant and *rad24Δ* cells: Mid1 shows higher localization to the nucleus in cells lacking *rad24*. (A) Mid1-GFP and Mid1^{4RXXSA}-GFP localization in *rad24*-deleted cells. WT Mid1-GFP cells show a clear Mid1-containing CAR. Mid1^{4RXXSA}-GFP is localized to cortical nodes. *rad24*-deleted cells show a concentration of Mid1 in the nucleus. *rad24Δ* Mid1^{4RXXSA}-GFP mutants show a cytoplasmic dispersion of Mid1. (B) Mid1 locations in the averaged percentage of cells counted within the corresponding cell types from two experimental replicates.

Ashley DeWitt and Dawn Clifford Hart, unpublished. Scale bar = 10 μ m.

These functions are, in effect, switched in Mid1^{4RXXSA} phosphomutant. In preliminary unpublished analysis of *rad24Δ* cells, Mid1-GFP accumulates in the nucleus (Figure 6 panel A3). Mid1^{4RXXSA}-GFP is localized to the cytoplasm, specifically the

nodes and cortex, when Imp1 fails to bind as compared to Mid1-GFP nuclear concentration when there is no *rad24* (Figure 6, panel A2 vs. panel A3). We hypothesize that the phenotype in Figure 6, panel A4 is due to both reduced Sid2 phosphorylation and the absence of *rad24* disrupting both nuclear import and Mid1-GFP (and Mid1^{4RXXSA}-GFP) localization, leading to overall cytoplasmic dispersion of Mid1. The lack of *rad24* may allow Mid1 to be returned to the nucleus early even though Sid2 has phosphorylated it, so perhaps this is due to increased Imp1 binding with no Rad24 to compete.

During interphase Mid1^{4RXXSA}-GFP remains only in the nodes, instead of in both the nucleus and nodes (Figure 6, panel A2). Double *rad24*Δ Mid1^{4RXXSA}-GFP mutants show an overall cytoplasmic dispersion of Mid1, which suggests that Sid2 phosphorylation plays a role in nuclear localization as well as Rad24 binding (Figure 6, panel A4). These data suggest a compelling role for Rad24 binding in Mid1 localization, through either an indirect or direct interaction between Mid1 and Rad24, and that Rad24 could play a role in transitioning Mid1 through its various oligomerization states.

1.8 Mid1 Structure and Oligomerization

A recent structural study (Sun, et al., 2015) revealed that both anillin and Mid1 contain a C2 domain, a β-sandwich composed of 8 β-strands (PFAM ID #PF00168). C2 domains are involved in targeting proteins to cell membranes, usually in a Ca²⁺ - dependent manner (Ponting and Parker, 1996). Anillin requires a Rho (Ras homolog) GTPase called RhoA (Figure 7A) for anchorage to phosphatidylinositol 4,5-bisphosphate (PI(4/5)P₂), a phospholipid component of the plasma membrane (Liu, et

al., 2012; Oegema, et al., 2000). RhoA is activated by Ect2, a guanine nucleotide exchange factor (RhoGEF) (Tatsumoto, et al., 1999). RhoA, together with a long disordered loop (aa 888-933) between $\beta 5$ and $\beta 6$ strands of the C2 domain, act synergistically with the PH (Pleckstrin Homology) domain to bind anillin in place (Sun, et al., 2015). C2 domains typically contain three Ca^{2+} -binding specific loops, and anillin's long disordered loop corresponds to the third Ca^{2+} -binding loop (L3) of a typical C2 domain (Malmberg, et al., 2003; Figure 7A, orange dotted line). However, Ca^{2+} did not promote anillin to bind to lipids, and deletion of this loop abolished the lipid binding ability altogether (Sun, et al., 2015). Targeting to PI(4/5)P2 may be mediated by eight positively charged and four hydrophobic residues within this loop rather than Ca^{2+} , indicative that anillin's C2 domain lacks Ca^{2+} binding ability in (Sun, et al., 2015).

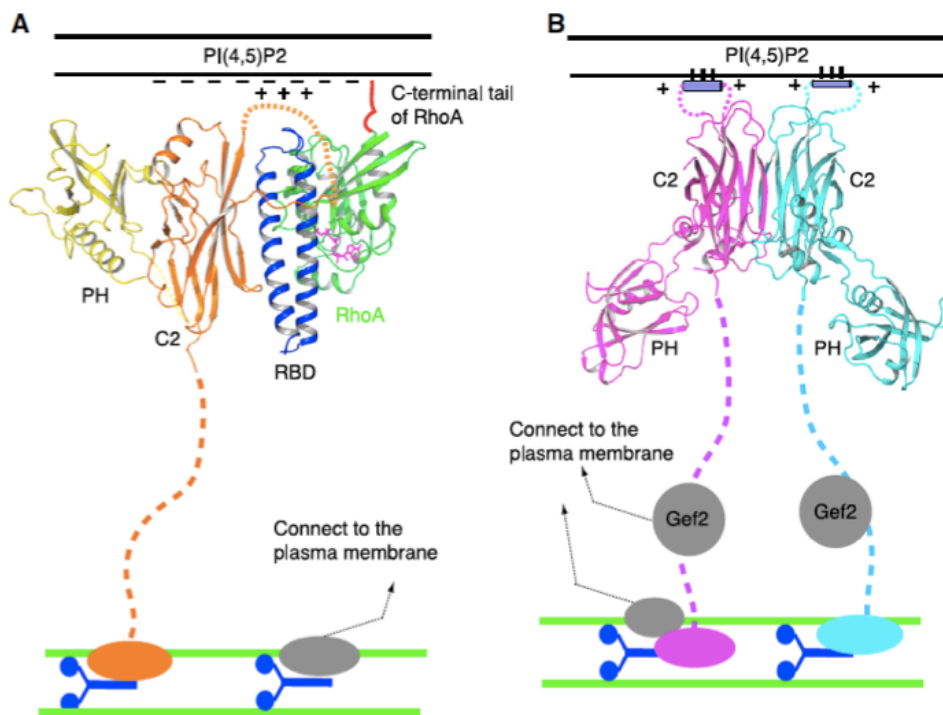


Figure 7. Protein structures of Anillin and Mid1.

(A) RhoA, the C2 domain, and the PH domain of Anillin act synergistically to bind PI(4,5)P2 in the plasma membrane (PDB ID # 4XOI). (B) Mid1 dimerizes by interactions between C2 domains while the L3 loop of the C2 domain binds to PI(4,5)P2 in the plasma membrane. Mid1 N-terminus is anchored to the plasma membrane further via Gef2 (PDB ID # 4XOH). From Sun, et al., 2015.

In *S. pombe*, GTPase is not required to tether Mid1 to the plasma membrane, so there is no Rho Binding Domain (RBD), and deletion of the PH domain does not disrupt normal cytokinesis (Lee and Wu, 2012). Instead, Mid1 dimerizes at the C2 domain (Figure 7B) to enhance binding to PI(4/5)P₂ as Gef2 facilitates placement at the division plane by interacting with Mid1's N-terminus (Ye, et al., 2012).

The N-terminal portion of anillin binds myosin II and IQGAP protein Rng2 (Eng, et al., 1998). A hybrid protein expressing the N-terminal portion of Mid1 and the C-terminal portion of anillin rescued the cytokinetic defects of anillin deletion. This, in addition to C2 domain membrane anchorage and the presence of PH domains, suggests that Mid1 and anillin evolved from a common ancestor and are homologous proteins (Sun, et al., 2015). The connector domain (Figure 8A, shown in red), not present in anillin, serves to attach both termini of the PH domain and pack them against the C2 domain (Sun, et al., 2015).

The amphipathic L3 loop (RKFFDKLF, aa 681-688) of the C2 domain (Figure 8A) stabilized by a nearby NLS (aa 691-695), anchors Mid1 to the cell membrane at the cortex (Figure 8C; Celton-Morizur, et al., 2004). It has been previously predicted that the Mid1 C2 domain L3 loop contains an amphipathic helix (shown in 8A and 8C), which, when bound to the cell membrane, obscures the NLS sequence to prohibit Mid1 nuclear accumulation (Celton-Morizur, et al., 2004). It is important to note that this amphipathic L3 loop (aa 681-709) was deleted from the protein to allow for crystallization (Sun, et al., 2015) so whether this region's architecture is a loop or helix remains unknown.

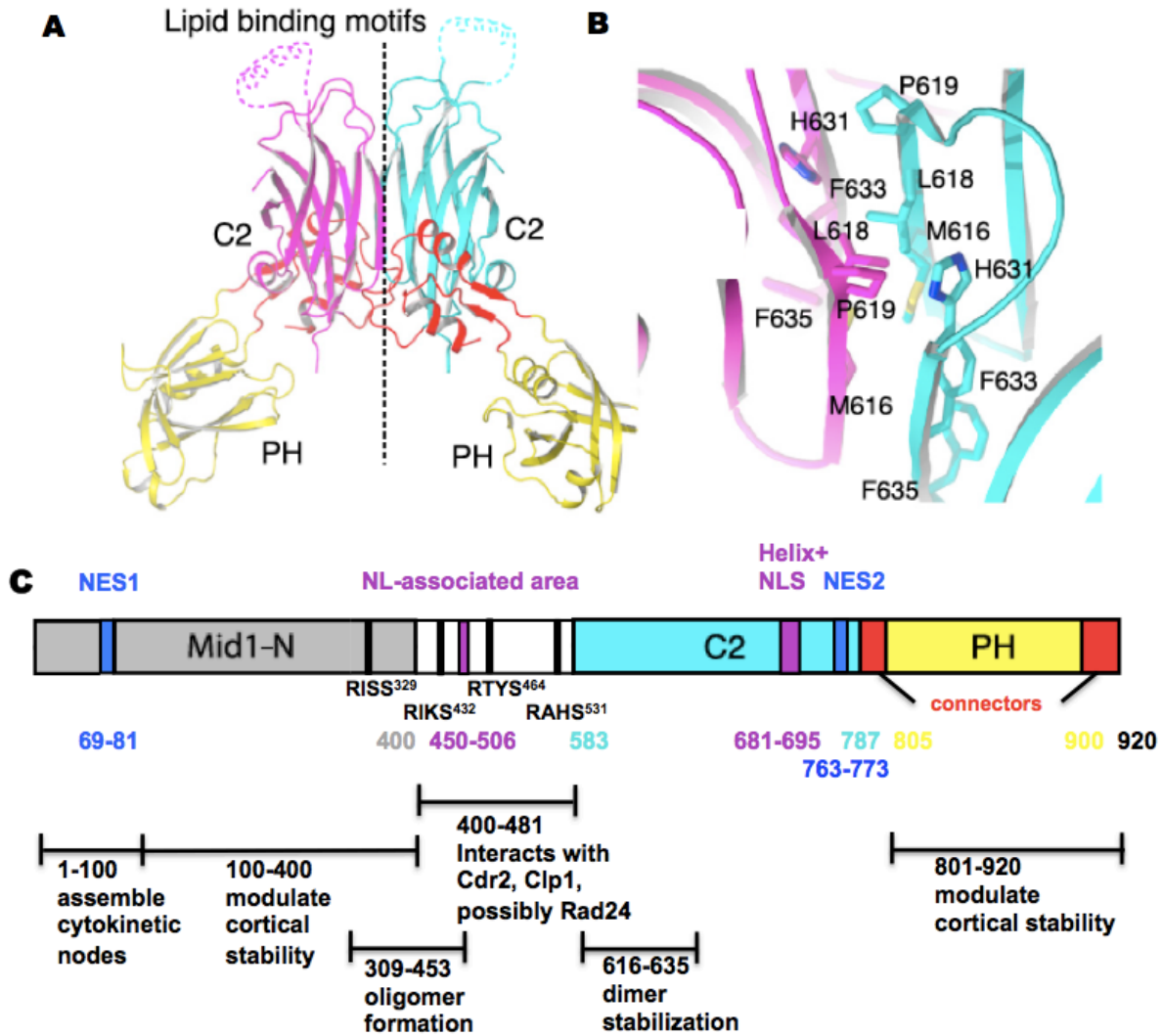


Figure 8. Mid1 dimerization interface and protein domain schematic.

(A) Interaction interface between C2 domains in Mid1. Dimers form through hydrogen bonds along the β_3 and β_4 strands. (B) Close up of additional hydrophobic contacts stabilizing the Mid1 dimer. (C) Schematic of Mid1 domains and their functions. Adapted from Sun, et al., 2015 and DeWitt A, Gould K, and Hart D.

Dimerization through the C2 domain is not common in other C2 domain containing proteins, including anillin (Nalefski, et al., 2001). Crystal structures of Mid1 (PDB ID# 4XOH) show almost identical interfaces on the C2 domain where dimerization occurs. The interaction between C2 interfaces occurs mainly through hydrogen bonding on main chains between the β_3 and β_4 strands, but dimer stability is enhanced by

hydrophobic contacts in the β 4 strand (Figure 8B). Dimerization in this way results in two amphipathic L3 loops anchoring Mid1 to the plasma membrane (Sun, et al., 2015).

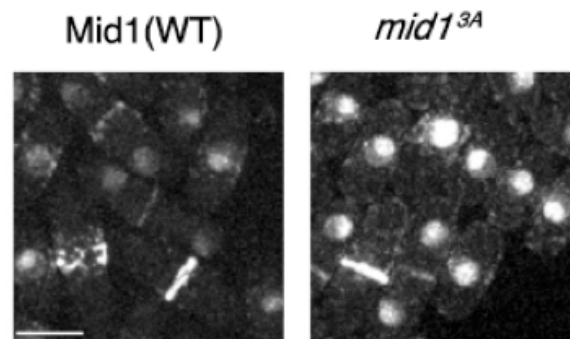


Figure 9. Dimerization of Mid1 is important for localization. Monomeric (*mid1*^{3A}) remains nuclear during interphase and if cytoplasmic, does not remain concentrated in the medial region where PI(4/5)P2 would be concentrated. In contrast, WT Mid1 localizes to the medial region (nodes) of the cell during interphase. From Sun, et al., 2015.

Analysis of cells expressing a mutant monomeric *mid1*^{3A}, in which Met616, Leu618, and Pro619 in the dimerization interface were mutated to alanine, shows that dimerization is needed for Mid1 to concentrate at the cell cortex during cytokinesis. During interphase, monomeric *mid1*^{3A} remained localized in the nucleus even though the CAR positioning and morphology was normal, and cytokinesis proceeded accordingly (Sun, et al., 2015; Figure 9, right). This could be because of redundant pathways involved in cell division or maybe that there was enough Mid1 present, or monomeric *mid1*^{3A} binding was sufficient, to tether the CAR. In contrast, WT Mid1 localized to the cell cortex and nodes during interphase (Figure 9, left). Monomeric *mid1*^{3A} was shown to have a low affinity for PI(4/5)P2. When both Mid1's interaction with the plasma membrane and its dimerization ability were disrupted by creating double *mid1*^{3A} *gef2* Δ mutants, strong CAR placement defects and septation difficulties were observed, suggesting that dimerization of Mid1 enhances affinity for PI(4/5)P2 (Sun, et al., 2015). Interestingly, PI(4/5)P2 has been previously shown to be enriched at

the cell division site (Zhang, et al., 2000), and its location there may help recruit extra-nuclear Mid1 to the division plane.

If dimerization of Mid1 increases affinity to PI(4,5)P2 and obscures the nuclear localization sequence (NLS) sequence (Sun, et al., 2015; Celton-Morizur, et al., 2004), then the decreased affinity of monomeric Mid1 for PI(4,5)P2 could make the NLS more available and could contribute to Mid1's accumulation in the nucleus in mutant *mid1*^{3A} cells. Since *mid1*^{3A} concentrates in the nucleus and we know this mutant fails to oligomerize, and we see the same phenotype in *rad24*-deleted cells, Rad24 may be playing a role in dimerization or stability of Mid1 conformation that retains Mid1 in the cytoplasm. Changes in Mid1 oligomeric status may also be impeded without Sid2 phosphorylation. While the various phosphorylation effects seen on Mid1 seem like opposite problems that lead to the same effect on the CAR, maybe neither *mid1*^{3A} or *mid1*^{4RXXSA} can transition through the needed oligomerization states. Rlc1 was recruited to the CAR early in *mid1*^{4RXXSA} mutant cells, and this contributed to impairment of CAR assembly, disordered CAR structures, and accelerated CAR constriction (DeWitt A, Gould K, and Hart D; article in progress).

Interestingly, CAR assembly was also faster in cells expressing monomeric *mid1*^{3A} than in wild-type cells (Sun, et al., 2015), but rates of CAR constriction were the same. There are definite phenotypic similarities seen between the monomeric *mid1*^{3A} and *rad24*-deleted cells.

Although the proteins and sequence of events involved in the cell cycle of fission yeast are well documented, the temporal and spatial details governing cell division are not well understood. Characterizing Mid1's interaction with Rad24 could possibly

connect oligomer stability of Mid1 to Rad24 binding. The Sid2 phosphorylation sites are in a central area of Mid1 that is known to oligomerize (aa309-453; Celton-Morizur, et al., 2004), rather than in the now-known dimerization site of the C2 domain (aa616-635). Mid1^{4RXXSA} phosphomutants could be demonstrating weakened dimerization due to Rad24 binding failure. Mid1 dimerization or octomerization could partially account for stabilization at the cell cortex during cytokinesis, as monomeric Mid1 is localized in the nucleus (Sun, et al., 2015). Similar results were obtained in our preliminary data with *rad24Δ* cells.

1.9 Hypothesis

Since Mid1 is known to form at least dimers (Sun, et al., 2015), and was shown to form octomers in sedimentation studies (Saha and Pollard, 2012b), it may be possible that Rad24 could stabilize Mid1 oligomers. There may be several “stages” of oligomerization that Mid1 passes through - nuclear Mid1 may be only monomeric, Mid1 dimers could provide enough stabilization for node formation at the cell membrane, and the higher orders of Mid1 oligomerization could occur during CAR assembly and maturation, where additional stability would be required to bolster scaffolding. Mid1 oligomerization in this capacity would also require a “disassembly” mechanism to disassociate Mid1 oligomers from the CAR during constriction when/where it is no longer needed. This would help explain why in *rad24Δ mid1^{4RXXSA}-GFP* double mutant cells, Mid1^{4RXXSA}-GFP is not binding to the nodes or being returned to the nucleus. Sid2 phosphorylation sites are located in the same region of Mid1 as oligomerization occurs,

which could relate to the Sid2 phosphorylation required for Mid1 to disperse from the division site.

We hypothesize that phosphorylation allows the NLS to become available and that Rad24 may play a role in oligomerization. In order to shed light on Rad24's involvement in this process and how it could sequester Mid1 in the cytoplasm, the focus of this thesis is to clarify the nature of Rad24 and Mid1's interaction. We hypothesize that this interaction could be direct, indirect, preferential to oligomers, and/or competitive with nuclear import proteins.

- 1) Direct, such as a change in the Mid1 oligomer conformation when Rad24 binds, or perhaps Rad24 favors binding to particular oligomer conformations.
- 2) Indirect, Rad24 and Mid1 could interact via a third party connector protein.
- 3) Rad24 binding preferentially to Mid1 oligomers could shift equilibrium towards oligomers and in effect reduce Mid1's translocation to the nucleus.
- 4) Rad24 could compete for the same binding pocket as Importin 1, which would also reduce Mid1's translocation to the nucleus.

2 Methods

2.1 Strains and Media

The *S. pombe* strains used in this study were grown in YE media, at 18°C, 25°C, or 32°C according to strain growth specifications. *S. pombe* yeast strains containing fluorescently tagged Mid1 (Mid1-GFP or Mid1-NeonGreen), F-Actin (LifeAct-GFP), and myosin regulatory light chain (Rlc1-tomato) were crossed into existing *rad24*-delete strains. New yeast strain crosses were created by random spore analysis. A toothpick was used to collect cells from the two strains containing tagged loci, one from each mating type, h^- and h^+ . The cells were mixed together in 5µl sterile water on the same glutamate (E) plate in a 1cm² area. The *S. pombe* sporulation and mating phase can only be induced under nutrient starved conditions. Glutamate (E) plates lack nitrogen and contain 1g/L of sodium glutamate. Newly formed zygotes enter meiosis immediately and sporulate, producing four spores in a tetrad ascus. Crosses were incubated at 25°C for 4 days on E plates until growth was evident, then examined for tetrads under light microscopy. Zygotic asci (diploid produced through conjugation of two mating types) can be distinguished from azygotic asci (sporulation of a heterozygous diploid strain) by the curvature of the ascus and separation of the spores.

Because mating and meiosis are linked in *S. pombe*, random spore analysis does not require isolation of a diploid. Vegetative cells were killed off by mixing 500 µl of sterile water, a pipette tip full of cells from the mating E plate, and 10 µl of glusulase (a snail gut enzyme). The cells were incubated overnight at 25°C in a shaking incubator, then washed with 30% ethanol and sterile water. A 1:1000 dilution was plated on a

standard YE plate and incubated at 25°C, and new yeast strains were replica plated on selective media plates once colonies formed.

To select only colonies that are unable to express Rad24, mutant *rad24*Δ strains were engineered to express uracil in place of Rad24 (*rad24::ura4* mutation). After sporulation of new strains, cells were plated on MAL selective plates. MAL is minimal media containing leucine and adenine, but no uracil. Only colonies able to produce uracil in place of Rad24 will be able to grow on selective MAL plates. Other tagged loci co-express a kanamycin or nourseothrycin resistance gene, and strains containing these loci were additionally plated on G418 or NTC (nourseothrycin N-acetyl transferase) plates for selection. The LifeAct-GFP strain co-expresses leucine (LifeAct-GFP:Leu mutation) and these strains were additionally selectively plated on MAU – minimal media containing adenine and uracil, but no leucine, and only colonies able to grow on both MAU and MAL separately were selected for use in this study.

Genotypes were confirmed by whole-cell PCR with primers specific to particular tags or genes of interest (Table 1), or by visual confirmation using the confocal microscope. For whole-cell PCR, a toothpick was used to pick a colony from new strains, and added to 20µl master mix containing primers, GoTaq polymerase MasterMix (Promega, #M7122), and sterile water. PCR program details are as follows: Lid, Hold at 105°C; 1-95°C 10 min.; 2-95°C 45 sec.; 3-60°C 1 min.; 4-72°C 1 min.; 5-Go to 2 repeat 11X; 6-95°C 45 sec.; 7-50°C 45 sec.; 8-72°C 1 min.; 9-Go to 6 repeat 24X; 10-72°C 8 min.; 11-Hold at 4°C.

All new *S. pombe* strains also contain a fluorescently tagged spindle pole body marker, Sid4-RFP. Sid4 is a scaffolding protein and a component of the SIN pathway.

Tracking the SPBs throughout cell division delineates the mitotic spindle and bipolar chromosome segregation, and is a way to monitor the cells progression through the cell cycle.

Table 1 PCR Primers used in this study

Mid1 1253bp	5'-CTTGAAC TTTTGCCTGCCCC-3'	Forward
Nat 296 bp	5'- TACGAGATGACCACGAAGCC -3'	Reverse
Sid4 1345 bp	5' -ACCCAAGCCCGTAAAGAGAT -3'	Forward
KanLinkChk	5'-CGGATGTGATGTGAGAACTGTATCCTAGC-3'	Reverse

Table 2 *S. pombe* strains used in this study

Strain#	Genotype	Literature Citation
0004	nda3-km311 mid1-4RXXS-GFP:kan ade6-M21X leu1-32 ura4-D18 h-	DeWitt, in progress
0110	mid1-GFP:kanR sid4-RFP:kanR ade6-M21X leu1-32 ura4-D18, h+	DeWitt, in progress
0143	LifeAct-GFP:Leu ade6-M216 leu1-32 ura4-D18 h+	Huang et al., 2012
0197	Mid1-Neongreen:kan rlc1-Tomato:nat sid4-RFP:kan ade6-M21X leu1-32 ura4-D18 h+	DeWitt, in progress
0216	LifeAct-GFP:leu1 sid4-RFP:kanMX6 ade6-m216 leu1-32 ura4-D18, h-	This study
0246	ade6-M210, ura4-D18, leu1-32, h-	Lab Stock
0251	rad24::ura4+ ura4-D18 leu1-32 ade6-704 h-	Mishra et al., 2005
0264	sid2-250 Mid1-GFP:kanMX6 ade6-M21X leu1-32 ura4-D18 h-	DeWitt, in progress
0266	rad24::ura4 Mid1-GFP ade6-X leu1-32 ura4-D18 h-	This study
0267	rad24::ura4 Mid1-4A-GFP ade6-X leu1-32 ura4-D18 h-	This study
0328	cdc16-116 Mid1-GFP:kanMX6 ura4-D18 leu1-32 ade6-M210	DeWitt, in progress
0353	rad24::ura4+ Mid1-GFP:kanR Sid4-RFP:kanR, ade6-M21X leu1-32 ura4-D18 h+	This study
0354	rad24::ura4+ Mid1-Neongreen:kanR rlc1-Tomato:natR Sid4-RFP:kanR, ade6-X leu1-32 ura4-D18 h+	This study
0355	rad24::ura4+ LifeAct-GFP:Leu Sid4-RFP:kanR, ade6-X leu1-32 ura4-D18 h-	This study
2415	mid1-GFP:KanR ade6-M210 ura4-D18 leu1-32 h+	Lab Stock
3173	mid1-GFP:KanR nda3-KM311 ade6-M210 leu-32 h+	Clifford et al., 2008
8566	mid1-4RXXSA-GFP(S329, 432, 464, 531):KanR ura4-D18 ade6-M21X leu1-32 h+	DeWitt, in progress

2.2 Confocal Microscopy

Confocal microscopy, or Confocal Laser Scanning Microscopy (CLSM), provides enhanced optical resolution and depth of focus by using a pinhole aperture to block out-of-focus light. This point illumination allows for two-dimensional images captured at different vertical points of depth throughout an entire specimen to be assembled post-hoc into a three-dimensional image with the microscope's software. The vertical plane throughout the depth of a specimen is referred to as the Z-plane, as opposed to the horizontal X-Y plane, and the collection of images referred to as a Z-stack.

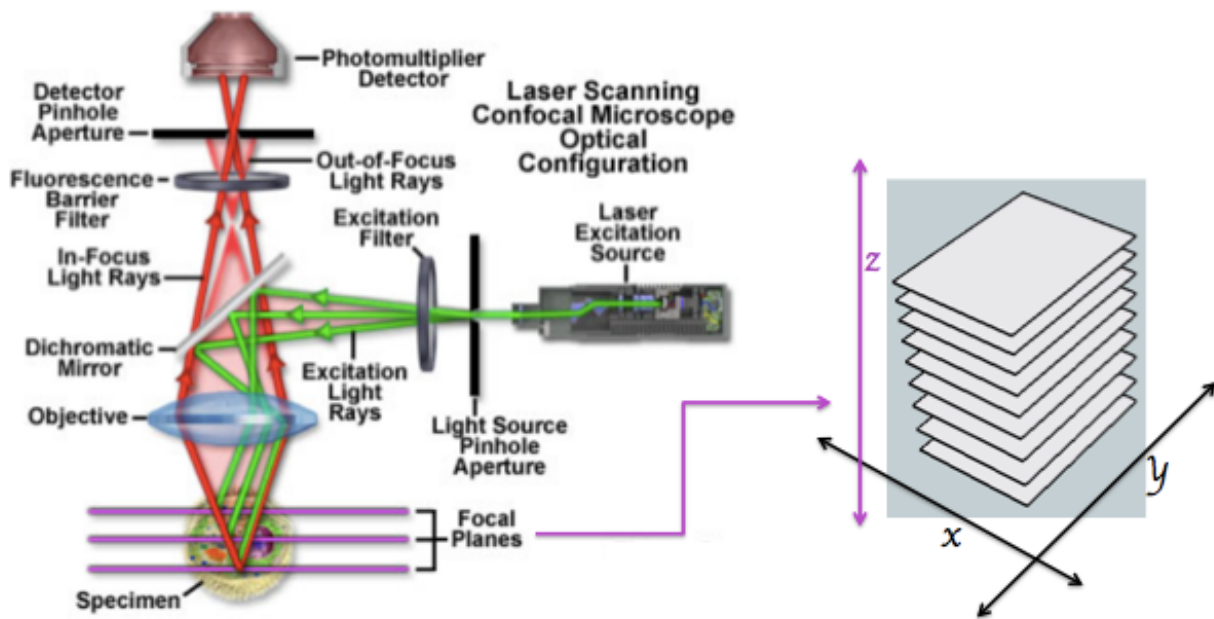


Figure 10. Concepts of confocal microscopy and Z-plane optical sectioning. Light rays from the excitation laser source are focused throughout the z-plane of a sample using dichroic mirrors. Out of focus light is excluded via pinhole apertures and only light emitted from the sample at a designated depth is picked up by the photomultiplier detector.

<https://www.olympus-lifescience.com/en/microscope-resource/primer/techniques/confocal/confocalintro/>

After passing through the first pinhole aperture, light from a laser excitation source is filtered and positioned using dichroic mirrors (Figure 10). The mirrors focus the light across the X-Y plane and within the desired Z-stack section. Only fluorescence

emitted from the sample in this particular focal plane are passed through a secondary pinhole aperture just before the photomultiplier tube (PMT) detector. A PMT is incorporated into the confocal system to amplify any signal lost from the exclusion of light outside of the pinhole aperture.

Newly constructed *rad24*-delete and corresponding WT live cells containing fluorescently tagged Sid4-RFP, Mid1-GFP, Rlc1-tomato, Mid1-NeonGreen, and/or LifeAct-GFP were immobilized on 1-1.5% YE agar pads on the surface of a glass microscope slide. A cover slip was placed on each specimen, and sealed in place using VELAP - a mixture of Vaseline, lanolin, and paraffin - to prevent agar media from drying during the three hours needed for movie collection. Movies were collected using a Nikon A1plus-Rsi scanning confocal microscope system equipped with an Anode PMT spectral detector and ORCA-Flash2.8 digital CMOS camera (Hamamatsu). The microscope objective used was an oil-immersion 100X objective with a numerical aperture of 1.45. Movies were created from Z-stacks of 14 images, spaced 0.279 μm apart, were collected every 60 seconds spanning a 3-hour observation window, giving approximately 180 time points per movie. The optical sections were compiled into maximum projection 3D images for analysis using the ND processing tool in the confocal microscope NIS-Elements software (<https://www.nikoninstruments.com/Products/Software/NIS-Elements-Confocal>). Images in figures 16 - 19 were maximum projections converted to 8 bit RGB files for analysis in ImageJ software (National Institutes of Health).

To track each cell's progression through the cell cycle, three manual measurements of each cell were taken using the spindle pole body (SPB) marker Sid4-

RFP, also using the ND analysis tool in NIS-Elements. The first measurement was taken at initial SPB separation, and indicates “time 0” in mitosis progression. The second measurement was of the widest point in SPB separation, indicating how far chromosome separation had progressed. The third measurement was of the cell length itself at the longest point, which is just before CAR constriction and the septation into two daughter cells.

2.3 Biochemical Assays

To produce GST (glutathione S-transferase) or GST-Rad24 fusion protein for *in vitro* binding assays, CaCL competent *E. coli* BL21-RiL cells (Agilent Technologies, #230245) were thawed on ice and heat-shocked for 45 seconds at 42°C for transformation with 100ng of either PGEX 4T (GST-containing plasmid; GE Life Sciences, #28954549) or PGEX 4T-Rad24 (GST-Rad24-containing plasmid). Bacterial cells were incubated with 900µl LB media for 37°C for 1 hour to recover, then pelleted, resuspended in LB, and plated on LBAC (LB plus 100 µg/mL ampicillin and 30 µg/mL chloramphenicol) selective media for growth at 37°C overnight. 5 mL starter cultures inoculated with colonies from the transformation plate were grown overnight in LBAC at 37°C. Starter cultures were added to 200mL LBAC and grown for 2 hours at 37°C to optical density₆₀₀ of 0.6. Recombinant protein expression was induced by adding 0.4mM IPTG (Isopropyl-β-D-thiogalactopyranoside, US Biological, #18500) to each bacterial culture and incubating for 4 hours at 37°C.

To isolate GST fusion proteins, cultures were pelleted and lysed by sonication. Lysates were centrifuged at 4°C, then resuspended and incubated with GST•Bind resin

(Millipore Sigma, #70541; 400 µl/protein) in TB1 buffer (50mM Tris-HCl, 120mM NaCl, 1mM EDTA, 1mM DTT, 0.1% Triton-X) for 1 hour at 4°C. The protein-resin complex was washed in TB1 buffer and proteins were eluted by adding 10mM glutathione into 400µl of TB1 buffer to compete off glutathione S-transferase and recombinant proteins from resin beads. Resin was centrifuged and the supernatants containing purified proteins were evaluated by SDS-PAGE (sodium dodecyl sulfate–polyacrylamide gel electrophoresis) for protein quality and concentration.

For yeast cell lysates, cold-sensitive *S. pombe* mutant *nda3-km311* cells expressing Mid1-GFP and *mid1*^{4RXXSA}-GFP were grown in 400 mL YE media overnight at the permissive temperature 32°C. Cultures were shifted to the restrictive temperature of 18°C and blocked in mitosis for 6.5-7 hours. Yeast pellets were collected and washed with NP40 buffer (6mM Na₂HPO₄, 4mM Na₂HPO₄H₂O, 1% Non-idet P-40, 150 mM NaCl, 2mM EDTA, 50 mM NaF, 0.1 mM Na₃Va₄) containing protease inhibitors (1X G Biosciences Protease Arrest, 1mM PMSF, 2mM Benzamidine, and 0.5mM DiFP). Pellets were lysed dry with glass beads (Sigma, #G8772) and lysed pellets were resuspended in NP40 buffer before clearing lysate by centrifugation. Total protein concentrations were normalized using BCA Protein Assay Kit (Thermo Scientific, #23227).

To immunoprecipitate Mid1-GFP and Mid1^{4RXXSA}-GFP for *in vitro* binding assays, Dynabeads Protein G (Invitrogen, #10007D; 75 µl /IP) were labeled with anti-GFP monoclonal antibody (Sigma-Aldrich, #11814460001; 4.5 µg/IP) in phosphate citrate buffer (0.1M Na₂PO₄, 0.05M Na₃C₆H₅O₇•2H₂O) overnight at 4°C. Equal amounts of the normalized lysates from mitotically synchronized, hyperphosphorylated cold-sensitive

mutant *nda3-km311 S. pombe* were incubated for 1 hour at 4°C with the previously labeled anti-GFP Protein G Dynabeads (80 µl/lysate).

To detect Mid1-GFP/Mid1^{4RXXSA}-GFP binding to GST-Rad24/GST, the Dynabead complex was then washed in NP40 buffer at 4°C then incubated with either bacterially expressed purified GST or GST-Rad24 fusion protein (2µg/190µl Dynabead complex) in TB1 buffer for 1 hour at 4°C. The entire Dynabead complex (anti-GFP Dynabeads/Mid1-GFP/Mid1^{4RXXSA}-GFP/Rad24/GST-Rad24) was washed with TB1 buffer by placing on Dyna-Mag2 magnet (Thermo-Fisher Scientific, #12321D) to remove supernatant and resuspended in 5X SDS sample buffer (250mM Tris-HCl, 10% SDS, 30% glycerol, 10mM DTT, 0.05% Bromophenol Blue). Samples were boiled for 7 minutes to denature proteins and placed on the Dyna-Mag2 magnet to separate them from Dynabeads prior to SDS-PAGE.

Samples were loaded onto a precast 10% polyacrylamide gel (Mini-Protean TGX; BioRad, #4651033) for SDS-PAGE using Mini-Protean Tetra system (BioRad, #1658004) with 1X Tris Glycine Running Buffer (25mM Tris, 192mM glycine, 0.1% SDS) at electrophoresed at 150V for 1.5 hours. Proteins were transferred to PVDF membrane (Immobilon-FL; Millipore Sigma, #IPFL00010) using XCell II blot module (Thermo Fisher Scientific, #EI9051) for XCell SureLock Mini-Cell Electrophoresis system (Thermo Fisher Scientific, #EI0001) in 1X NuPage transfer buffer (Thermo Fisher Scientific, 20X, #NP0006) for 1 hour 20 minutes at 30V.

For Western Blots, membranes were blocked for one hour in 1:1 PBS:Odyssey Blocking Buffer (Licor, #927-40000) at room temperature before incubating with monoclonal anti-GST antibody (Thermo Fisher Scientific, #MA4-004) and anti-GFP

(Sigma-Aldrich, #11814460001) antibodies at 1:1000 dilution in 1:1 PBS:Odyssey Blocking Buffer overnight at 4°C. Membranes were washed with PBST (PBS, 0.1% Tween-20) and incubated with IRDye secondary antibodies (IR800CW goat anti-mouse; Licor, #925-32210 or IR680RD goat anti-rabbit; Licor, #925-68071) for 1 hour at room temperature. Membranes were washed with PBST/PBS and visualized with the Licor Odyssey Fc Imaging System.

Mid1-GFP was also immunoprecipitated from a SIN kinase hyperactive strain, *cdc16-116*, and a SIN kinase inactive strain, *sid2-250*. Immunoprecipitation, binding assays, SDS-PAGE, and western blots were carried out as detailed above with *nda3-km311* cell lysates, with the exception that *cdc16-116* and *sid2-250* cultures were grown at 25°C overnight before shifting to the restrictive temperature of 36°C for 4 hours to induce SIN phenotypes before pellet collection and lysis.

2.4 Computational Tools

Since the crystal structures for Rad24 and the N-terminal portion of Mid1 have yet to be determined, comparative modeling can be used to generate models based on homologous structures. In the absence of homologous structures, protein fold recognition can be used. If such models are built successfully, they can help formulate hypotheses about potential interaction sites or reveal features in Mid1's structure that are conducive to its aggregation and/or localization.

Sequence analysis (MSA and MEME): To search for homologs to the N-terminal portion of Mid1 (aa1-582), PSI-BLAST (Altschul, et al., 1997) with 25 iterations was performed with *S. pombe* Mid1 sequence as the query sequence (NP_588075.1). Algorithm parameters for this search were as follows - word size: 3; expect threshold: 10; matrix

used: BLOSUM62 with conditional compositional score matrix adjustment; Non-redundant protein sequences database was searched with no exclusions. An MSA of resultant sequences obtained through the PSI-BLAST was created using EMBL Clustal Omega Alignment (Sievers, et al., 2011). A MEME motif analysis was performed on the same set of sequences using MEMESuite (Bailey, et al., 2009), set for zero or one occurrence of a contributing motif site per sequence and searching for 6 motifs with widths between 6 and 50 amino acids (default settings).

Structural Modeling: A high-quality structure of a Rad24 homolog, *Cryptosporidium parvum* 14-3-3 protein homodimer (PDB ID #2NPM), was found by submitting Rad24 protein sequence (NP_594167.1) to the Phyre2 protein fold recognition server (Kelley, et al., 2015). This structure has 63% sequence identity with Rad24, therefore a structure was obtained by comparative modeling also using Phyre2 (Kelley, et al., 2015).

For Mid1, there are no suitable templates on which to base a comparative model, so Mid1's N-terminal sequence (aa 1-582) was submitted to I-TASSER (Yang, 2009; Roy, et al., 2012; Yang and Zhang, 2015) for threading. Threading aligns each amino acid in a target protein's sequence to a template protein's structure - template proteins are determined using fold recognition, rather than known structures of a homologous protein. Predicted models were aligned using the STAMP structural alignment (Russell and Barton, 1992) available in the MultiSeq plugin within the Visual Molecular Dynamics (Humphrey, et al., 1996) software package.

2.5 Statistical Analysis

Kolmogorov-Smirnoff (K-S) tests were done to generate average intensity profiles of WT strains in relation to average intensity profiles of *rad24*Δ strains, using SAS (https://www.sas.com/en_us/software/stat.html) software. The K-S test is a nonparametric measure of empirical distribution between two samples. The K-S test was chosen because it can be used under a continuity assumption for the univariate population/model distribution, giving valid probabilities for any underlying distribution of the original (WT) and comparison (*rad24*Δ) dataset.

The two-sample K-S test is one of the most useful and general nonparametric methods for comparing two samples, as it is sensitive to differences in both location and shape of the empirical cumulative distribution functions. It shows one-dimensional probability distributions between two samples.

In order to statistically compute distribution probabilities using confocal data, intensity profiles were drawn across the length of each cell using the ND analysis tool in NIS-Elements (Figure 11), which takes a fluorescence reading every 0.211 micrometers (μm) across the length of a cell. After adjusting for individual background levels in each movie, raw fluorescent reading data for each profile was exported into individual Excel spreadsheets for each yeast strain. Since individual cells varied in their maximum lengths, intensity profile measurements were converted from μm into percentage of cell length. This allowed for data across all strains to be compared equally. There were 15-20 cells per strain analyzed, as indicated in the figure legend, and average intensities were created for all cells in each strain, for each time point. In essence, handling the

intensity profile data this way creates a "graph" of average (for all cells in a strain) intensities (y axis) over % cell distance (x axis) for each time point.

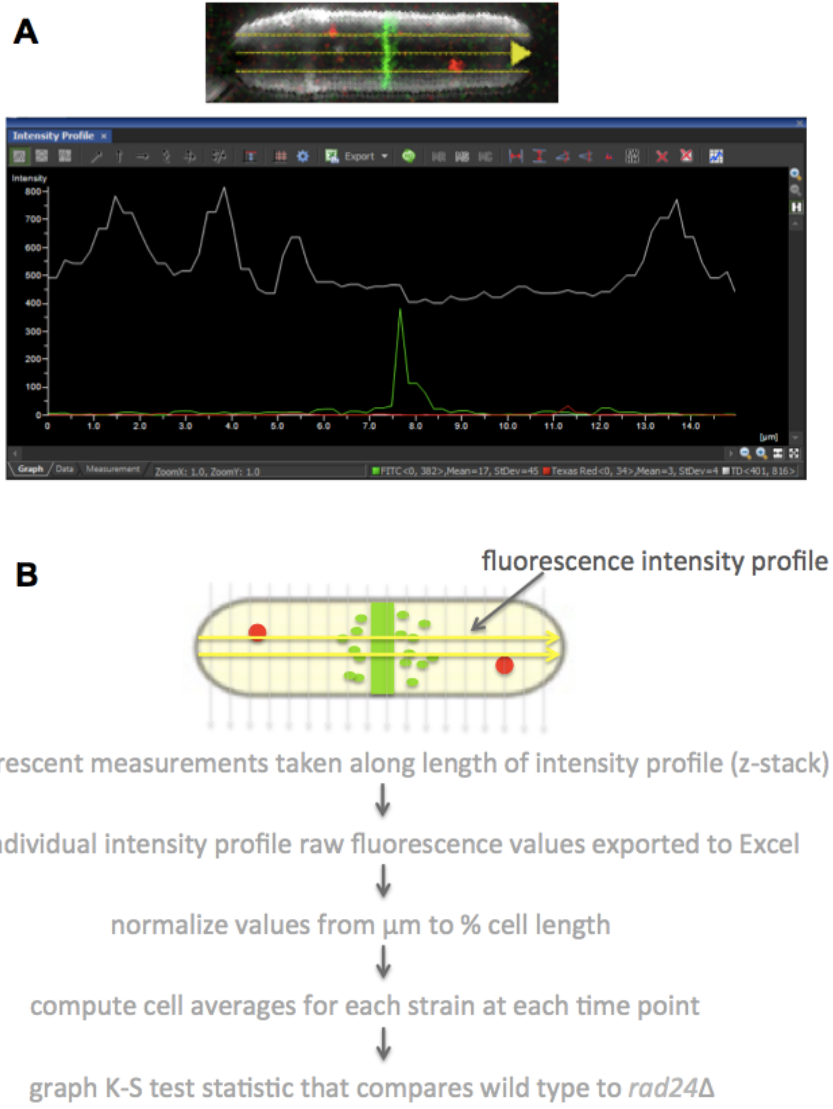


Figure 11. Schematic of Fluorescence Intensity Distribution Profiles and Data Processing. (A) Example of a fluorescently-tagged Mid1-GFP Sid4-RFP wild-type *S. pombe* cell and its corresponding intensity profile. (B) Fluorescence intensity profiles drawn across cells shows intensity values across the length of the profile. Raw fluorescence values were normalized for cell length and averaged for all cells in each strain before statistical analysis.

Therefore, each of six strains had 180 time points to analyze – one for each Z-stack collected during movie acquisition, and this would theoretically result in 180

graphs for each of the 6 strains. The K-S test was selected in this regard to carry out the remaining statistical work, in order to quantitatively compare *rad24*Δ distributions to WT distributions, from the amount of data collected from the intensity averages. The K-S test statistic in this instance is numerically representative of the differences in signal distribution over intensity profiles for cells in WT strains in comparison to cells from *rad24*Δ strains. The ratio of the K-S value for WT vs. *rad24*Δ is graphed (y-axis) vs. time (x-axis) in Figures 15-17 – a ratio of 1 means no difference in distribution; values above and below 1 would indicate a difference.

3 Characterization of the Interaction between Mid1 and Rad24

3.1 Determination of Phospho-dependence of Mid1 and Mid1^{4RXXSA}/Rad24 Interaction

To test the importance of Sid2 phosphorylation on Mid1 and Rad24's interaction, hyperphosphorylated Mid1-GFP and hypophosphorylated Mid1^{4RXXSA}-GFP were isolated to assay for Rad24 binding. Mid1-GFP and Mid1^{4RXXSA}-GFP were expressed in cell lines that had been previously crossed into cold-sensitive *nda3-km311* mutant background. The NDA3 gene encodes β -tubulin, and a mutation in this gene results in the inability to form microtubules, a blockage of spindle formation, and a lapse in the movement of chromosomes (Hiraoka, et al., 1984). The *nda3-km311* mutation specifically arrests yeast cells synchronously in prometaphase when shifted from the permissive temperature of 32°C to the restrictive temperature of 18°C, following the loss of β -tubulin function.

During early mitosis (prometaphase), the point at which Mid1 is exported from the nucleus, Mid1 would be in its most phosphorylated form. *nda3-km311* mutant cells were used to capture Mid1-GFP in this most hyperphosphorylated state, and to evaluate whether Mid1^{4RXXSA}-GFP would have less Rad24 binding capacity because of reduced Sid2 phosphorylation. Mid1-GFP and Mid1^{4RXXSA}-GFP were immunoprecipitated from mitotically synchronized *nda3-km311* cell lysates with α GFP-labeled magnetic beads, incubated with either bacterially-expressed GST or GST-Rad24, separated by SDS-PAGE, transferred to PVDF membranes, and probed with α GFP and α GST antibodies.

Since SIN activity also peaks during mitosis, Sid2 phosphorylation in the Mid1^{4RXXSA}-GFP phosphomutant cell line should be diminished during mitosis, and Mid1-GFP isolated from this cell line should, in theory, demonstrate a reduced GST-

Rad24 binding ability. This reduced binding ability would be apparent on the WB as either a lighter or nonexistent 56 kDa sized GST-Rad24 band (Rad24's molecular weight is 30kDa; GST's is 26 kDa) in the Mid1^{4RXXSA}-GFP/GST-Rad24 immunoprecipitation/*in vitro* binding assay lane.

However, Mid1-GFP did not bind more efficiently to Rad24 than Mid1^{4RXXSA} - GFP; there was not a marked difference in band intensity between phosphosite mutant Mid1^{4RXXSA} -GFP and Mid1-GFP (Figure 12). Additionally, results obtained were inconsistent between two separate experiments, with two ~56 kDa GST-Rad24 bands showing up in the GST-Rad24-containing IP lanes on one occurrence, and four ~56 kDa GST-Rad24 bands showing up in all IP lanes, GST only included, on a separate occurrence. This would suggest that another protein that is roughly ~56 kDa in size in the GST only IP lanes is binding nonspecifically to the magnetic beads. Perhaps the conformations of either Mid1 (Mid1 is a large ~120 kDa nonsoluble protein that tends to break apart when purified) or Rad24 were not in their native state as they would be *in vivo*, which may be necessary for binding affinity.

There are, in fact, more than Sid2 phosphorylation sites on Mid1. Mid1's protein sequence shows 9 serines that fit the consensus motif for Sid2 phosphorylation, and phosphopeptide mapping has shown that there are additional sites as well (DeWitt A, Gould K, and Hart D; article in process). Since all of the Sid2 phosphorylation sites are not removed in the Mid1^{4RXXSA} -GFP mutant, there could still be significant binding occurring between Rad24 and Mid1, even though 4 of the 9 of the phosphorylation sites were destroyed. This may account for the binding of GST-Rad24 to both Mid1-GFP and Mid1^{4RXXSA} -GFP in the binding assay. (Figure12).

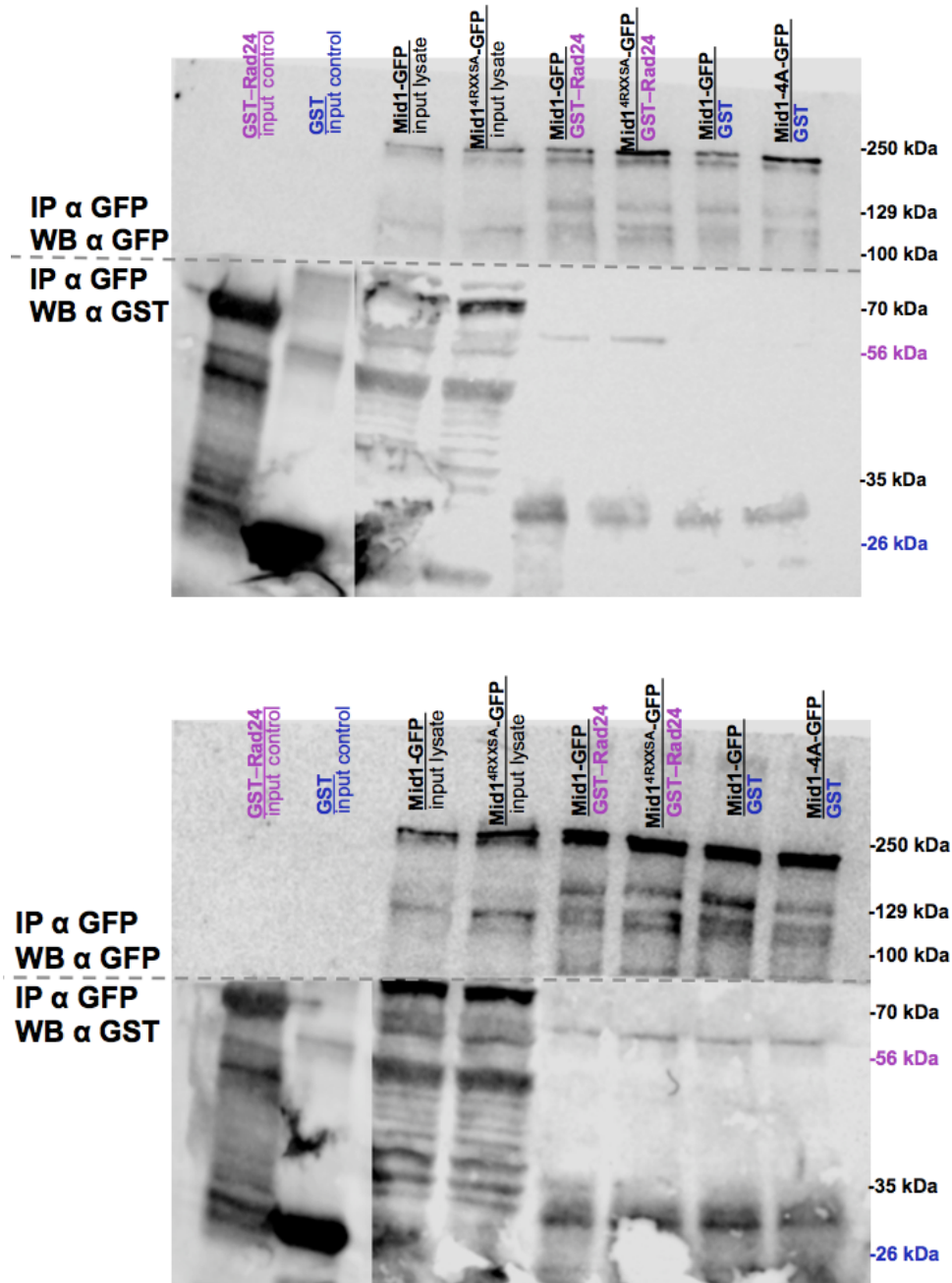


Figure 12. Mid1-GFP does not bind more efficiently to GST-Rad24 than Mid1^{4RXXSA}-GFP. Two separate IP/*in vitro* BA/WB experiments are shown. Immunoprecipitated Mid1-GFP and Mid1^{4RXXSA}-GFP from mitotically-synchronized, prometaphase-arrested *nda3-km311* mutant *S.pombe* strains #3173 and #4 were incubated with bacterially expressed GST or GST-Rad24. Proteins were separated using SDS-PAGE and transferred to PVDF membrane prior to cutting membrane between 100 kDa and 70 kDa. Blots were probed with αGFP/αGST on the top and bottom of blot, respectively, along with corresponding secondary antibodies.

3.2 Determination of Phospho-dependence of Rad24/Mid1 Interaction in SIN Mutants

As an alternative, and specifically SIN-dependent, method to induce different phosphorylation states of Mid1, Mid1-GFP was isolated from two *S. pombe* cell lines that express the temperature-sensitive SIN mutations *cdc16-116* and *sid2-250*. Sid2 is activated and inactivated, respectively, in each of these strains, and their use explicitly couples the SIN pathway to Mid1 phosphorylation. In *cdc16-116* cells, the SIN is constitutively activated due to inactivation of Cdc16. The *cdc16* gene encodes one of the two components of the GTPase-activating protein (GAP) for GTPase Spg1, and inactivating GAP activity is necessary for SIN activation (Furge, et al., 1998). The *cdc16-116* phenotype is small, multiseptated cells that display cytokinetic failure at a restrictive temperature (Fankhauser, et al., 1993; see Figure 5 of this thesis). The *sid2-250* mutation inactivates Sid2's kinase ability and results in elongated, multinucleate cells with missing or misshapen septa (Balasubramanian, et al., 1998; see Figure 5 of this thesis). To assay for Rad24 binding, Mid1-GFP was immuno-precipitated from *cdc16-116* and *sid2-250* lysates, incubated with bacterially-expressed GST or GST-Rad24, separated by SDS-PAGE, transferred to PVDF membranes, and probed with α GFP and α GST antibodies.

Mid1-GFP was isolated from SIN mutant strains to evaluate whether forcing Mid1 phosphorylation in a SIN-dependent manner has an effect on Rad24's binding ability with Mid1. SIN mutant *cdc16-116* cells arrest in cytokinesis because their mitotic, nuclear division has become uncoupled from their cytokinetic, physical separation. *sid2-250* cells also show marked cytokinetic failure because they cannot form a new cell wall and thus can never complete physical separation, even though they contain

multiple septa. It is a possibility that perhaps since SIN mutant cells arrest in cytokinesis, we could miss the Mid1 and Rad24 interaction if it happens during early mitosis, and that cytokinesis is too late to show binding. But the SIN mutants in this case are being used to induce specific phosphorylation states on Mid1, so cell cycle stage at the time of pellet collection should not be a factor for Rad24 binding once Mid1 is purified from lysates, and since the binding assay is performed *in vitro*, not *in vivo*.

If Mid1 were reliant on Sid2 phosphorylation for Rad24 binding, we would expect reduced or nonexistent Mid1-GFP/GST-Rad24 binding with immunoprecipitation of hypophosphorylated Mid1-GFP from *sid2-250* lysate. Likewise, we would expect a concurrent increase in Mid1-GFP/GST-Rad24 binding with immunoprecipitation of hyperphosphorylated Mid1-GFP from the SIN hyperactive strain, *cdc16-116*.

However, hyperphosphorylation did not result in more Rad24 binding to Mid1 (Figure 13). In fact, Mid1-GFP and GST-Rad24 show no evidence of binding in either *cdc16-116* or *sid2-250* lysates. SIN elongated and multiseptated phenotypes were confirmed by examination under light microscopy before collecting cell pellets, so Mid1 hypo and hyperphosphorylation should be insured. The rather dark ~50 kDa band in the immuno-precipitation/*in vitro* binding assay lanes is the α -mouse secondary antibody picking up the Immunoglobulin G (IgG) heavy chain from the immunoprecipitation using and mouse α -GFP antibody.

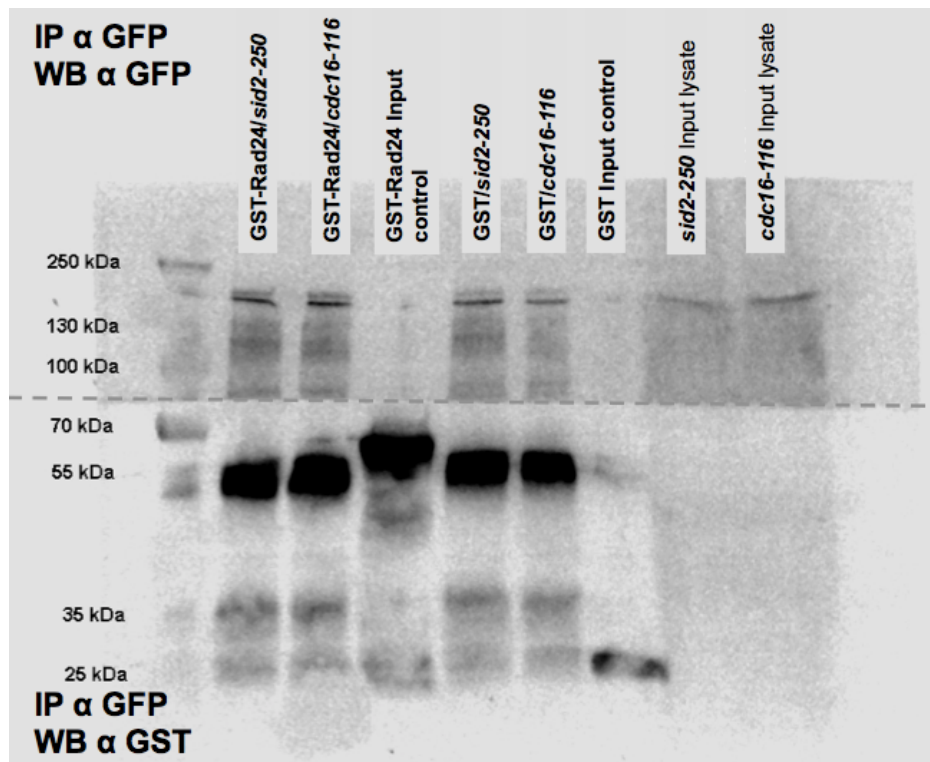
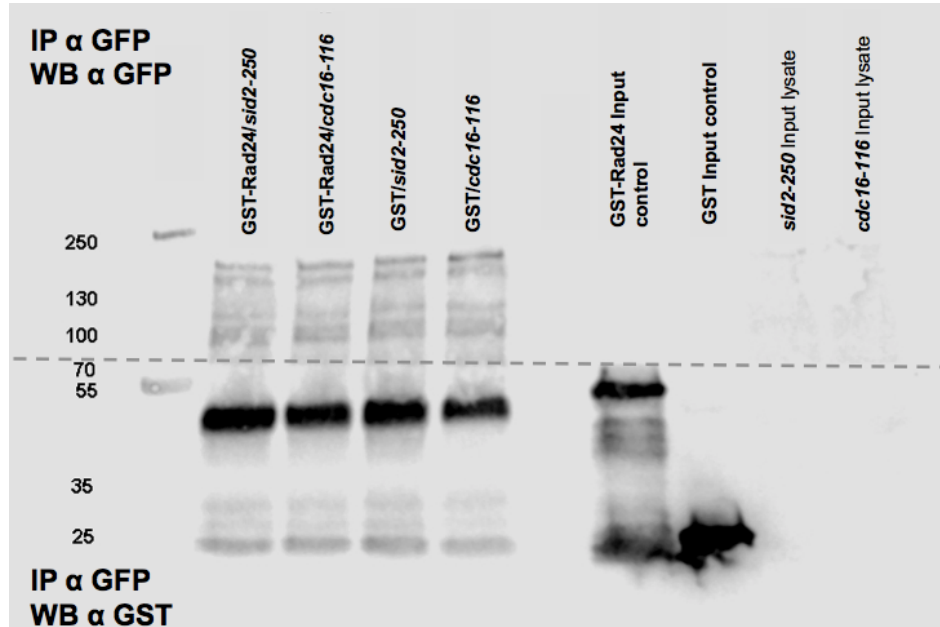


Figure 13. Hyperphosphorylation did not result in Rad24 binding to Mid1 more readily. Two separate IP/*in vitro* BA/WB experiments are shown. Immunoprecipitated Mid1-GFP from asynchronous SIN hyperactive and SIN inactive mutant *S.pombe* cells were incubated with bacterially expressed GST or GST-Rad24. Proteins were separated using SDS-PAGE and transferred to PVDF membrane prior to cutting membrane between 100 kDa and 70 kDa. Blots were probed with αGFP/αGST on the top and bottom of blot, respectively, along with corresponding secondary antibodies for detection.

There may be technical reasons to consider in addressing these results. The Mid1-GFP/GST-Rad24 binding assay itself does not have a positive control, so issues such as buffer conditions and incubation times may or may not be optimal. It may also be possible that there are various post-translational modifications that necessitate Rad24 binding. It could be that Rad24 itself, since it is also a phosphoprotein, requires post-translational modifications such as phosphorylation, or quaternary structure shifts such as dimerization, that would not happen in its bacterially-expressed, purified form. Also, Mid1 or Rad24 may not be in the correct protein conformation to facilitate binding to one another or their interaction may require another binding partner not present in this particular assay. And lastly, even though Rad24 may bind Mid1 at some point during the cell cycle, phosphorylation of RXXS sites may be accomplished by another NDR2 kinase.

It may be that Mid1, even though in a constitutively active phosphorylation state, does not bind Rad24 *permanently*. With purified proteins, the post-translational modifications or additional binding partners that may be necessary to drive this interaction *in vivo* are not present. Nevertheless, the fact that Mid1-GFP/GST-Rad24 binding was not detected in SIN mutant lysates may be reflective of the transience of the interaction. And although this shows an *in vitro* test, perhaps Rad24 only binds Mid1 for a short time. The interaction could be dependent on Mid1's conformation or oligomerization state after it is exported from the nucleus, or when Mid1 is separated from the CAR and heading back to the nucleus. Rad24 and Mid1 are known to interact through tandem-affinity purification (TAP), with a significantly high recovery of Mid1 with Rad24 (Hart D and Gould K, unpublished data). There was 73.6% peptide coverage of

Mid1 with 55.8% coverage of Rad24, which are considered high for a large, hydrophobic protein like Mid1 that is difficult to purify. The mixed results obtained from our lysate binding assays could be more of a reflection of the relative difficulty of isolating and working with Mid1, and its transient interaction time with Rad24, rather than there not being an interaction at all. TAP is also a method in which the proteins are purified as a complex from live cells and any post-translational modifications or binding partners will still be intact, so all of these factors may play a role in failure to detect binding *in vitro*.

3.3 Sequence analysis and structural models of Rad24 and Mid1 N-terminus

To identify distant homologs of Mid1's N-terminus, PSI-BLAST (Altschul, et al., 1997) was performed. Resultant sequences, shown in Table 3, were submitted along with the sequence from *S. pombe* (UniProt ID# P78953) Mid1 for a multiple sequence alignment (Figure S2) and conserved motif search using MEMESuite (Bailey, et al., 2009).

Table 3 PSI-BLAST result sequences with Mid1 N-terminus (aa 1-582) as query

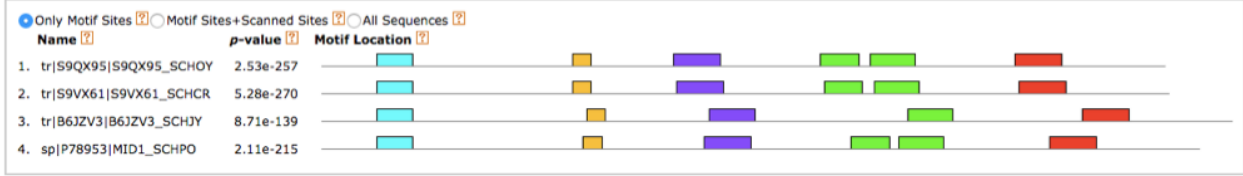
Species	UniProt ID	E Value	Identity	Sequence Coverage
<i>S. cryophilus</i>	S9VX61	0.0	42%	99%
<i>S. octosporus</i>	S9QX95	0.0	40%	99%
<i>S. japonicus</i>	B6JZV3	9e-175	31%	94%
<i>C. nigoni</i>	A0A2G5THJ6	0.027	17%	80%

MSA shows conserved serine residues at Sid2 phosphosites RIKS⁴³², RTYS⁴⁶⁴, and RAHS⁵³¹, which indicates evolutionary importance of these sites, at least among yeasts (Figure S2). The site where Plo1 phosphorylates *S. pombe* Mid1 and binds Rng2 (aa 59-96) to modulate cytokinetic node assembly is highly conserved among yeasts as well. There are several serines in the MSA (S⁴⁶, S⁶², S⁶⁷, S¹⁷⁴, S³³⁵, and S⁴⁹²) that are highly conserved but located outside of the MEME motifs. MEME results indicate several conserved motifs present in the N-terminal segment of Mid1. Of particular interest was a motif (number 3, aa 401- 450) that contains aforementioned S⁴³² of Sid2 phosphosite RIKS in *S. pombe* Mid1 (Figure 14, shown in purple). This is one of the main sites located in phosphopeptide studies (DeWitt A, Gould K, and Hart D; article in process), and could be an indicator of evolutionary importance. The site where Plo1 phosphorylates *S. pombe* Mid1 and binds Rng2 is also located within a conserved motif (number 1, aa 59-96, shown in teal in Figure 14).

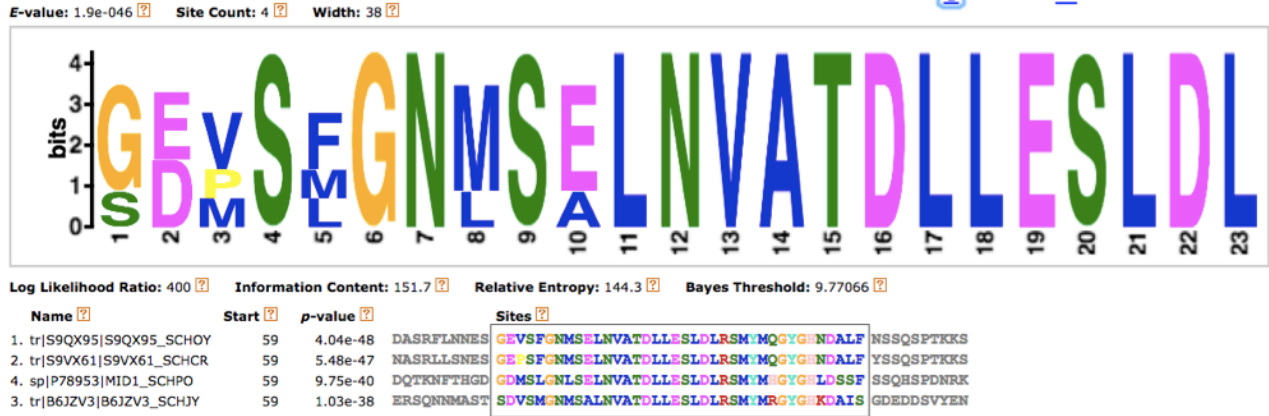
The most conserved part of motif number 3, RGRI[KR]SSS[ST] (Figure 14), containing S⁴³² is predominantly polar but there are hydrophobic residues flanking it, which would fit the description of an amphipathic binding cleft consistent with Rad24 binding (Muslin, et al., 1996).

Other motifs found among yeasts contain several conserved residues including glutamic acid, proline, tyrosine, threonine, leucine, aspartic acid, and phenylalanine (aa274-294, aa605-652, aa763-812; Figure S3). These motifs could be important for regulatory processes that occur outside of the scope of this thesis or have yet to be elucidated.

A Motif Locations



B



C



Figure 14. Motif analysis shows consensus between four yeast Mid1 protein sequences. (A) Six conserved motifs found across *S. cryophilus* (UniProt ID# S9VX61), *S. octosporus* (UniProt ID# S9QX95), *S. japonicus* (UniProt ID# B6JZV3), and *S. pombe* (UniProt ID# P78953) Mid1 sequences. (B) Close up logo of motif 1 shown in A (teal) where Plo1 phosphorylates and Mid1 binds Rng2 (aa 59-96). (C) Close up of motif 3 shown in A (purple). The grey box indicates conserved consensus RXXS site where Sid2 phosphorylates Mid1 at S432. This region is also where Clp1 and Cdr2 interact with Mid1.

The Rad24 model based on the 14-3-3 protein (PFAM ID #PF00244; Figure 15) has 9 antiparallel alpha helices that could form a concave amphipathic groove to

interact with target peptides when dimerized. The core of 14-3-3 proteins, where the dimerization interface and the functional regulatory domain are located, are more conserved than the N and C termini (Isobe, et al., 1991). The quality of the *S. pombe* Rad24 model was quite high, with a 100% confidence score and a 63% sequence identity with the structure of the *C. parvum* 14-3-3 homodimer (PDB ID# 2NPM) at 2.52 Å resolution. The structure obtained fits the description of a regulatory molecule with the ability to bind a variety of functionally diverse ligands (Fu, et al., 2000).

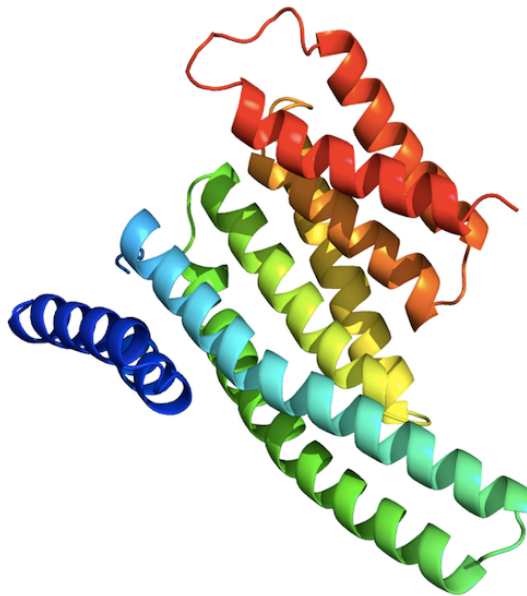


Figure 15. Phyre2 comparative model of *S. pombe* Rad24. Like other 14-3-3 proteins, helices 3 and 5 contain charged and polar residues while helices 7 and 9 contain hydrophobic residues. This amphipathic groove constitutes the dimerization interface as well as mediating interactions with phosphoamino acids in binding partners (Fu, et al., 2000). There is 100% confidence and 63% sequence identity based on the structure of *C. parvum* 14-3-3 homodimer in complex with a peptide (PDB ID # 2NPM).

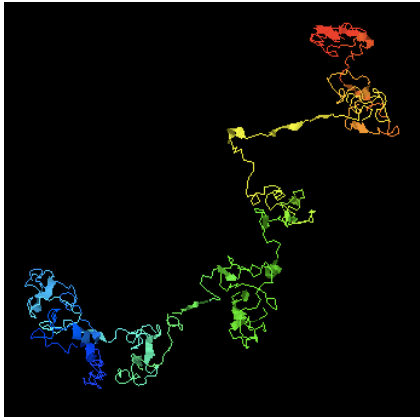
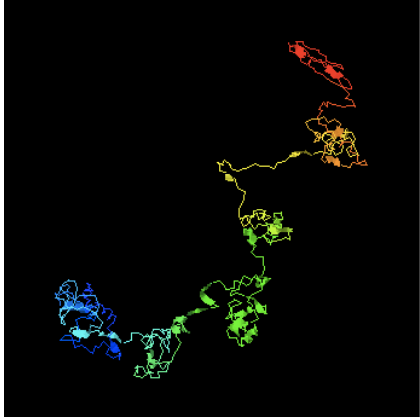
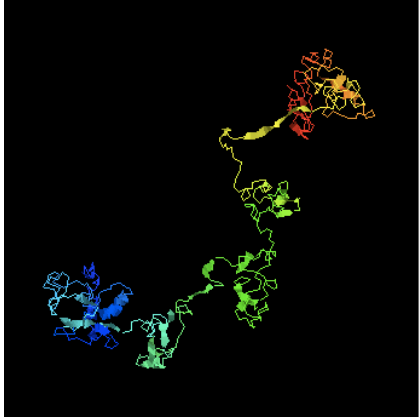
The Phyre 2 query of Mid1 N-terminus revealed that there are no close, high sequence similarity homologs available. Since there was not a homologous crystal structure to base a model on for Mid1's N-terminus (aa 1-582), the sequence was submitted to I-TASSER for fold recognition via PSI-BLAST and threading to identify

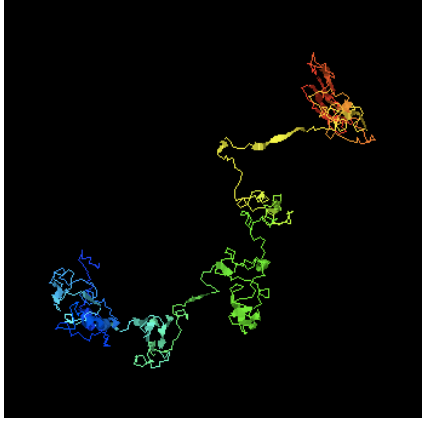
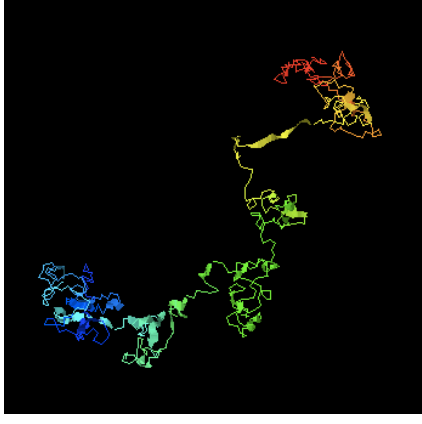
distant relatives. The top five model structures of Mid1's N-Terminus are represented in Table 4, with their corresponding C-scores. The C-score is a quality measure of each model that is calculated based on significance of alignment to the template used. C-scores range from -5 to 2, with higher scores being associated with high confidence in the model's predicted structure (Roy, et al., 2012). The models of Mid1 were constructed from multiple different partial templates that were identified using fold recognition, rather than from a single known structure of a homologous protein. Thus the predicted models are built based on similar protein domains from various structures, and not on a *single* structure.

Due to their low C-scores, the Mid1 N-terminal structures obtained through I-TASSER were not considered reliable enough to be used for protein-protein docking to Rad24. Nevertheless, these predicted models can offer potential insight into the Sid2 phosphosite residues involved, and the biochemical properties of the surrounding residues can be evaluated. Though highly speculative, these models can be used to evaluate Sid2 phosphorylation sites on Mid1, their exposure to solvent, and availability to interact with binding partners.

The five models were aligned using the STAMP structural alignment (Russell and Barton, 1992) in VMD (Humphrey, et al., 1996). All predicted models are very similar as shown in the Figure 16 alignment. There was an agreement in structure of Sid2 phosphosites, and these regions, with the exception of S³²⁹, constitute more compactly folded segments joined together by more flexible (possibly disordered) regions of the structure. The serines at Sid2 phosphosites RISS³²⁹, RIKS⁴³², RTYS⁴⁶⁴, and RAHS⁵³¹ are located in areas of moderate solvent accessibility according to the I-TASSER

Table 4 I-Tasser modeling results of Mid1 amino acids 1-582

Model 1		C-score: -2.63 Template(s) PDB accession number: 2NBI 3CHN 2PFF 4V58 3HMJ 1XI4 5I8I 4O9X 5L5G 3K1Q
Model 2		C-score: -2.64 Template(s) PDB accession number: 2NBI 3CHN 2PFF 4V58 3HMJ 1XI4 5I8I 4O9X 5L5G 3K1Q
Model 3		C-score: -2.81 Template(s) PDB accession number: 2NBI 3CHN 2PFF 4V58 3HMJ 1XI4 5I8I 4O9X 5L5G 3K1Q

Model 4		C-score: -3.24 Template(s) PDB accession number: 2NBI 3CHN 2PFF 4V58 3HMJ 1XI4 5I8I 4O9X 5L5G 3K1Q
Model 5		C-score: -3.15 Template(s) PDB accession number: 2NBI 3CHN 2PFF 4V58 3HMJ 1XI4 5I8I 4O9X 5L5G 3K1Q

predicted solvent accessibility report (data not shown) with an average of 3.25 on a scale of 0-9. The predicted structures of the phosphosites are helical in two of the four sites mentioned.

It is plausible that Mid1's N-terminus, due to its role as a scaffolding protein, is highly flexible, perhaps intrinsically disordered. The N-terminus is known to play a role in node assembly and modulating cortical stability at the plasma membrane (see Figure 8C). The threading models obtained may reflect this inherent flexibility in that the conserved "joint" regions are connected via extensive linker loops (Figure 16).

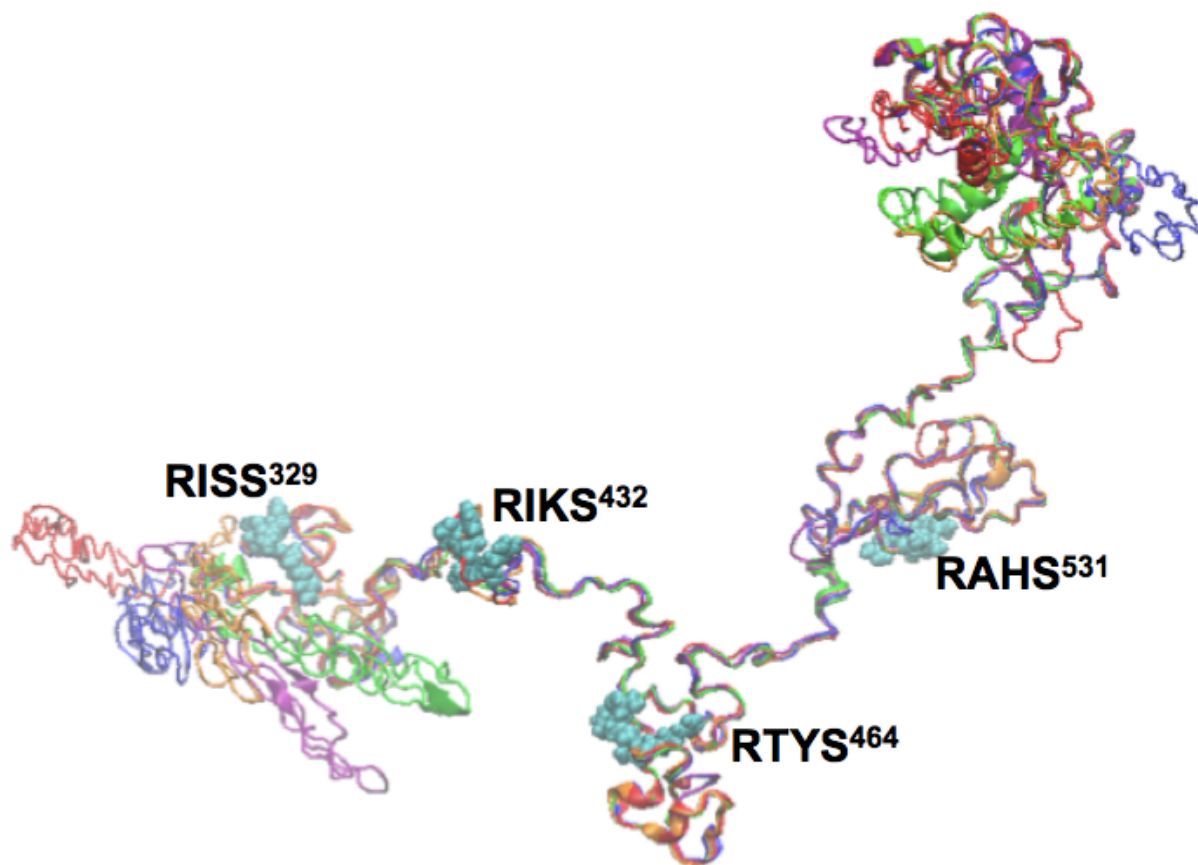


Figure 16. STAMP structural alignment of putative Mid1 N-terminus (aa 1-582) models rendered in VMD shows consensus around Sid2 phosphosites. The aqua colored VDW (Van Der Waals) residues represent the four Sid2 binding sites mutated in the Mid1-4^{RXXSA} mutant.

In the context of the Mid1 N-terminus structural models (Table 4 and Figure 16), the MSA results suggest that the conserved regions containing Sid2 phosphosites with conserved serines are in the more ordered, folded regions of the protein, while the highly disordered and flexible regions do not contain conserved residues. Phosphosite RISS³²⁹ does not contain a conserved serine - this is the most N-terminal phosphosite and lies within a region where the predicted models vary the most (Figure 16 and Figure S2). Extensive dynamics simulations that are beyond the scope of this thesis would be necessary to generate the conformational ensemble of this complex structure.

4 Consequences of Rad24 deletion on timing and morphology of CAR formation

4.1 Difference in F-actin distribution between wild type and *rad24* Δ *S. pombe*

Restructuring the actin cytoskeleton for cell division requires relocalization of actin from the cell ends during cell growth in interphase to the cell cortex at mitosis to form the CAR. In fission yeast, the Morphogenesis Orb6 Network (MOR) pathway is essential for bipolar growth by promoting actin polarization at cell tips during interphase (Verde, et al., 1998) and has also been implicated in F-actin patch assembly (Huang, et al., 2005). The MOR pathway is another conserved NDR-pathway in fission yeast, and like the SIN, is regulated through a GTPase, Cdc42 (Das, et al., 2009). The G2/M interphase-to-mitosis transition is coordinated by interplay between the SIN and MOR pathways (Ray, et al., 2010; Gupta and McCollum, 2011) and Sid2-related kinase Orb6 binds to Mob1-related protein Mob2 (Hou, et al., 2003). The SIN disrupts the interphase actin cytoskeleton by directly impeding MOR activity through Nak1 kinase-mediated Orb6 inhibition (Gupta and McCollum, 2011). Therefore, we hypothesized that F-actin temporal and spatial localization is altered when SIN targets are misregulated.

Three-dimensional structures such as the CAR and the actin relocalization needed to form it are more easily visualized using the confocal microscope. The migration and timing of proteins involved in CAR assembly are more easily visualized as well, and the aim of the methods employed here are to gain insight into the whole picture of the CAR, as it assembles and constricts during mitosis. More specifically, confocal microscopy enables visualization of the effects that deleting *rad24* has on CAR formation. These effects could be due, in part, on SIN activity regulating Rad24, or may be tied into the MOR pathway in a SIN-dependent manner.

Live cell videomicroscopy was used to monitor the intensity of F-actin across the length of each cell, followed by a multi-step statistical approach to generate K-S values (complete details provided in Sections 2.2 and 2.5 of this thesis). The ratio of K-S value in WT vs. *rad24* Δ cells was plotted to show differences in F-actin distribution. A ratio of 1 would mean there is no difference in protein distributions, and any value above or below 1 would indicate that there is a difference. The K-S ratio plots also show cytokinetic events, such as sharp rings or CAR constriction, as they occur in each strain. To do this, individual cells were observed and the movie frame was recorded and averaged for each cytokinetic event, with the frame number at which the SPBs separated marked as time 0 to follow the timing of mitotic events in individual cells. All cells in which fluorescent intensity profiles were analyzed for the statistical data were timed for cytokinetic events in this way, and WT values were compared to *rad24* Δ in an unpaired student t-test (<https://www.graphpad.com/quickcalcs/ttest1.cfm>) for statistical significance. Differences in mean cytokinetic event times considered to be statistically significant (p value ≤ 0.01) are marked on the plot with a red asterisk.

In *rad24* Δ cells, F-actin recruitment to the CAR is not significantly early (WT mean 7.07 min, SD 4.74 vs. *rad24* Δ mean 8.40 min, SD 5.28; $p = 0.4727$), even though CAR constriction is significantly early in comparison to WT cells (WT mean 64.75 min, SD 26.04 vs. *rad24* Δ mean 37.53 min, SD 11.59; $p < 0.0001$) (Figures 16B and C, 64 min vs. 35 min) and the cells separate sooner (WT mean 89.14 min, SD 25.29 vs. *rad24* Δ mean 66.80 min, SD 14.25; $p = 0.0147$) (Figure 17A). CAR constriction also ends earlier in *rad24* Δ cells (WT mean 76.57 min, SD 20.74 vs. *rad24* Δ mean 54.07 min, SD 12.67; $p = 0.0049$). Interestingly, the SPBs are at their widest separation much

earlier in *rad24* Δ cells (WT mean 34.47 min, SD 5.55 vs. *rad24* Δ mean 19.93 min, SD 5.51; $p < 0.0001$) even though the difference in timing that the rings were sharp in both cell lines was not significant (WT mean 23.2 min, SD 9.26 vs. *rad24* Δ mean 24.67 min, SD 8.62; $p = 0.6568$). This would indicate a potential disconnect between mitotic division and cytokinesis that could be brought on by a delay in F-actin cables assembling for timely CAR constriction. The delay in CAR constriction could be brought on by the failure of Rad24 to sequester Cdr2 in the cytoplasm during mitosis and therefore indirectly resulting in the timing/misplacement of Mid1. This would incorrectly situate Mid1 during late interphase, when actin is supposed to be recruited to the CAR. Or perhaps SIN signaling controls the MOR pathway in a Cdr2 or 14-3-3 – dependent manner. Orb6 is also an NDR kinase and could potentially be involved with Rad24 somehow since it also phosphorylates RXXS motifs.

The difference in LifeAct-GFP distribution between WT and *rad24* Δ cells is most evident from 40 to 65 minutes into cell division, during the overlap when the CAR is constricting (Figure 17A) in both WT and *rad24* Δ cells. If Rad24 were required to modulate Mid1's presence in the cytoplasm during interphase, we would expect to see delays in recruitment of F-actin or problems with actin filamentation or bundling due to lack of actin regulator Cdc15 recruitment, which needs Mid1 for proper placement (Laporte, et al., 2011). Cdc15 is also reliant on Clp1, whose placement in the cytoplasm during interphase requires Rad24 (Mishra, et al., 2005; Clifford, et al., 2008). F-actin is also more localized to the cell tips at the end of CAR constriction in WT cells (Figure 17A and B, starting at ~80 minutes). In sum, there are detectable differences in F-actin distribution during key cytokinetic events and early CAR constriction in *rad24* Δ cells.

LifeAct-GFP Sid4-RFP WT vs. *rad24* Δ

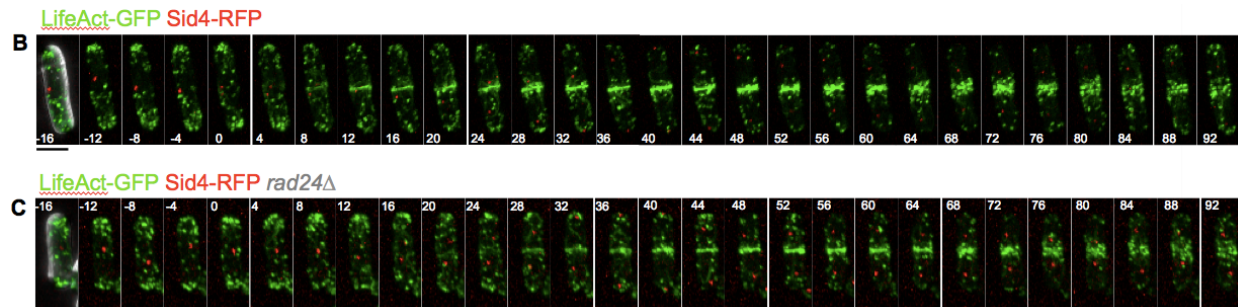
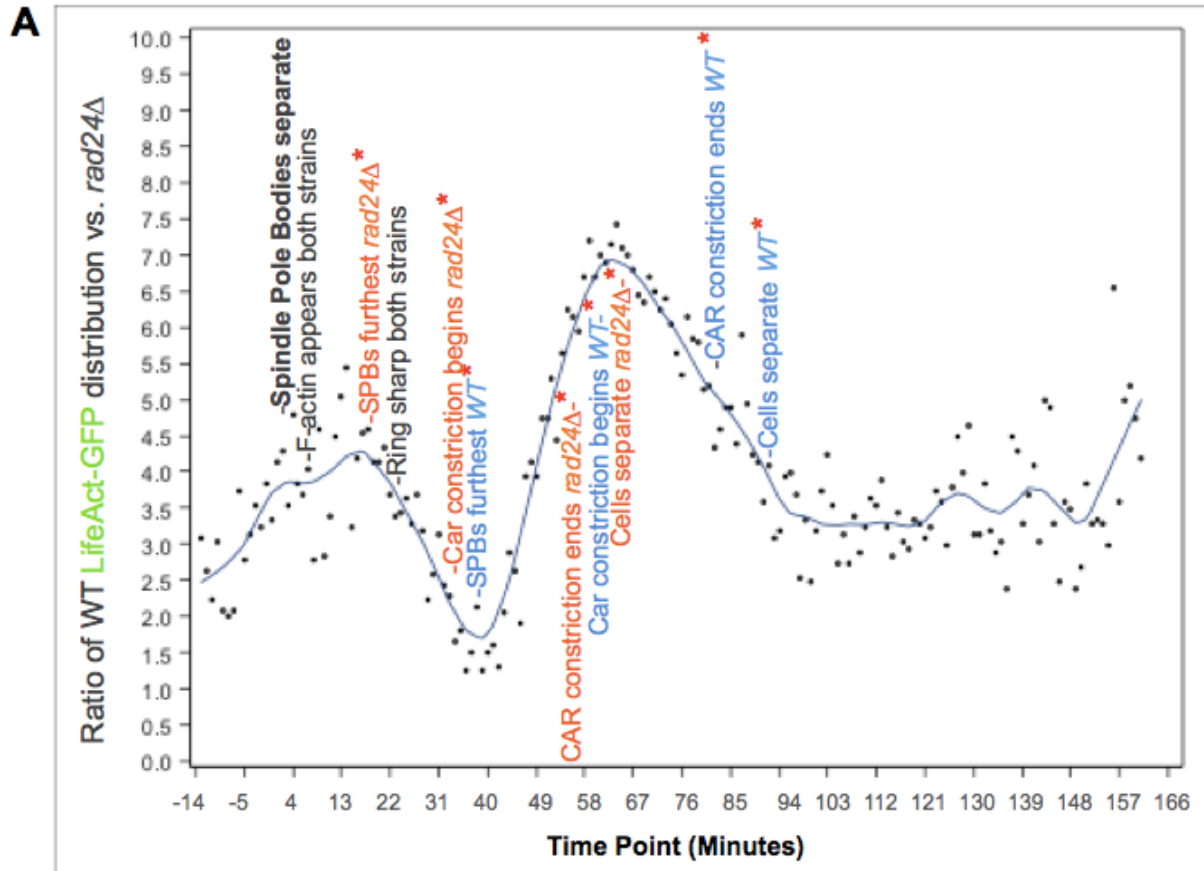


Figure 17. *rad24* Δ cells show a delay in F-actin recruitment to the CAR but premature CAR constriction and septation. (A) K-S test graph of distribution ratio of LifeAct-GFP in WT vs. *rad24* Δ *S. pombe* strains. Number of cells analyzed: n=15 for both strains LifeAct-GFP sid4-RFP, strain #216 and LifeAct-GFP sid4-RFP *rad24* Δ , strain #355 (B) Localization of LifeAct-GFP in an example WT cell from strain #216 throughout mitosis, the beginning of which is marked at timepoint 0, when SPBs separate. (C) Localization of LifeAct-GFP in an example *rad24* Δ cell from strain #355 throughout mitosis. Scale bar = 5 μ m.

4.2 Difference in Myosin-II and Mid1 distributions in WT and *rad24Δ S. pombe*

Myosin-II is a motor protein and, like other CAR constriction machinery components, is recruited to the CAR via Mid1 at the onset of mitosis (Wu, et al., 2003). Myosin-II in fission yeast is composed of three subunits - heavy chain Myo2, and light chains Cdc4 and Rlc1. During cytokinesis, myosin-II cables are thought to condense oppositely situated F-actin filaments into closer proximity and cause CAR constriction (Kamasaki, et al., 2007), often times called the “purse-string model.” Myosin-II subunits and IQGAP Rng2 are recruited to the CAR at roughly the same time, ~6-9 minutes before SPB separation, and earlier than Cdc15 and formin Cdc12, which contribute to F-actin polymerization at ~2 minutes into mitosis (Wu, et al., 2003).

Even though Mid1 is present at the medial cortex throughout G2 (Paoletti and Chang, 2000), assembly of all the necessary contractile components and maturation of medial cortical nodes is initiated by mitotic entry and fuels mitotic commitment (Tanaka, et al., 2001). Plo1, in addition to its regulation of Mid1 nuclear export at mitotic onset, phosphorylates Mid1 and provides a binding site for IQGAP Rng2 (Eng, et al., 1998) to influence the timing of myosin-II recruitment (Almonacid et al., 2011; Takaine, et al., 2012). Maturation of nodes at mitotic onset is marked by the loss and gain of numerous components, and myosin-II motor activity has been shown to be involved in cortical actin turnover during cytokinesis, which indicates it may play a role in F-actin disassembly (Guha, et al., 2005). In *mid1Δ* cells, the C-terminal portion of Myo2 (Myo2Ct-YFP; aa 1394-1596) failed to accumulate at the medial cortex during G2 or at maturing nodes during mitosis (Motegi, et al., 2004), indicating that Myo2’s N-terminus is required to bind Mid1. Even though Mid1 was shown to be essential for myosin-II’s

initial accumulation, an abnormal CAR was slowly formed by Myo2 in *mid1* Δ cells which disintegrated during F-actin disassembly, while the CAR in WT cells did not (Motegi, et al., 2004). A similar result was seen in SIN inactive mutants that form an ectopic CAR early in mitosis that dissipate in anaphase, suggesting that SIN signaling is required for CAR maintenance in late mitosis (Balasubramanian, et al., 1998). We hypothesized that Rad24 could play a role in both of these processes and assayed fluorescent Rlc1 using the same live cell videomicroscopy, statistical analysis, timed cytokinetic events, and K-S ratio plots as F-actin in WT and *rad24* Δ cells to check for spatial and temporal differences in myosin-II localization.

Unlike F-actin, Myosin Rlc1 exhibits significantly delayed recruitment to the CAR in *rad24* Δ cells (WT mean -10.33 min, SD 6.01 vs. *rad24* Δ mean -3.13 min, SD 1.55; $p=0.0039$) (Figure 18B and C), which also resulted in a delay of the onset of CAR constriction (WT mean 15.8 min, SD 6.52 vs. *rad24* Δ mean 27.73 min, SD 7.91; $p < 0.0001$) (Figure 18B and C) as well as delayed completion of CAR constriction (WT mean 44.57 min, SD 3.98 vs. *rad24* Δ mean 74.4 min, SD 6.22; $p < 0.0001$). A lag in CAR dissolution was also evident in *rad24* Δ cells (WT mean 48 min, SD 3.78 vs. *rad24* Δ mean 80.80 min, SD 6.18; $p < 0.0001$) (Figure 18B and C). The delay in CAR dissolution is visibly evident in the K-S distribution ratio curve for Rlc1, as the differences increase throughout cell division and are drawn out over a period of ~2 hours (Figure 18A).

rad24 Δ cells also displayed significant differences in the timing of ring sharpness, an indicator of full myosin-II recruitment to the CAR (WT mean 8.4 min, SD 5.42 vs. *rad24* Δ mean 18 min, SD 6.24; $p < 0.0001$) (Figure 18B and C). SPB maximum

separation (WT mean 22.6 min, SD 7.42 vs. *rad24* Δ mean 39.13 min, SD 7.07; $p < 0.0001$) (Figure 18B and C) and completed cytokinesis were also deferred (WT mean 68.56 min, SD 7.83 vs. *rad24* Δ mean 104.83 min, SD 6.7; $p < 0.0001$).

Since myosin-II is recruited to the CAR slightly earlier than the onset of actin polymerization (Laporte, et al., 2011), *rad24* Δ cells may have delayed CAR constriction, due to the lapse in timely recruitment of Myosin because of misplaced Mid1 (See supplemental figure S1 of this thesis for an overlay of Mid1-NeonGreen and Rlc1-tomato). This is in contrast to the accelerated CAR constriction seen in the Mid1^{4RXXSA} mutant and may be because although Sid2 phosphorylation is required for Mid1 to dissociate from the CAR prior to constriction, Rad24 is needed for the correct timing of Clp1 or Mid1 in the cytoplasm during mitosis. Since Clp1 is a regulator of mitotic exit, perhaps Rad24 is required for completion of the cytokinetic checkpoint. Additionally, if Rad24 is required for Mid1 to stay in the cytoplasm, a delay in Myosin recruitment to the CAR and CAR constriction would be consistent with Mid1 being stuck at the nodes, as in the Mid1^{4RXXSA} mutant. However, CAR constriction is not accelerated in *rad24* Δ cells as was noted in the Mid1^{4RXXSA} mutant, so this effect seems to be Rad24-dependent.

Mid1-NeonGreen Sid4-RFP Rlc1-Tomato WT vs. *rad24* Δ

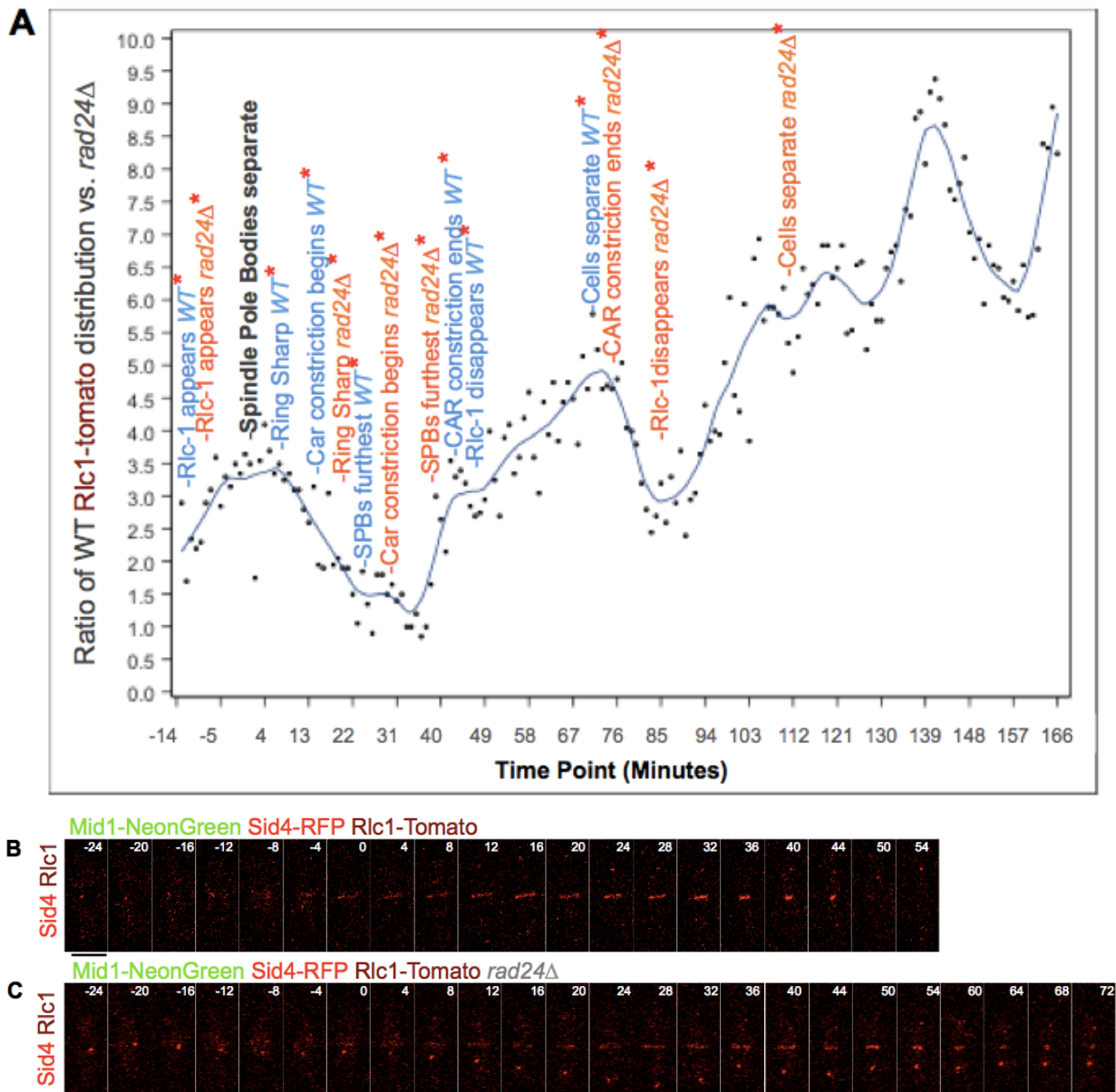


Figure 18. *rad24* Δ cells show delayed Myosin recruitment to the CAR and delays in CAR constriction (A) K-S test graph of distribution ratio of Rlc1-Tomato in WT vs. *rad24* Δ *S. pombe* strains. Number of cells analyzed: n=20 for Mid1-NG sid4-RFP Rlc1-tomato, strain #197 and n=25 for Mid1-NG sid4-RFP Rlc1-tomato *rad24* Δ , strain #354. (B) Rlc1-Tomato in WT strain #197. (C) Rlc1-Tomato in *rad24* Δ strain #354. Scale bar = 5 μ m.

If, like Clp1 and Cdr2, Mid1 requires Rad24 binding in order to sequester it in the cytoplasm during mitosis and prolong SIN signaling until the completion of the cytokinetic checkpoint, we hypothesized that Mid1-NeonGreen would return to the nucleus earlier in *rad24Δ* cells. We also surmised that Rad24 may play a role in transitioning Mid1 through various oligomerization states – Rad24 may bind to and prevent only Mid1 monomers from returning to the nucleus early or it may stabilize oligomers at the cell membrane. To test these hypotheses, Mid1-NeonGreen was expressed in the same cell line as Rlc1-tomato and assayed using the same live cell videomicroscopy, statistical analysis, timed cytokinetic events, and K-S ratio plots as stated above and in Methods section 2.2.

The ratio of WT Mid1-NeonGreen protein distribution vs. *rad24Δ* shows changes that are concentrated early on in cell division and continue to increase up to ring constriction (Figure 19A). This could be because of misplaced Cdr2 during the previous round of mitosis resulting in a deficient Cdr2 amount at the cell cortex to anchor Mid1 correctly. Mid1-NeonGreen's full recruitment to the CAR was delayed in *rad24Δ* cells (WT mean 9.27 min, SD 5.35 vs. *rad24Δ* mean 25.47 min, SD 7.92; $p < 0.0001$) (Figure 19B and C), and Mid1-NeonGreen disperses from the CAR later (WT mean 34.53 min, SD 7.78 vs. *rad24Δ* mean 92.47 min, SD 23.95; $p < 0.0001$) (Figure 19B and C) resulting in significantly deferred completion of cytokinesis (WT mean 68.56 min, SD 7.83 vs. *rad24Δ* mean 105.67 min, SD 6.8; $p < 0.0001$). This effect was also observed in the Mid1^{4RXXSA} phosphosite mutant; Mid1^{4RXXSA}-GFP was stuck at the cell cortex when it should have dispersed at CAR constriction (DeWitt A, Gould K, and Hart D; article in process) as was seen with WT Mid1-GFP.

Mid1-NeonGreen also appears to be more concentrated at the cell cortex and nodes rather than in the nucleus ~20 minutes prior to the onset of mitosis (Figure 19B and C, -20 min). It also appears that Mid1-NeonGreen is more concentrated in the new daughter cells' nuclei after dissociation from the CAR (Figure 19C, 40 min through 72min). This is what we would expect to see if Rad24 is required for Mid1 to be sequestered in the cytoplasm during interphase – a return of Mid1 to the nucleus early that is suggestive of a SIN/Rad24-dependent mechanism for control over Mid1 localization. SPBs also show a delay in reaching their furthest separation (WT mean 22.6 min, SD 7.42 vs. *rad24*Δ mean 38.4 min, SD 7.38; $p < 0.0001$), which indicates a delayed coupling of cytokinesis to mitosis. Rad24 has been shown to colocalize with SIN components Sid4 and Cdc11 at the SPBs (Mishra, et al., 2005), so perhaps the delay in mitotic progression is due to a lack of Rad24 to prolong SIN signaling.

In addition to these delays, which were also observed in LifeAct-GFP and Rlc1-tomato distributions, there is an additional peak in the Mid1-NeonGreen distribution ratio at 140 minutes past the onset of mitosis. This may be attributed to Mid1-NeonGreen localizing to the nucleus earlier in *rad24*Δ cells than WT and would support the hypothesis that Rad24 may sequester Mid1 monomers before returning to the nucleus. This result is similar to what was seen in the *mid1*^{3A} mutant (Sun, et al., 2015).

Mid1-NeonGreen Sid4-RFP Rlc1-Tomato WT vs. *rad24* Δ

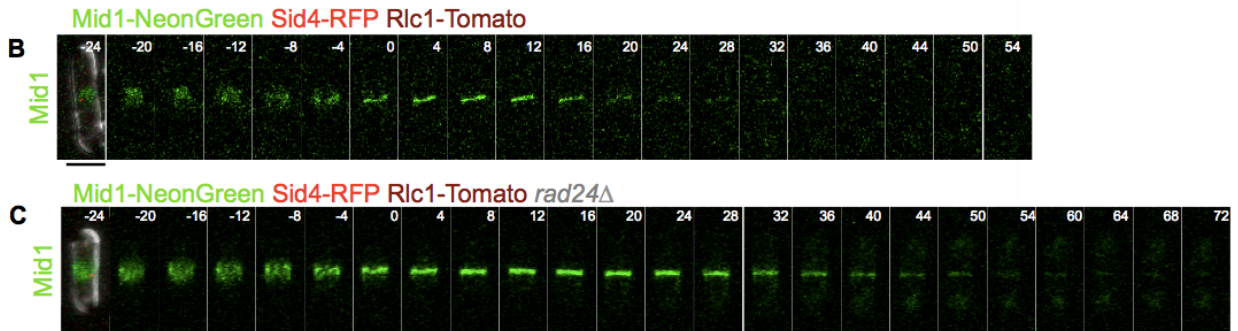
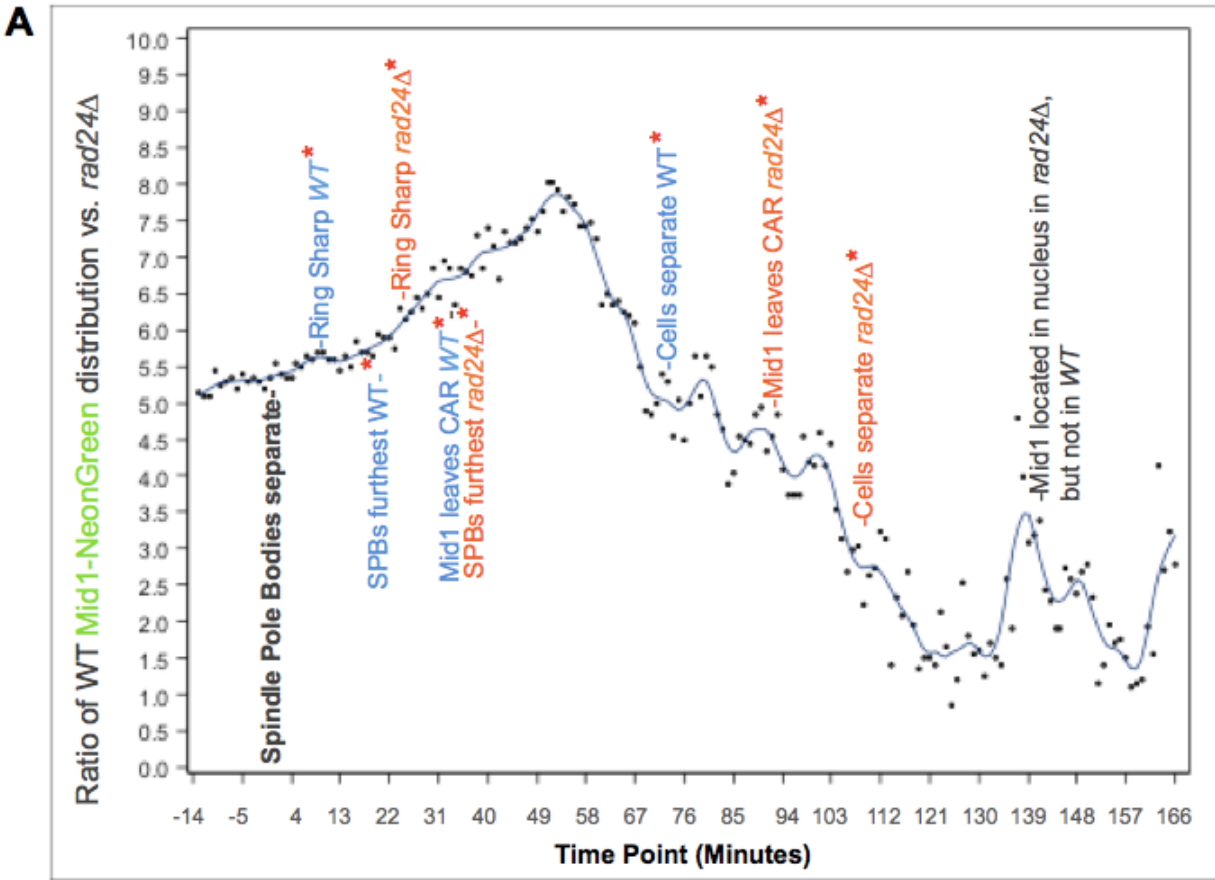


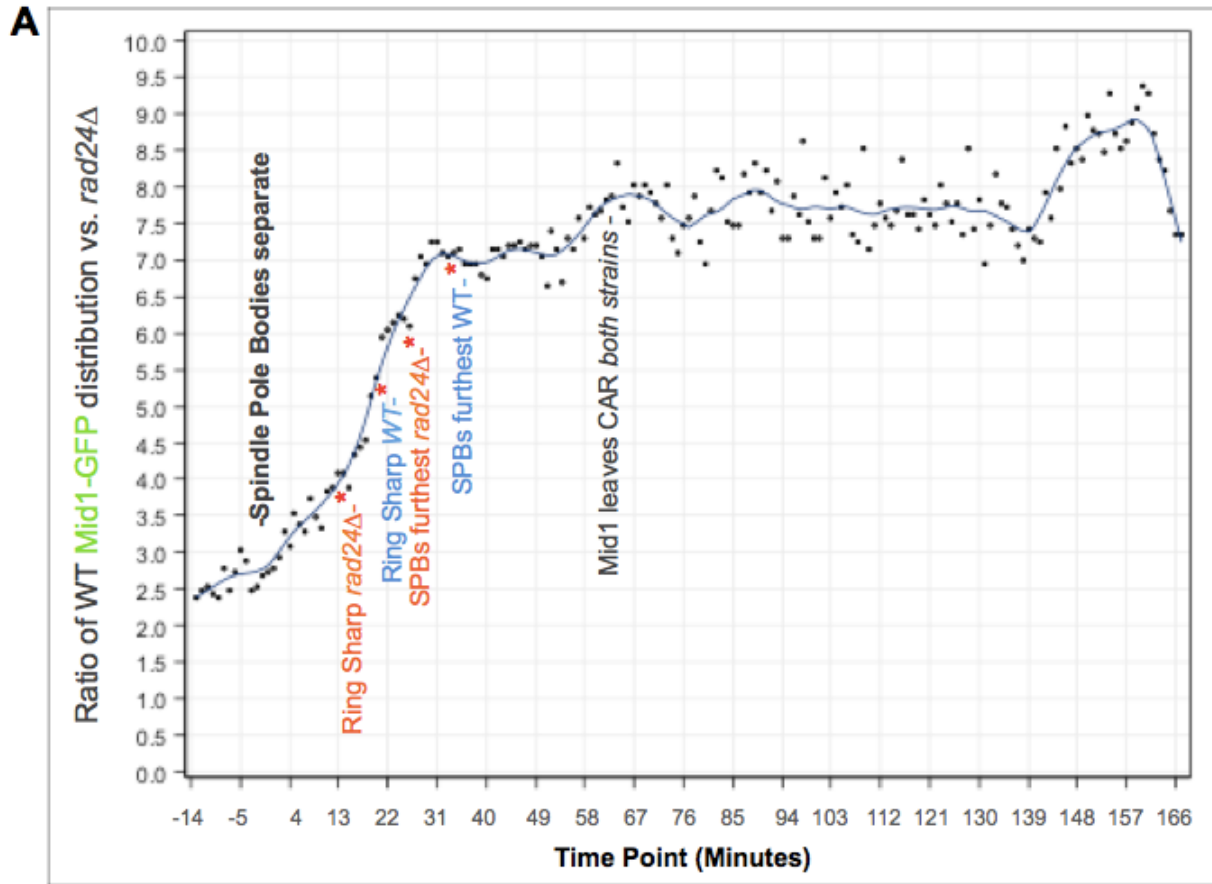
Figure 19. *rad24* Δ cells show cortical adherence of Mid1 during G2 and a premature return to the nucleus. (A) K-S test graph of distribution ratio of Mid1-NeonGreen in WT vs. *rad24* Δ *S. pombe* strains. Number of cells analyzed: $n=20$ for Mid1-NG sid4-RFP Rlc1-tomato, strain #197 and $n=25$ for Mid1-NG sid4-RFP Rlc1-tomato *rad24* Δ , strain #354. (B) Mid1-NeonGreen in WT strain #197. (C) Mid1-NeonGreen in *rad24* Δ strain #354. *rad24* Δ cells show significant delays in full Mid1-NG recruitment (Figure B:8 min vs. Figure C:20 min), Mid1-NG dispersion from the CAR (B:36 min vs. C:72 min), and increased nuclear Mid1-NG after CAR constriction. Scale bar = 5 μ m.

4.3 Difference in Mid1 distribution between wild type and *rad24* Δ *S. pombe*

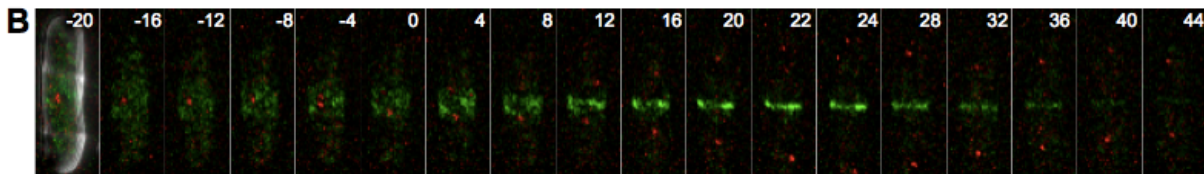
To test Mid1 localization in *rad24* Δ cells independent of Rlc1 fluorescent labeling, and to test labeling Mid1 with a second fluorescent tag, *S. pombe* strains expressing Mid1-GFP and Sid4-RFP only were assayed for differences in protein distributions using the same live cell videomicroscopy, statistical analysis, timed cytokinetic events, and K-S ratio plots as stated above with Mid1-NeonGreen. Mid1-NeonGreen gives a brighter signal with lower background, and is a more accurate depiction of Mid1 protein localization in these assays, and final conclusions were based off the Mid1-NeonGreen data. Nevertheless, Mid1-GFP localization (Figure 20) shows similar delays to the Mid1-NeonGreen localization (Figure 19) when comparing WT to *rad24* Δ cells.

It appears that Mid1-GFP was fully recruited (sharp ring) to the cell cortex earlier in *rad24* Δ cells (WT mean 23.08 min, SD 9.25 vs. *rad24* Δ mean 15.32 min, SD 8.47; $p = 0.0022$) (Figure 20B and C; ~22 min vs. ~16min). This effect was not apparent in the Mid1-NeonGreen data. The SPBs again showed a delay in reaching their furthest separation (WT mean 34.69 min, SD 10.74 vs. *rad24* Δ mean 26.79 min, SD 6.96; $p = 0.0021$). The unpaired student t-test was not significant for timing of Mid1 leaving the CAR in analysis of these cells, but roughly occurred at the same time, ~62 minutes after mitotic onset. The peak in ratio distribution difference shown again at ~140 minutes could be due to Mid1-GFP returning to the nucleus earlier, as in the Mid1-NeonGreen data. Also, as in the Mid1-NeonGreen data, most of the difference in distribution occurs as the CAR is forming and constricting.

Mid1-GFP Sid4-RFP WT vs. *rad24* Δ



Mid1-GFP Sid4-RFP



Mid1-GFP Sid4-RFP *rad24* Δ

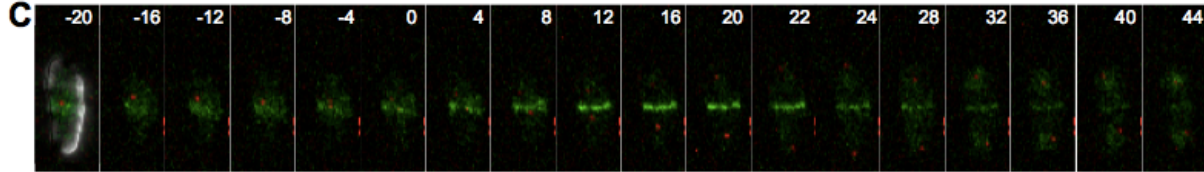


Figure 20. *rad24* Δ cells show cortical adherence of Mid1 during G2 and a premature return to the nucleus. (A) K-S test graph of distribution ratio of Mid1-GFP in WT vs. *rad24* Δ *S. pombe* strains. Number of cells analyzed: n=26 for Mid1-GFP Sid4-RFP, strain #110 and n=28 for Mid1-GFP Sid4-RFP *rad24* Δ , strain #353. (B) Mid1-GFP in WT strain #110. (C) Mid1-GFP in *rad24* Δ strain #353. Scale bar = 5 μ m.

5 Discussion

In animal and yeast cells, the proper CAR formation and constriction is heavily reliant on the temporal regulation, phosphorylation, and localization of key proteins. Removal of one of these key proteins, Rad24, has distinct consequences on the timing of major events in cell division. Rad24 is known to interact with a handful of cytokinetic proteins and some of their regulators, such as Cdc14-like Phosphatase Clp1, a temporary CAR component and regulator of mitotic exit (Wolfe, et al., 2006). Clp1 binds to Mid1 and is anchored to the division site through an interaction with the central region of Mid1 (aa 431-481; Clifford, et al., 2008), and SIN activity restricts Clp1 from returning to the nucleolus until cell division is complete (Chen, et al., 2008). Our results show that Mid1 is affected by the deletion of Rad24 by remaining nodal during G2 and returning to the nucleus early after CAR constriction, similar to Clp1-6A phosphomutant cells (Chen, et al., 2008). Additionally, it has been shown that Clp1 activity regulates Cdc15 and other components of CAR assembly and stability – myosin II in particular – and that Mid1 is required to recruit Clp1 to the CAR (Clifford, et al., 2008). The absence of Rad24 to directly facilitate cytoplasmic sequestration of Mid1, in the same manner as with Clp1, would cause delays and/or perturbations in CAR formation and constriction.

Rad24 also plays an important role in Cdr2 localization, which is essential for the formation of Type I CAR precursor nodes (Rincon, et al., 2017; Almonacid, et al., 2009; Moseley, et al., 2009). Cortical targeting of Mid1 is dependent on its interaction with Cdr2 (Breeding, et al., 1998; Almonacid, et al., 2009) and Mid1 localization is controlled by Cdr2-containing Type I medial cortical nodes throughout interphase (Akamatsu, et al., 2014). Sid2 plays a role in Cdr2 dissociating from the cell cortex during division

(Rincon, et al., 2017). In *rad24* Δ cells, Cdr2-mEGFP did not leave the cell cortex during mitosis, was redistributed from the medial cortex toward the cell tips, and the intensity of Cdr2-mEGFP did not increase in the cytoplasm during mitosis (Rincon, et al., 2017). SIN activity restricts Cdr2 from returning to the medial cortex until cell division is complete (Rincon, et al., 2017). The loss of Rad24 could also affect Cdr2 localization to the cytoplasm during mitosis and cytokinesis, which in turn could have an effect on recruiting Mid1 to Type I nodes during the next round of cell division, producing a prolonged cytokinesis. This could account for changes in Mid1 distribution early in cell division, before CAR constriction occurs.

However, the interactions of Rad24 with Clp1 and Cdr2 would most likely only indirectly affect Mid1. Although Cdr2 recruits Mid1 to cell cortex and Type I nodes during interphase (Almonacid, et al., 2009; Moseley, et al., 2009), both proteins disperse from the CAR in a SIN-dependent manner as specific and separate entities; Cdr2 prior to mitotic entry (Akamatsu et al, 2014), and Mid1 in late anaphase just before CAR constriction (DeWitt A, Gould K, and Hart D; article in progress). The interaction that Cdr2 has with Rad24 is most likely independent from Mid1 because of this. Since SIN activation during cell division promotes Cdr2 interaction with Rad24 (Rincon, et al., 2017), Rad24 would not be in complex with Cdr2 at the same time that it interacts with Mid1 in the Type I interphase nodes (Rincon, et al., 2014). Likewise, Clp1 remained in its typical localization configuration - nucleolar during interphase and cytoplasmic during mitosis - even in *rad24* Δ cells. Clp1 was ectopically bound to the nucleolus in *rad24* Δ cells only when cytokinetic stress was induced with Latrunculin A (Mishra, et al., 2005), which depolymerizes actin filaments (Ayscough, et al., 1997). The delays brought on in

the data presented here would not be influenced by this effect on Clp1 without the presence of Latrunculin A.

The cytokinetic delays seen in this work may be explained more readily when we examine the timing of key events in WT *S. pombe* cells during cytokinesis (Wu, et al., 2003). Mid1 shuttles from nucleus to nodes in G2 roughly 90 minutes before mitotic onset marked by SPB separation (Nabeshima, et al., 1998), but is mostly located in the nucleus during interphase. Myo2, Cdc4, Rlc1, Rng2 are located in the cytoplasm during interphase (Wu, et al., 2003). The G2/M transition occurs roughly 10 minutes prior to mitotic onset; upon mitotic entry, Mid1 is exported from the nucleus, and cortical Mid1 concentration increases with Plo1 activation and initiates the recruitment of CAR components to maturing cytokinetic nodes, starting with Rng2 and the myosin II subunits (Bähler, et al., 1998; Almonacid, et al., 2011). Plo1 phosphorylation triggers Rng2 binding on Mid1's N-terminus (aa 1-422), the portion of the protein associated with assembling the cytokinetic nodes and modulating cortical stability (Almonacid, et al., 2011).

Interestingly, the region of Mid1 phosphorylated by Plo1 where Rng2 binds, along with the Sid2 phosphorylation site at S432, were found to be conserved in Mid1, at least among some yeasts (section 3.3 of this thesis). By 2 minutes after mitotic onset, Mid1 has completed nuclear export and is stably dimerized at its C2 domains at the cell cortex (Sun, et al., 2015), and its need for Cdr2-anchorage is bypassed by its amphipathic helix binding directly to the plasma membrane (Almonacid, et al., 2011). Cdc15 and Cdc12 join Mid1 as nodes begin to condense and coalesce into the CAR (Fankhauser, et al., 1995; Carnahan and Gould, 2003). It is of note that actin regulator

Cdc15 and formin Cdc12 are known SIN targets (Hatchet and Simanis, 2008; Bohnert, et al., 2013), and their mislocalization could have definitive effects on the CAR formation and constriction events downstream, such as actin filamentation and bundling. Also, Clp1 localization to the CAR is required for Cdc15 dephosphorylation, which affects CAR stability (Clifford, et al., 2008).

From 2 to 10 minutes after mitotic onset, actin polymerization begins (Arai and Mabuchi, 2002) and Tropomyosin Cdc8 as well as α -actinin Ain1 join the CAR at this time (Wu, et al., 2001; Balasubramanian, et al., 1992). By 10 minutes after mitotic onset, the CAR is fully mature (sharp) with all the necessary components for constriction in place - Mid1, Myo2, Cdc4, Rlc1, Rng2, Cdc15, Cdc12, actin, Cdc8, and Ain1 (Wu, et al., 2003). As the onset of CAR constriction coincides with the peak in SIN signaling (Sparks, et al., 1999; Bohnert, et al., 2013), at this point Sid2 has relocated from the SPBs to the CAR to form the mitosis-cytokinesis link. The Septins, GTP-binding proteins that associate with the plasma membrane (Longtine, et al., 1996; Berlin et al., 2003; Tasto et al., 2003), and the second myosin heavy chain, Myp2, join the CAR 20 minutes into cytokinesis to facilitate CAR maintenance and eventual cell separation (Wu, et al., 2003; Takaine, et al., 2015). Mid1 is dispersed from the CAR, and at 37 minutes past mitotic entry, anaphase has completed and CAR contraction and disassembly begins (Wu, et al., 2003). CAR constriction is complete 67 minutes past mitotic onset, and daughter cells separate at 102 minutes (Wu, et al., 2003). Looking at these interactions, the cytokinetic delays brought on by the lack of Rad24 are most likely due to mislocalization of Mid1 early in CAR formation, while the cytokinetic nodes are maturing, just before mitotic onset.

SIN-dependent localization of Mid1 requires Rad24. It would make sense in light of the timing of these known interactions, that Rad24 transiently binds and sequesters Mid1 monomers in the cytoplasm. Mid1's dimer stabilization sites (aa 616-635) in the C2 domain (Sun, et al., 2015) are in close proximity to the region where Mid1 interacts with Clp1, Cdr2, and Rad24 (aa 329-531), and also to a site known to be involved in oligomer stabilization (aa 309-453; Clifford, et al., 2008; Almonacid, et al., 2009; Saha and Pollard, 2012b). It could be possible that dimerization and/or oligomerization inhibits Rad24 binding simply because phosphorylated Sid2 sites are structurally unavailable due to the number of Mid1 binding partners. The interaction between Mid1 and Rad24 potentially occurs when Mid1 is exported from the nucleus, or when it disperses from the CAR before constriction, or both. That Mid1 may bind to Rad24 in binding assays with Mid1-GFP and Mid1^{4RXXSA}-GFP isolated from cells mitotically synchronized in prometaphase may be more evidence for Mid1 monomers interacting preferentially with Rad24 (section 3.1 of this thesis). Even though our binding assays were an *in vitro* test, they remain a reflection of Mid1's phosphorylation state in early mitosis. The Mid1-NG mislocalization and cytokinetic delays seen in this data would make sense if this were the case. It would also preclude the notion of Rad24 stabilizing Mid1 oligomers at the cell cortex. Further research would be needed, however, to resolve how *mid1*^{3A} monomers are still shuttled back to the nucleus early in the presence of Rad24 (Sun et al., 2015).

Myosin regulatory light chain and F-actin recruitment are reliant on Rad24 for proper CAR recruitment and constriction. Delays in myosin regulatory light chain and actin recruitment to the CAR are consistent with previous results obtained with the

Mid1^{4RXXSA} mutant (DeWitt A, Gould K, and Hart D; article in progress), however, we report significantly deferred CAR constriction (section 4.1 and 4.2 of this thesis) with the absence of Rad24, as compared to accelerated CAR constriction seen in the Mid1^{4RXXSA} mutant. Rlc1 was recruited to the CAR early in Mid1^{4RXXSA} mutant cells, and this contributed to impairment of CAR assembly, disordered CAR structures, and accelerated CAR constriction (DeWitt A, Gould K, and Hart D; article in progress).

CAR assembly was also faster in cells expressing monomeric *mid1*^{3A} than in wild-type cells (Sun, et al., 2015), but rates of CAR constriction were the same. There are definite phenotypic similarities seen between the Mid1^{4RXXSA} phosphomutant, monomeric *mid1*^{3A} mutant, and *rad24*Δ cells, but it seems that the timing of events is affected differently. Further research to test for Sid2-dependent interactions between Rad24 and Cdc15 or Cdc12 could shed more light on how Rad24 affects CAR formation.

Mid1 is the common factor for division plane positioning through the CGN and SIN (Rincon and Paoletti, 2012). In addition, Mid1 could be the common factor for polarized cell growth and actin reorganization through the MOR and the SIN. More research is needed in this area to uncover the mechanistic link between the SIN and the MOR pathway. Further research in this area could involve more *in vivo* studies such as live cell videomicroscopy in *cdc12* and *cdc15* temperature sensitive mutants crossed with a *rad24*Δ strain, or more biochemical assays such as coimmunoprecipitation *in vivo* of Rad24/Mid1 from mitotically synchronized cells. Elucidation of Mid1's N-terminal crystal structure would also be extremely helpful. We conclude that Rad24 modulates CAR formation through Mid1 and that Rad24 is necessary for correct placement of F-

actin and myosin-II and proper CAR constriction. Due to the highly conserved nature of proteins involved in major *S. pombe* cytokinetic pathways, these findings could have wider implications for the study of cell division and cancer in humans and other higher organisms.

6 Supplemental

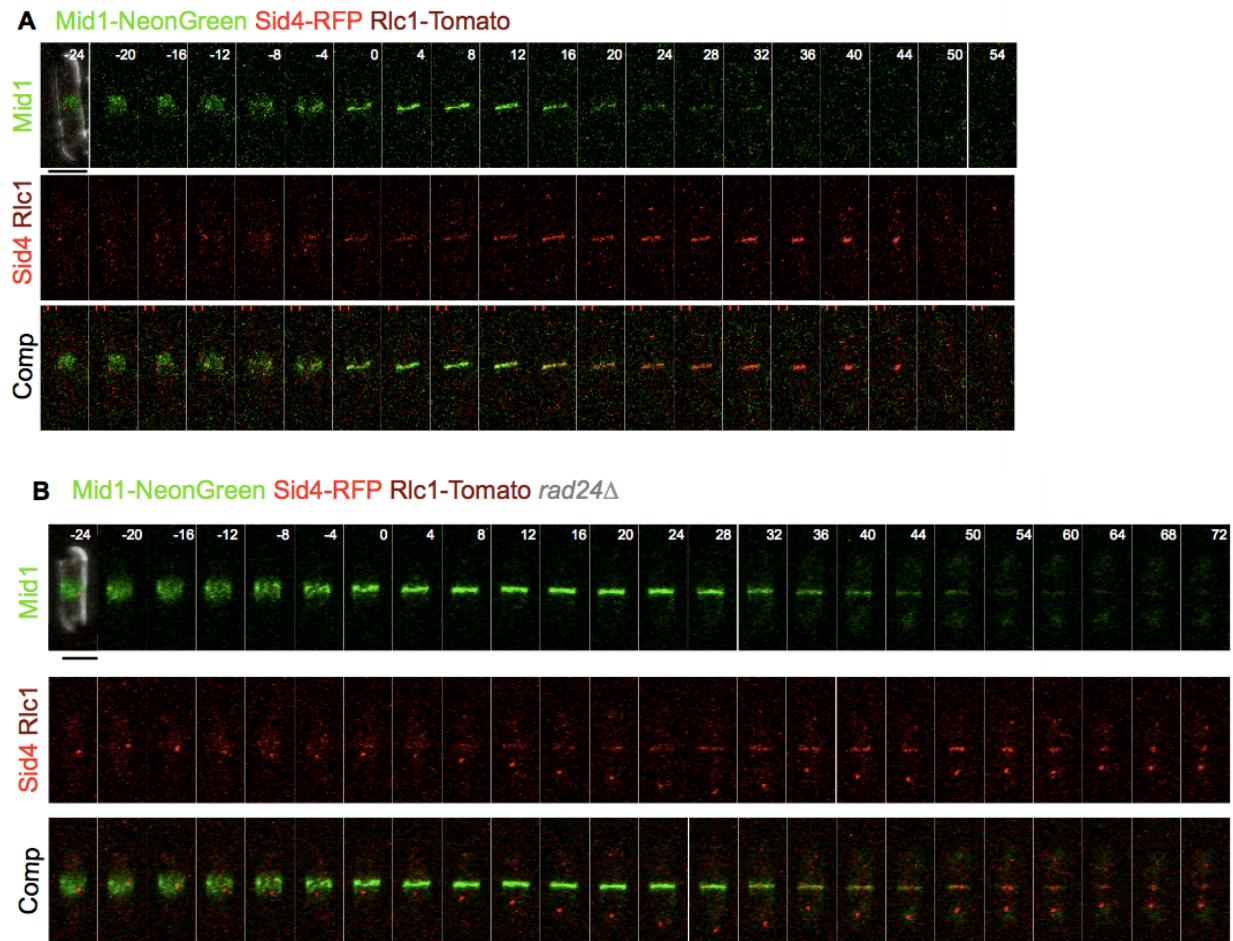


Figure S1. Delay in Mid1-facilitated assembly of the CAR coincides with a delay in Myosin recruitment to the CAR and deferred CAR constriction. An overlay of Mid1-NeonGreen and Rlc1 in the same dividing *S. pombe* cells is shown. (A) Mid1-NeonGreen and Rlc1-Tomato in Mid1-NG Sid4-RFP Rlc1-tomato strain #197. (B) Mid1-NeonGreen and Rlc1-Tomato in Mid1-NG Sid4-RFP Rlc1-tomato *rad24* Δ strain #354.

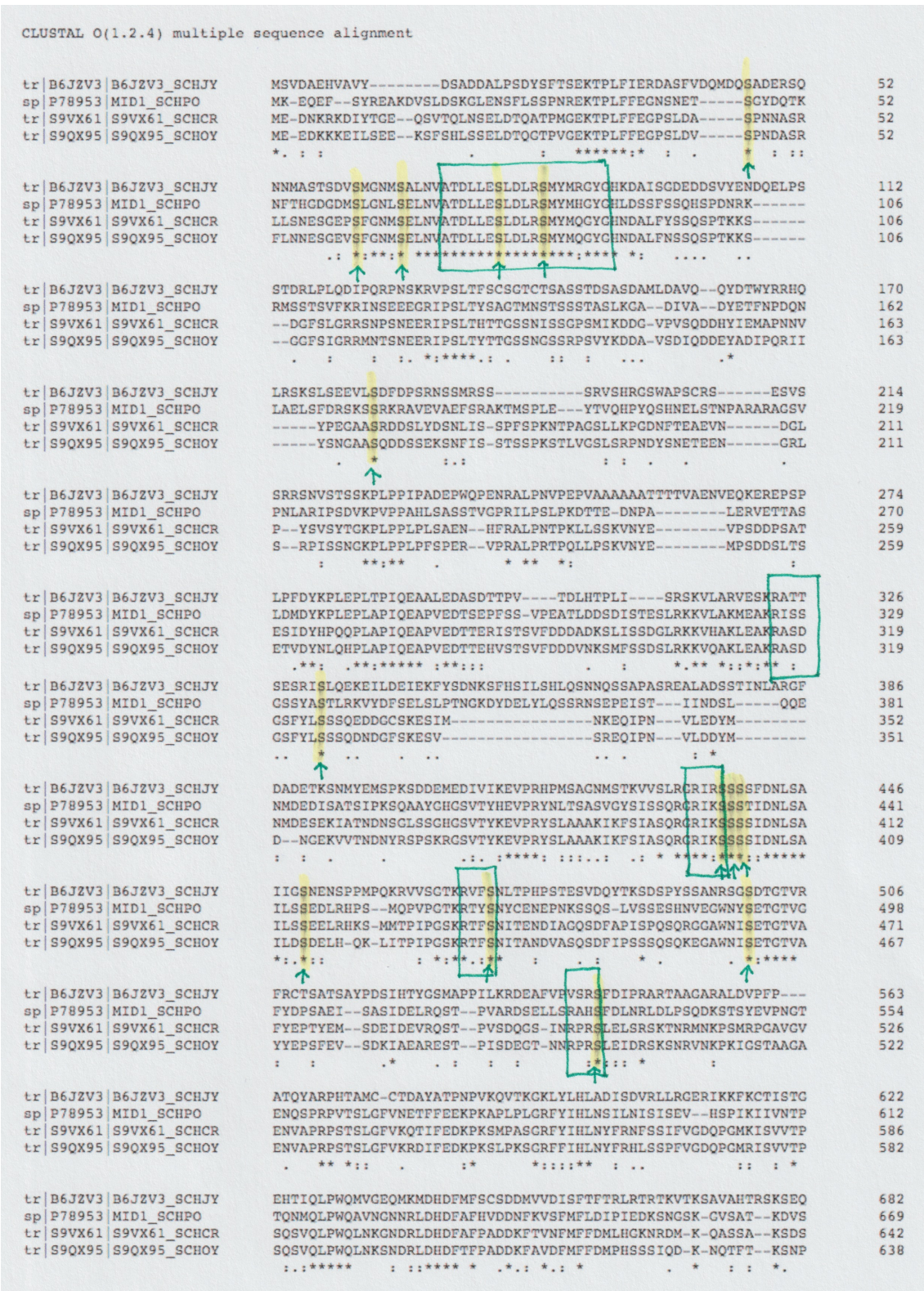
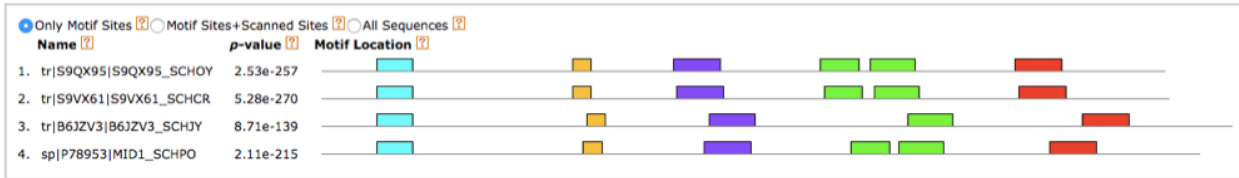


Figure S2. Clustal Omega Multiple Sequence Alignment of yeast Mid1 sequences reveals multiple conserved motifs and serines. Motifs important for node assembly and Sid2 phosphorylation are shown in green boxes. Conserved serines are highlighted in yellow.

A Motif Locations



B

E-value: 2.0e-017 Site Count: 4 Width: 21



Log Likelihood Ratio: 214 Information Content: 80.9 Relative Entropy: 77.3 Bayes Threshold: 9.79847

Name	Start	p-value	Sites
2. tr S9VX61 S9VX61_SCHCR	263	6.68e-28	SDDPSATESI DYKPPQLAPLQEAAPVEDTTE RISTSVFDDD
4. sp P78953 MID1_SCHPO	274	1.61e-25	RVETTASLDM DYKLEPLAPLQEAAPVEDTSE PFSSVFEATL
1. tr S9QX95 S9QX95_SCHOY	263	1.76e-24	SDDSLTSETV DYNLQPLAPLQEAAPVEDTTE HVTSTVFDDD
3. tr B6JZV3 B6JZV3_SCHJY	278	8.07e-20	KEREPSPLPF DYKLEPLTQEAALDASD TTFVTDLHTP

C

E-value: 5.4e-044 Site Count: 4 Width: 48



Log Likelihood Ratio: 468 Information Content: 165.4 Relative Entropy: 168.8 Bayes Threshold: 10.4917

Name	Start	p-value	Sites
2. tr S9VX61 S9VX61_SCHCR	579	2.02e-58	SSIFVGDQPG MKISVYTPSQTSPVQLPWQQLVKNV GKNRDMKQAS
1. tr S9QX95 S9QX95_SCHOY	575	4.42e-56	SSPFVGDQPG MKISVYTPSQTSPVQLPWQQLVKNV SSSIQDKNQI
4. sp P78953 MID1_SCHPO	605	3.39e-47	NISISEVHSP IKIIVNTPQNMQLPWQAVN EDKSNKSGV
3. tr B6JZV3 B6JZV3_SCHJY	615	5.44e-34	RLLRGERIKK FKCTISTGELIQLWQVGEQ RTRTKVKKSA

D

E-value: 3.7e-047 Site Count: 4 Width: 50



Log Likelihood Ratio: 490 Information Content: 180.8 Relative Entropy: 176.8 Bayes Threshold: 9.75071

Name	Start	p-value	Sites
1. tr S9QX95 S9QX95_SCHOY	727	1.50e-60	GKTGLKINDV IGNLSLCLYIPPELSPVPESS GTSVRRRFVAV
2. tr S9VX61 S9VX61_SCHCR	731	1.17e-58	GKSDLSLNDI IGNLSLCLYIPPELSPVPESS GTSVRRRFVAV
4. sp P78953 MID1_SCHPO	763	5.69e-50	VKINSIGKRT LGNLTLCLYIPPELSPVPESS DSSIRRRFVAV
3. tr B6JZV3 B6JZV3_SCHJY	797	4.65e-40	PSESLVPCV IGRISLRCLVPELMDDEL KGALQKRFAM

Figure S3. Additional Logos from MEME Motif Analysis reveals conserved residues among yeasts. B, C, and D are #2 (gold), #5 (green), and #6 (red) motifs, respectively.

7 References

Akamatsu M, Berro J, Pu KM, Tebbs IR, Pollard TD. Cytokinetic Nodes in Fission Yeast Arise from Two Distinct Types of Nodes That Merge during Interphase. *The Journal of Cell Biology*. 2014;204.6: 977–988.

Almonacid M, Moseley JB, Janvore J, Mayeux A, Fraiser V, Nurse P, Paoletti A. Spatial control of cytokinesis by Cdr2 kinase and Mid1/anillin nuclear export. *Curr Biol*. 2009 Jun 9;19(11):961-6.

Almonacid M, Celton-Morizur S, Jakubowski JL, Dingli F, Loew D, Mayeux A, Chen JS, Gould KL, Clifford DM, Paoletti A. Temporal control of contractile ring assembly by Plo1 regulation of myosin II recruitment by Mid1/anillin. *Curr Biol*. 2011 Mar 22;21(6):473-9.

Altschul SF, Madden TL, Schäffer AA, Zhang J, Zhang Z, Miller W, Lipman DJ. Gapped BLAST and PSI-BLAST: a new generation of protein database search programs. *Nucleic Acids Res*. 1997 Sep 1;25(17):3389-402.

Arai R, Mabuchi I. F-actin ring formation and the role of F-actin cables in the fission yeast *Schizosaccharomyces pombe*. *J Cell Sci*. 2002 Mar 1;115(Pt 5):887-98.

Ayscough KR, Stryker J, Pokala N, Sanders M, Crews P, Drubin DG. High rates of actin filament turnover in budding yeast and roles for actin in establishment and maintenance of cell polarity revealed using the actin inhibitor latrunculin-A. *J Cell Biol*. 1997 Apr 21;137(2):399-416.

Bähler J and Pringle JR. Pom1p, a fission yeast protein kinase that provides positional information for both polarized growth and cytokinesis. *Genes Dev*. 1998 May 1;12(9):1356-70.

Bähler J, Steever AB, Wheatley S, Wang YI, Pringle JR, Gould KL, McCollum D. Role of polo kinase and Mid1p in determining the site of cell division in fission yeast. *J Cell Biol*. 1998 Dec 14;143(6):1603-16.

Bailey TL, Boden M, Buske FA, Frith M, Grant CE, Clementi L, Ren J, Li WW, Noble WS. MEME Suite: tools for motif discovery and searching. *Nucleic Acids Res*. 2009 Jul 1; 37(Web Server issue): W202–W208.

Balasubramanian MK, McCollum D, Chang L, Wong KC, Naqvi NI, He X, Sazer S, Gould KL. Isolation and characterization of new fission yeast cytokinesis mutants. *Genetics*. 1998 Jul;149(3):1265-75.

Balasubramanian MK, Helfman DM, Hemmingsen SM. A new tropomyosin essential for cytokinesis in the fission yeast *S. pombe*. *Nature*. 1992 Nov 5; 360(6399):84-7.

Barnum KJ and O'Connell MJ. Cell cycle regulation by checkpoints. *Methods Mol Biol.* 2014;1170:29-40.

Berlin A, Paoletti A, Chang F. Mid2p stabilizes septin rings during cytokinesis in fission yeast. *J Cell Biol.* 2003 Mar 31; 160(7):1083-92.

Bohnert KA, Grzegorzewska AP, Willet AH, Vander Kooi CW, Kovar DR, Gould KL. SIN-dependent phosphoinhibition of formin multimerization controls fission yeast cytokinesis. *Genes Dev.* 2013 Oct 1;27(19):2164-77.

Breeding CS, Hudson J, Balasubramanian MK, Hemmingsen SM, Young PG, Gould KL. The *cdr2(+)* gene encodes a regulator of G2/M progression and cytokinesis in *Schizosaccharomyces pombe*. *Mol Biol Cell.* 1998 Dec;9(12):3399-415.

Carnahan RH, Gould KL. The PCH family protein, Cdc15p, recruits two F-actin nucleation pathways to coordinate cytokinetic actin ring formation in *Schizosaccharomyces pombe*. *J Cell Biol.* 2003 Sep 1;162(5):851-62.

Celton-Morizur S, Bordes N, Fraissier V, Tran PT, Paoletti A. C-terminal anchoring of mid1p to membranes stabilizes cytokinetic ring position in early mitosis in fission yeast. *Mol Cell Biol.* 2004 Dec;24(24):10621-35.

Celton-Morizur S, Racine V, Sibarita JB, Paoletti A. Pom1 kinase links division plane position to cell polarity by regulating Mid1p cortical distribution. *J Cell Sci.* 2006 Nov 15;119(Pt 22):4710-8.

Chang F, Woollard A, Nurse P. Isolation and characterization of fission yeast mutants defective in the assembly and placement of the contractile actin ring. *J Cell Sci.* 1996 Jan;109 (Pt 1):131-42.

Chang F, Drubin D, Nurse P. Cdc12p, a Protein Required for Cytokinesis in Fission Yeast, Is a Component of the Cell Division Ring and Interacts with Profilin. *J Cell Biol.* 1997 Apr 7; 137(1): 169–182.

Chang L and Gould KL. Sid4p is required to localize components of the septation initiation pathway to the spindle pole body in fission yeast. *Proc. Natl. Acad. Sci. USA* 2000 May 9;97:5249–5254.

Chen CT, Feoktistova A, Chen JS, Shim YS, Clifford DM, Gould KL, McCollum D. The SIN Kinase Sid2 Regulates Cytoplasmic Retention of the *S. pombe* Cdc14-like Phosphatase Clp1. *Current Biology.* October 2008; 18, no. 20:1594–99.

Clifford DM, Wolfe BA, Roberts-Galbraith RH, McDonald WH, Yates JR 3rd, Gould KL. The Clp1/Cdc14 phosphatase contributes to the robustness of cytokinesis by association with anillin-related Mid1. *J Cell Biol.* 2008 Apr 7;181(1):79-88.

Cortés JC, Sato M, Muñoz J, Moreno MB, Clemente-Ramos JA, Ramos M, Okada H, Osumi M, Durán A, Ribas JC. Fission yeast Ags1 confers the essential septum strength needed for safe gradual cell abscission. *J Cell Biol.* 2012 Aug 20;198(4):637-56.

Eng K, Naqvi NI, Wong KC, Balasubramanian MK. Rng2p, a protein required for cytokinesis in fission yeast, is a component of the actomyosin ring and the spindle pole body. *Curr Biol.* 1998; 8:611–621.

Deng L, Baldissard S, Kettenbach AN, Gerber SA, Moseley JB. Dueling kinases regulate cell size at division through the SAD kinase Cdr2. *Curr Biol.* 2014 Feb 17; 24(4): 428–433.

Daga RR, Lahoz A, Muñoz MJ, Moreno S, Jimenez J. Etd1p is a novel protein that links the SIN cascade with cytokinesis. *EMBO J.* 2005 Jul 6; 24(13): 2436–2446.

Das M, Wiley DJ, Chen X, Shah K, Verde F. The conserved NDR kinase Orb6 controls polarized cell growth by spatial regulation of the small GTPase Cdc42. *Curr Biol.* 2009 Aug 11;19(15):1314-9.

DeWitt A, Schneider P, Foxa G, Gould K, and Hart D. NDR Kinase Sid2 phosphorylates and disperses Anillin-related Mid1 from the Division Site Contributing to Contractile Actomyosin Ring Integrity During Cytokinesis. Article in progress.

Fankhauser C, Marks J, Reymond A, and Simanis V. The *S. pombe* cdc16 gene is required both for maintenance of p34cdc2 kinase activity and regulation of septum formation: a link between mitosis and cytokinesis? *EMBO J.* 1993 Jul;12(7):2697-704.

Fankhauser C, Reymond A, Cerutti L, Utzig S, Hofmann K, Simanis V. The *S. pombe* cdc15 gene is a key element in the reorganization of F-actin at mitosis. *Cell.* 1995 Aug 11;82(3):435-44.

Ford J, al-Khodairy F, Fotou E, Sheldrick KS, Griffiths DJ, Carr AM. 14-3-3 protein homologs required for the DNA damage checkpoint in fission yeast. *Science.* 1994; 265:533–535.

Fu H, Subramanian RR, Masters SC. 14-3-3 proteins: structure, function, and regulation. *Annu Rev Pharmacol Toxicol.* 2000;40:617-47.

Furge KA, Wong K, Armstrong J, Balasubramanian M, Albright CF. Byr4 and Cdc16 form a two-component GTPase-activating protein for the Spg1 GTPase that controls septation in fission yeast. *Curr Biol.* 1998 Aug 27;8(17):947-54.

Gould KL, Moreno S, Tonks NK, Nurse P. Complementation of the mitotic activator, p80cdc25, by a human protein-tyrosine phosphatase. *Science.* 1990 Dec14;250(4987):1573-6.

Guertin DA, Chang L, Irshad F, Gould KL, McCollum D. The role of the sid1p kinase and cdc14p in regulating the onset of cytokinesis in fission yeast. *EMBO J*. 2000 Apr 17;19(8):1803-15.

Guha M, Zhou M, Wang YL. Cortical actin turnover during cytokinesis requires myosin II. *Curr Biol*. 2005 Apr 26;15(8):732-6.

Gupta S and McCollum D. Crosstalk between NDR kinase pathways coordinates cell cycle dependent actin rearrangements. *Cell Div*. 2011 Nov 11;6:19.

Gupta S, Mana-Capelli S, McLean JR, Chen CT, Ray S, Gould KL, McCollum D. Identification of SIN pathway targets reveals mechanisms of crosstalk between NDR kinase pathways. *Curr Biol*. 2013 Feb 18;23(4):333-8.

Hachet O and Simanis V. Mid1p/anillin and the septation initiation network orchestrate contractile ring assembly for cytokinesis. *Genes Dev*. 2008 Nov 15;22(22):3205-16.

Hao Y, Chun A, Cheung K, Rashidi B, Yang X. Tumor suppressor LATS1 is a negative regulator of oncogene YAP. *J Biol Chem*. 2008 Feb 29;283(9):5496-509.

Hall PA, Todd CB, Hyland PL, McDade SS, Grabsch H, Dattani M, Hillan KJ, Russell SE. The Septin-Binding Protein Anillin Is Overexpressed in Diverse Human Tumors. *Clin Cancer Res*. 2005 Oct 1;11(19 Pt 1):6780-6.

Hayles J and Nurse P. A review of mitosis in the fission yeast *Schizosaccharomyces pombe*. *Exp Cell Res*. 1989 Oct;184(2):273-86.

Hermeking H and Benzinger A. 14-3-3 proteins in cell cycle regulation. *Semin Cancer Biol*. 2006 Jun;16(3):183-92.

Hergovich A and Hemmings BA. Hippo signalling in the G2/M cell cycle phase: lessons learned from the yeast MEN and SIN pathways. *Semin Cell Dev Biol*. 2012 Sep;23(7):794-802.

Hiraoka Y, Toda T, Yanagida M. The NDA3 gene of fission yeast encodes beta-tubulin: a cold-sensitive nda3 mutation reversibly blocks spindle formation and chromosome movement in mitosis. *Cell*. 1984 Dec;39(2 Pt 1):349-58.

Hou MC, Wiley DJ, Verde F, and McCollum D. Mob2p interacts with the protein kinase Orb6p to promote coordination of cell polarity with cell cycle progression. *J Cell Sci*. 2003 Jan 1;116 (Pt 1):125-35.

Hou MC, Guertin DA, McCollum D. Initiation of cytokinesis is controlled through multiple modes of regulation of the Sid2p-Mob1p kinase complex. *Mol Cell Biol*. 2004 Apr;24(8):3262-76.

Hou MC, Salek J, McCollum D. Mob1p interacts with the Sid2p kinase and is required for cytokinesis in fission yeast. *Curr Biol*. 2000 May 18;10(10):619-22.

Huang J, Huang Y, Yu H, Subramanian D, Padmanabhan A, Thadani R, Tao Y, Tang X, Wedlich-Soldner R, Balasubramanian MK. Nonmedially Assembled F-Actin Cables Incorporate Into the Actomyosin Ring in Fission Yeast. *J Cell Biol*. 199 (5), 831-847.

Huang TY, Renaud-Young M, Young D. Nak1 interacts with Hob1 and Wsp1 to regulate cell growth and polarity in *Schizosaccharomyces pombe*. *J Cell Sci*. 2005 Jan 1;118 (Pt 1):199-210.

Humbel BM, Konomi M, Takagi T, Kamasawa N, Ishijima SA, Osumi M. In situ localization of beta-glucans in the cell wall of *Schizosaccharomyces pombe*. *Yeast*. 2001 Mar 30;18(5):433-44.

Humphrey W, Dalke A, and Schulten K. VMD:Visual Molecular Dynamics. *Journal of Molecular Graphics*. 1996 Feb;14(1):33-8, 27-8.

Isobe T, Ichimura T, Sunaya T, Okuyama T, Takahashi N, Kuwano R, Takahashi Y. Distinct forms of the protein kinase-dependent activator of tyrosine and tryptophan hydroxylases. *J Mol Biol*. 1991 Jan 5;217(1):125-32.

Johnson AE, McCollum D, and Gould KL. Polar opposites: Fine-tuning cytokinesis through SIN asymmetry. *Cytoskeleton*. 2012 Oct;69(10):686-99.

Kamasaki T, Osumi M, Mabuchi I. Three-dimensional arrangement of F-actin in the contractile ring of fission yeast. *J Cell Biol*. 2007 Aug 27;178(5):765-71.

Krapp A, Gulli MP, and Simanis V. SIN and the art of splitting the fission yeast cell. *Curr Biol*. 2004 Sep 7;14(17):R722-30.

Krapp A and Simanis V. An overview of the fission yeast septation initiation network (SIN). *Biochem Soc Trans*. 2008 Jun;36(Pt 3):411-5.

Kelley LA, Mezulis S, Yates CM, Wass MN, Sternberg MJ. The Phyre2 web portal for protein modeling, prediction and analysis. *Nat Protoc*. 2015 Jun;10(6):845-58.

Laporte D, Coffman VC, Lee IJ, Wu JQ. Assembly and architecture of precursor nodes during fission yeast cytokinesis. *J Cell Biol*. 2011 Mar 21;192(6):1005-21.

Laporte D, Ojkic N, Vavylonis D, Wu JQ. α -Actinin and fimbrin cooperate with myosin II to organize actomyosin bundles during contractile-ring assembly. *Mol Biol Cell*. 2012 Aug;23(16):3094-110.

Lee IJ and Wu J-Q. Characterization of Mid1 domains for targeting and scaffolding in fission yeast cytokinesis. *J Cell Sci*. 2012 Jun 15;125(Pt 12):2973-85.

Le Goff X, Woollard A, Simanis V. Analysis of the *cps1* gene provides evidence for a septation checkpoint in *Schizosaccharomyces pombe*. *Mol Gen Genet*. 1999 Aug;262(1):163-72.

Liu J, Wang H, and Balasubramanian MK. A checkpoint that monitors cytokinesis in *Schizosaccharomyces pombe*. *J Cell Sci*. 2000 Apr;113 (Pt 7):1223-30.

Liu J, Fairn GD, Ceccarelli DF, Sicheri F, Wilde A. Cleavage furrow organization requires PIP(2)-mediated recruitment of anillin. *Curr Biol*. 2012 Jan 10;22(1):64-9.

Longtine MS, DeMarini DJ, Valencik ML, Al-Awar OS, Fares H, De Virgilio C, Pringle JR. The septins: roles in cytokinesis and other processes. *Curr Opin Cell Biol*. 1996 Feb; 8(1):106-19.

Mah AS, Elia AE, Devgan G, Ptacek J, Schutkowski M, Snyder M, Yaffe MB, Deshaies RJ. Substrate specificity analysis of protein kinase complex Dbf2-Mob1 by peptide library and proteome array screening. *BMC Biochem*. 2005 Oct 21;6:22.

Malmberg NJ, Van Buskirk DR, and Falke JJ. Membrane-Docking Loops of the cPLA2 C2 Domain: Detailed Structural Analysis of the Protein-Membrane Interface via Site-Directed Spin-Labeling. *Biochemistry*. 2003 Nov 18; 42(45): 13227–13240.

Marks J, Hagan IM, and Hyams JS. Growth polarity and cytokinesis in fission yeast: the role of the cytoskeleton. *J Cell Sci Suppl*. 1986;5:229-41.

Martin SG and Berthelot-Grosjean M. Polar gradients of the DYRK-family kinase Pom1 couple cell length with the cell cycle. *Nature*. 2009 Jun 11;459(7248):852-6.

McCollum D and Gould KL. Timing is everything: regulation of mitotic exit and cytokinesis by the MEN and SIN. *Trends Cell Biol*. 2001 Feb;11(2):89-95.

Minet M, Nurse P, Thuriaux P, Mitchison JM. Uncontrolled septation in a cell division cycle mutant of the fission yeast *Schizosaccharomyces pombe*. *J Bacteriol*. 1979 Jan;137(1):440-6.

Mishra M, Karagiannis J, Sevugan M, Singh P, Balasubramanian MK. The 14-3-3 protein rad24p modulates function of the *cdc14p* family phosphatase *clp1p/flp1p* in fission yeast. *Curr Biol*. 2005 Aug 9;15(15):1376-83.

Moroishi T, Hayashi T, Pan WW, Fujita Y, Holt MV, Qin J, Carson DA, Guan KL. The Hippo Pathway Kinases LATS1/2 Suppress Cancer Immunity. *Cell*. 2016 Dec 1;167(6):1525-1539.e17.

Motegi F, Mishra M, Balasubramanian MK, Mabuchi I. Myosin-II reorganization during mitosis is controlled temporally by its dephosphorylation and spatially by Mid1 in fission yeast. *J Cell Biol.* 2004 Jun 7;165(5):685-95.

Mulvihill DP and Hyams JS. Cytokinetic actomyosin ring formation and septation in fission yeast are dependent on the full recruitment of the polo-like kinase Plo1 to the spindle pole body and a functional spindle assembly checkpoint. *J Cell Sci.* 2002 Sep 15;115(Pt 18):3575-86.

Muslin AJ, Tanner JW, Allen PM, Shaw AS. Interaction of 14-3-3 with signaling proteins is mediated by the recognition of phosphoserine. *Cell.* 1996 Mar 22;84(6):889-97.

Nalefski EA, Wisner MA, Chen JZ, Sprang SR, Fukuda M, Mikoshiba K, and Falke JJ. C2 Domains from Different Ca²⁺ Signaling Pathways Display Functional and, Mechanistic Diversity. *Biochemistry.* 2001 Mar 13; 40(10): 3089–3100.

Nabeshima K, Nakagawa T, Straight AF, Murray A, Chikashige Y, Yamashita YM, Hiraoka Y, Yanagida M. Dynamics of centromeres during metaphase-anaphase transition in fission yeast: Dis1 is implicated in force balance in metaphase bipolar spindle. *Mol Biol Cell.* 1998 Nov;9(11):3211-25.

Nurse P, Thuriaux P, Nasmyth K. Genetic control of the cell division cycle in the fission yeast *Schizosaccharomyces pombe*. *Mol Gen Genet.* 1976 Jul 23;146(2):167-78.

Oegema K, Savoian MS, Mitchison TJ, Field CM. Functional analysis of a human homologue of the *Drosophila* actin binding protein anillin suggests a role in cytokinesis. *J Cell Biol.* 2000 Aug 7;150(3):539-52.

Paoletti A and Chang F. Analysis of mid1p, a protein required for placement of the cell division site, reveals a link between the nucleus and the cell surface in fission yeast. *Mol Biol Cell.* 2000 Aug;11(8):2757-73.

Pollard TD and Wu JQ. Understanding cytokinesis: lessons from fission yeast. *Nat Rev Mol Cell Biol.* 2010 Feb; 11(2): 149.

Ponting CP and Parker PJ. Extending the C2 domain family:C2s in PKCs delta, epsilon, eta, theta, phospholipases, GAPs, and perforin. *Protein Sci.* 1996 Jan;5(1):162-6.

Pu KM, Akamatsu M, and Pollard TD. The septation initiation network controls the assembly of nodes containing Cdr2p for cytokinesis in fission yeast. *J Cell Sci.* 2015 Feb 1;128(3):441-6.

Rachfall N, Johnson AE, Mehta S, Chen JS, Gould KL. Cdk1 promotes cytokinesis in fission yeast through activation of the septation initiation network. *Mol Biol Cell.* 2014 Aug 1;25(15):2250-9.

Ray S, Kume K, Gupta S, Ge W, Balasubramanian M, Hirata D, McCollum D. The mitosis-to-interphase transition is coordinated by cross talk between the SIN and MOR pathways in *Schizosaccharomyces pombe*. *J Cell Biol.* 2010 Sep 6;190(5):793-805.

Rice P, Longden I, and Bleasby A. EMBOSS: the European Molecular Biology Open Software Suite. *Trends Genet.* 2000 Jun;16(6):276-7.

Rincon SA, Estravis M, Dingli F, Loew D, Tran PT, Paoletti A. SIN-Dependent Dissociation of the SAD Kinase Cdr2 from the Cell Cortex Resets the Division Plane. *Curr Biol.* 2017 Feb 20;27(4):534-542.

Rincon SA and Paoletti A. Mid1/anillin and the spatial regulation of cytokinesis in fission yeast. *Cytoskeleton.* 2012 Oct;69(10):764-77.

Rincon SA and Paoletti A. Molecular Control of Fission Yeast Cytokinesis. *Seminars in Cell & Developmental Biology.* May 2016; 53: 28–38.

Roberts-Galbraith RH and Gould KL. Stepping into the ring: the SIN takes on contractile ring assembly. *Genes Dev.* 2008 Nov 15;22(22):3082-8.

Roberts-Galbraith RH, Ohi MD, Ballif BA, Chen JS, McLeod I, McDonald WH, Gygi SP, Yates JR 3rd, Gould KL. Dephosphorylation of F-BAR protein Cdc15 modulates its conformation and stimulates its scaffolding activity at the cell division site. *Mol Cell.* 2010 Jul 9;39(1):86-99.

Roy A, Yang J, Zhang Y. COFACTOR: an accurate comparative algorithm for structure-based protein function annotation. *Nucleic Acids Research.* 2012; 40: W471-W477.

Russell RB and Barton GJ. Multiple protein sequence alignment from tertiary structure comparison: assignment of global and residue confidence levels. *Proteins.* 1992 Oct;14(2):309-23.

Russell P and Nurse P. *cdc25+* functions as an inducer in the mitotic control of fission yeast. *Cell.* 1986 Apr 11;45(1):145-53.

Russell P and Nurse P. Negative regulation of mitosis by *wee1+*, a gene encoding a protein kinase homolog. *Cell.* 1987 May 22;49(4):559-67.

Saha S and Pollard TD (a). Anillin-related protein Mid1p coordinates the assembly of the cytokinetic contractile ring in fission yeast. *Mol Biol Cell.* 2012 Oct;23(20):3982-92.

Saha S and Pollard TD (b). Characterization of structural and functional domains of the anillin-related protein Mid1p that contribute to cytokinesis in fission yeast. *Mol Biol Cell.* 2012 Oct;23(20):3993-4007.

Sievers F, Wilm A, Dineen D, Gibson TJ, Karplus K, Li W, Lopez R, McWilliam H, Remmert M, Söding J, Thompson JD, Higgins DG. Fast, scalable generation of high-quality protein multiple sequence alignments using Clustal Omega. *Mol Syst Biol.* 2011 Oct 11;7:539.

Simanis, V. Events at the end of mitosis in the budding and fission yeasts. *J Cell Sci.* 2003 Nov 1;116(Pt 21):4263-75.

Simanis, V. Pombe's thirteen - control of fission yeast cell division by the septation initiation network. *J Cell Sci.* 2015 Apr 15;128(8):1465-74.

Sohrmann M, Fankhauser C, Brodbeck C, Simanis V. The *dmf1/mid1* gene is essential for correct positioning of the division septum in fission yeast. *Genes Dev.* 1996 Nov 1;10(21):2707-19.

Song K, Mach KE, Chen CY, Reynolds T, Albright CF. A novel suppressor of *ras1* in fission yeast, *byr4*, is a dosage-dependent inhibitor of cytokinesis. *J Cell Biol.* 1996 Jun;133(6):1307-19.

Sparks CA, Morphew M and McCollum D. Sid2p, a Spindle Pole Body Kinase That Regulates the Onset of Cytokinesis. *The Journal of Cell Biology.* Aug 1999;146, no. 4: 777–90.

Sun L, Guan R, Lee IJ, Liu Y, Chen M, Wang J, Wu JQ, Chen Z. Mechanistic insights into the anchorage of the contractile ring by anillin and Mid1. *Dev Cell.* 2015 May 26;33(4):413-26.

Takaine M, Numata O, Nakano K. Fission yeast IQGAP maintains F-actin-independent localization of myosin-II in the contractile ring. *Genes Cells.* 2014 Feb;19(2):161-76.

Takaine M, Numata O, Nakano K. An actin-myosin-II interaction is involved in maintaining the contractile ring in fission yeast. *J Cell Sci.* 2015 Aug 1;128(15):2903-18

Tanaka K, Petersen J, MacIver F, Mulvihill DP, Glover DM, Hagan IM. The role of Plo1 kinase in mitotic commitment and septation in *Schizosaccharomyces pombe*. *EMBO J.* 2001 Mar 15;20(6):1259-70.

Tasto JJ, Morrell JL, Gould KL. An anillin homologue, Mid2p, acts during fission yeast cytokinesis to organize the septin ring and promote cell separation. *J Cell Biol.* 2003 Mar 31; 160(7):1093-103.

Tatsumoto T, Xie X, Blumenthal R, Okamoto I, Miki T. Human ECT2 is an exchange factor for Rho GTPases, phosphorylated in G2/M phases, and involved in cytokinesis. *J Cell Biol.* 1999 Nov 29;147(5):921-8.

Tran PT, Marsh L, Doye V, Inoué S, Chang F. A mechanism for nuclear positioning in fission yeast based on microtubule pushing. *J Cell Biol.* 2001 Apr 16;153(2):397-411.

Vavylonis D, Wu JQ, Hao S, O'Shaughnessy B, Pollard TD. Assembly mechanism of the contractile ring for cytokinesis by fission yeast. *Science.* 2008 Jan 4;319(5859):97-100.

Verde F, Wiley DJ, and Nurse P. Fission yeast orb6, a ser/thr protein kinase related to mammalian rho kinase and myotonic dystrophy kinase, is required for maintenance of cell polarity and coordinates cell morphogenesis with the cell cycle. *Proc Natl Acad Sci U S A.* 1998 Jun 23;95(13):7526-31.

Visser S and Yang X. LATS tumor suppressor: a new governor of cellular homeostasis. *Cell Cycle.* 2010 Oct 1;9(19):3892-903.

Wolfe BA, McDonald WH, Yates JR 3rd, Gould KL. Phospho-regulation of the Cdc14/Clp1 phosphatase delays late mitotic events in *S. pombe*. *Dev Cell.* 2006 Sep;11(3):423-30.

Wu JQ, Bähler J, Pringle JR. Roles of a fimbrin and an alpha-actinin-like protein in fission yeast cell polarization and cytokinesis. *Mol Biol Cell.* 2001 Apr; 12(4):1061-77.

Wu JQ, Sirotkin V, Kovar DR, Lord M, Beltzner CC, Kuhn JR, Pollard TD. Assembly of the cytokinetic contractile ring from a broad band of nodes in fission yeast. *J Cell Biol.* 2006 Jul 31; 174(3):391-402.

Wu JQ, Kuhn JR, Kovar DR, Pollard TD. Spatial and temporal pathway for assembly and constriction of the contractile ring in fission yeast cytokinesis. *Dev Cell.* 2003 Nov;5(5):723-34.

Yang J, Roy A, Zhang Y. Protein-ligand binding site recognition using complementary binding-specific substructure comparison and sequence profile alignment. *Bioinformatics.* 2013; 29: 2588-2595.

Yang J and Zhang Y. I-TASSER server: new development for protein structure and function predictions. *Nucleic Acids Research.* 2015; 43: W174-W181.

Yang X, Lee WH, Sobott F, Papagrigoriou E, Robinson CV, Grossmann JG, Sundström M, Doyle DA, Elkins JM. Structural basis for protein-protein interactions in the 14-3-3 protein family. *Proc Natl Acad Sci U S A.* 2006 Nov 14;103(46):17237-42.

Ye Y, Lee IJ, Runge KW, Wu JQ. Roles of putative Rho-GEF Gef2 in division-site positioning and contractile-ring function in fission yeast cytokinesis. *Mol Biol Cell.* 2012 Apr;23(7):1181-95.

Zeng Y and Piwnica-Worms, H. DNA Damage and Replication Checkpoints in Fission Yeast Require Nuclear Exclusion of the Cdc25 Phosphatase via 14-3-3 Binding. *Mol Cell Biol*. 1999 Nov; 19(11): 7410–7419.

Zeng Y, Forbes KC, Wu Z, Moreno S, Piwnica-Worms H, Enoch T. Replication checkpoint requires phosphorylation of the phosphatase Cdc25 by Cds1 or Chk1. *Nature*. 1998 Oct 1;395(6701):507-10.

Zhang Y, Sugiura R, Lu Y, Asami M, Maeda T, Itoh T, Takenawa T, Shuntoh H, Kuno T. Phosphatidylinositol 4-phosphate 5-kinase Its3 and calcineurin Ppb1 coordinately regulate cytokinesis in fission yeast. *J Biol Chem*. 2000 Nov 10;275(45):35600-6.

Zhang Y. I-TASSER: Fully automated protein structure prediction in CASP8. *Proteins*, 77 (Suppl 9): 100-113, 2009.

Zhu YH, Ye Y, Wu Z, Wu JQ. Cooperation between Rho-GEF Gef2 and its binding partner Nod1 in the regulation of fission yeast cytokinesis. *Mol Biol Cell*. 2013 Oct;24(20):3187-204.